DANMARKS OG GRØNLANDS GEOLOGISKE UNDERSØGELSE RAPPORT 2008/66

Burial anomalies estimated from sonic data for the Mesozoic-Palaeogene succession in 31 Norwegian wells in the Egersund Basin and adjacent areas

Peter Japsen

GEOLOGICAL SURVEY OF DENMARK AND GREENLAND
MINISTRY OF CLIMATE AND ENERGY

G E U S

DANMARKS OG GRØNLANDS GEOLOGISKE UNDERSØGELSE RAPPORT 2008/66

Burial anomalies estimated from sonic data for the Mesozoic-Palaeogene succession in 31 Norwegian wells in the Egersund Basin and adjacent areas

A contribution to the project "Erogen 2008, Norwegian Danish Basin. Recent erosion and deposition offshore Norway - Effects on heat flow and hydrocarbon generation"

Peter Japsen

Released 01.06.2011

GEOLOGICAL SURVEY OF DENMARK AND GREENLAND
MINISTRY OF CLIMATE END ENERGY

G E U S

1. Summary

This report documents estimated values of burial anomalies from sonic data for the Mesozoic-Palaeogene succession in 31 offshore Norwegian wells in the Egersund Basin and adjacent areas.

The burial anomaly is the difference between the present-day burial depth of a rock and the depth corresponding to normal compaction for the measured velocity as predicted by a normal velocity-depth trend for the lithology in question. The burial anomaly is zero for normally compacted sediments, whereas high velocities relative to depth give negative burial anomalies which may be caused by a reduction in overburden thickness. A positive burial anomaly may indicate undercompaction due to overpressure. Post-exhumational burial will mask the magnitude of the removed overburden section

The conversion of the estimated burial anomalies to amounts of removed section requires that the timing of maximum burial is known and thus that the amount of post-exhumational burial can be estimated. These parameters cannot be assessed from sonic data but requires input from apatite fission-track analysis data, stratigraphy and seismic data. Based on results from similar studies in adjacent areas in Denmark (Japsen et al. 2007a) candidates for the timing of maximum burial are either early or late Neogene; i.e. c. 25 or 5 Ma.

The burial anomalies are estimated qualitatively for the Mesozoic–Palaeogene successions in each well and are primarily based on a comparison between (1) the sonic data for the chalk of the Shetland Group and a revised chalk baseline and (2) the sonic data for the Paleogene shale and a published shale baseline. Furthermore, the interpretation has been supported by a comparison between the sonic data for shales below the chalk and the shale baseline and a comparison between the sonic data for Triassic-Jurassic sandstone intervals and a baseline for relatively pure sandstone.

The qualitative estimation of the burial anomaly is based on depth-shifting all three baselines by the same amount until a match is obtained with the sonic data for the intervals of the identified lithology that are considered more reliable; typically the chalk and the Palaeogene shale. The benefit of this qualitative approach is that whereas the velocity-depth trend for one of the lithologies may be difficult to identify from the sonic data, the comparison of the sonic data for two or more lithologies with the respective baseline effectively limits the range of the possible burial anomalies.

The estimated burial anomalies are shown in Figure *i* that reveals a consistent trend of negative anomalies (indicating exhumation) increasing in magnitude in direction of the Norwegian coast and a narrow belt of burial anomalies near zero m (indicating maximum burial) towards the central North Sea where overpressure is reflected in positive anomalies (see Table 6-1).

For 20 wells the Mesozoic-Palaeogene succession is found to have been more deeply buried. The maximum magnitude of the burial anomalies is estimated to -2500 m for well 11/9-1 drilled on a salt structure, but this is not very well constrained because only the Hegre

Group is penetrated by this well. Burial anomalies for the other wells range from -200 and -700 m with maximum values in Block 9 of -600 m (well 9/3-1) and -700 m in Block 10 (well 10/7-1).

For 9 wells the Mesozoic-Palaeogene succession is found to be near maximum burial (absolute value of the burial anomaly equal to or less than 150 m) whereas the succession was found to be overpressured in two wells.

The result presented here are in good agreement with previous studies. The mean difference between the burial anomalies presented here and those of Hansen (1996) that were based on sonic data for shale intervals is 160 m for the 18 wells in common between the studies. This indicates a slight reduction in the amount of exhumation (or increase in the amount of overpressure) estimated in this study relative to that of Hansen (1996).

The mean difference between the burial anomalies presented here and those of Japsen (2000) that were based on interval velocities for the chalk of the Shetland Group is 38 m for the 17 wells in common between the studies indicating that the two studies arrived at almost identical results. This similarity in results is obtained despite several differences in the methods applied by the two studies; e.g. the revised chalk baseline presented here and the use of a qualitative comparison between sonic data and baselines for different lithologies rather than computing the burial anomaly with only the chalk interval velocity as input.

Anomalously low velocities are found in the uppermost part of the chalk below high-velocity carbonates with bryozoans in several wells on the Yme field; i.e. wells 9/2-1, 9/2-2 and 9/2-4s. It is a possible explanation that these low velocities (high porosities) are caused by the presence of hydrocarbons in the chalk at an early stage during the compaction of the chalk. Presence of hydrocarbons is known to have a porosity-preserving effect in chalk where coating of the grains with hydrocarbons prevents pressure solution of the carbonates (e.g. Fabricius et al. 2008).

Improved constraints on the estimated burial anomalies could be obtained from a better definition of uniform shale in the Lower Cretaceous succession where pronounced velocity variations are observed. Furthermore, the deeper intervals of sand-rich sediments of Jurassic and Triassic age need to be studied in more detail for a reliable identification of intervals dominated by pure sandstone that are not affected by high-velocity anhydrite or limestone. A further investigation of the well data presented in this report will benefit from the well-defined velocity-depth relations for the Palaeogene shales and the Upper Cretaceous chalks in the study area.

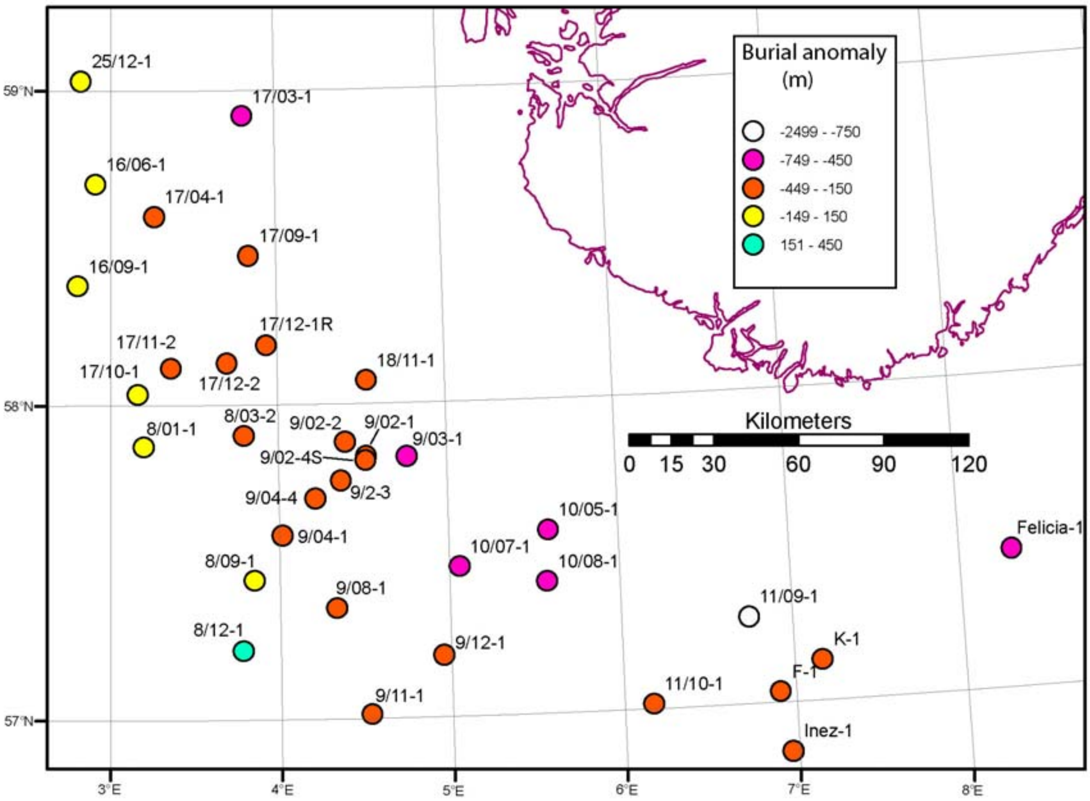

Figure i. *Map of the estimated burial anomalies based on Norwegian wells investigated in this report together with results from Danish wells (Japsen & Bidstrup 1999; Japsen et al. 2007a).*

2. Introduction

The present report is a contribution to the project “Erogen 2008, Norwegian Danish Basin. Recent erosion and deposition offshore Norway – Effects on heat flow and hydrocarbon generation” carried out by GEUS for Exploro AS, Tondheim, Norway. The report documents the interpretation of burial anomalies relative to maximum burial based on sonic logs in 31 Norwegian offshore wells.

The report is based on digital log data provided by Exploro and stratigraphic and other information available at the web site of the Norwegian Petroleum Directorate (www.npd.no). Legend to the plots in the report is found in Appendix A.

The report is structured in the following way:

Chapter 3. Velocity anomalies and burial anomalies. The basic principles of estimating maximum palaeoburial using sonic data and a summary of how sonic data for shale and chalk can be used for estimating overpressure. As a supplement to this and the following chapter, Appendix B contains the paper ‘Constraints on velocity-depth trends from rock physics models’ by Japsen, Mukerji & Mavko (2007).

Chapter 4. Normal velocity-depth trends for different lithologies. A revised baseline for chalk is suggested based on sonic data in this report and (B) the observations presented by Japsen et al. (2005) – reproduced in Appendix C. Furthermore, the chapter contains a short presentations of baselines for marine shale and for the Lower Triassic Bunter ‘Shale’ as well as a revised baseline for sandstone.

Chapter 5. Discussion of lithological indicators and identification of velocity-depth trends. This chapter contains a discussion of general and specific aspects of the sonic data in the studied wells for which the log data are shown in Appendix A.

Chapter 6. Estimation of burial anomalies. This chapter describes the method of quantitative estimation of the burial anomalies and the estimated burial anomalies for the drilled sections in the individual wells are presented in Table 6-1. The results are compared with previous studies.

Chapter 7. Suggestions for future work.

Chapter 8. References.

Appendix A. Plots and comments to log data.

Appendix B. Appendix B – Constraints on velocity-depth trends from rock physics models (Japsen et al. 2007b).

Appendix C. Chalk background velocity: Influence of effective stress and texture (Japsen et al. 2005).

3. Velocity anomalies and burial anomalies

3.1 Estimation of maximum palaeoburial using sonic data

The technique for estimating maximum palaeoburial of a sedimentary unit – and thus the amount of erosion of its overburden – from sonic data has been known for decades (e.g. Marie, 1975; Magara, 1976; Scherbaum, 1982; Chapman, 1983; Bulat & Stoker, 1986; Japsen, 1993, 1998, 2000; Hillis, 1995; Heasler & Kharitonova, 1996; Al-Chalabi & Rosenkranz, 2002). There is, however, no generally accepted methodology of how such estimates are best derived (see Corcoran & Doré, 2005 for a review). The technique is based on the general observation that the sonic velocity of most sedimentary rocks increases as the porosity of the sediment is reduced through deeper burial. Porosity is reduced due to increased effective stress that causes mechanical compaction and pressure solution. Sonic velocity is increased due to porosity-reduction and stiffer grain contacts, and as these processes are considered largely irreversible, measured velocity will depend on the maximum effective stress experienced by the sedimentary rock – and hence on its maximum burial if the burial depth has been reduced by erosion. The timing of the erosion of the overburden is represented by any of the unconformities in the overburden.

A normal velocity-depth trend is thus a function that describes how sonic velocity increases with depth in a relatively homogenous, brine-saturated sedimentary formation when porosity is reduced during normal compaction (mechanical or chemical). Compaction is 'normal' when the fluid pressure of the formation is hydrostatic, and the formation is at maximum burial depth. Simple boundary conditions for such trends are that the velocity at the surface equals the velocity of the sediment when it was first deposited (Nur et al., 1998), and that velocity approaches the matrix velocity of the rock while the velocity-depth gradient approaches zero with increasing depth (see Japsen et al., 2007b).

The derivation of a normal velocity-depth trend involves three steps of generalisation: 1) Identification of a relatively, laterally homogenous lithological unit, 2) selection of data points that represent normal compaction and 3) assignment of a function that expresses the velocity-depth trend (see Japsen et al., 2007). Few attempts have been made to constrain normal velocity-depth trends for different lithologies rather than just considering velocity-depth trends as fits of arbitrary functions to local data sets. The increase of velocity with depth for a uniform sedimentary formation (and thus the shape of the baseline) has been shown to depend on the mineralogical composition of the formation (Japsen et al., 2007b).

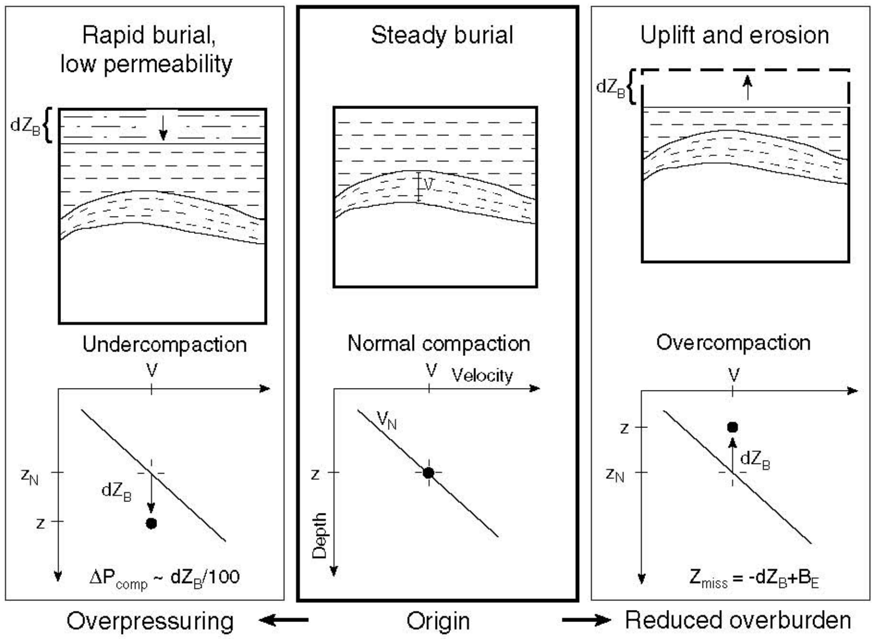

Figure 3-1. *Burial anomaly, dZ_B [m], relative to a normal velocity-depth trend, V_N, for a sedimentary formation. In the North Sea Basin, burial anomalies of ±1 km for pre-Miocene formations result from late Cenozoic exhumation along basin margins and overpressuring due to rapid, late Cenozoic burial in the basin centre. Rapid burial and low permeability cause undercompaction and overpressure, ΔP_{comp} [MPa], and velocities low relative to depth (positive dZ_B) (cf. Eq. 3-3). Exhumation due to uplift reduce the overburden thickness, and causes overcompaction expressed as velocities high relative to depth (negative dZ_B); however, post-exhumational burial, B_E, will mask the magnitude of the missing section, Δz_{miss}. The normalized depth, z_N, is the depth corresponding to normal compaction for the measured velocity (cf. Terzaghi's principle). Modified after Japsen (1998).*

Normal velocity-depth trends for chalk (V_N^{ch}), marine shale dominated by smectite/illite (V_N^{sh}) and quartz-dominated Triassic deposits (V_N^{B}) were defined by Japsen (1998, 1999, 2000) in such a way that the velocity at the surface agreed with those of recently deposited sediments, and that velocity did not approach infinity at depth. Velocity-depth anomalies relative to these trends were found to be in agreement with estimates of erosion along the margins of the North Sea Basin as well as with measurements of overpressure in the centre of this basin. Furthermore, these baselines are in agreement with those of previous workers even though such analytical expressions have often not fulfilled simple boundary conditions (e.g. Marie, 1975; Scherbaum, 1982; Bulat & Stoker, 1987; Hillis, 1995; Hansen, 1996).

The burial anomaly, dZ_B, is the difference between the present-day burial depth of a rock, z, and the depth, $z_N(V)$, corresponding to normal compaction for the measured velocity, V (Japsen 1998):

$$dZ_B = z - z_N(V) \tag{3-1}$$

The burial anomaly is zero for normally compacted sediments, whereas high velocities relative to depth give negative burial anomalies which may be caused by a reduction in overburden thickness when lithology is relatively homogenous over the study area, and if lateral variations of horizontal stress are minor. A positive burial anomaly may indicate undercompaction due to overpressure. To assess whether the burial anomaly for a stratigraphic unit is a measure of exhumation requires an integrated evaluation: The burial anomalies should thus agree with other estimates of erosion and should correspond geographically to where there is a missing section in the stratigraphic record. Any post-exhumational burial, B_E, will mask the magnitude of the missing (removed) overburden section, Δz_{miss}:

$$\Delta z_{miss} = -dZ_B + B_E \qquad (3\text{-}2)$$

where the minus indicates that erosion reduces depth (Hillis, 1995; Japsen, 1998). The timing of the exhumation events is thus important for understanding the succession of events, their true magnitude and for identifying the age of the eroded succession.

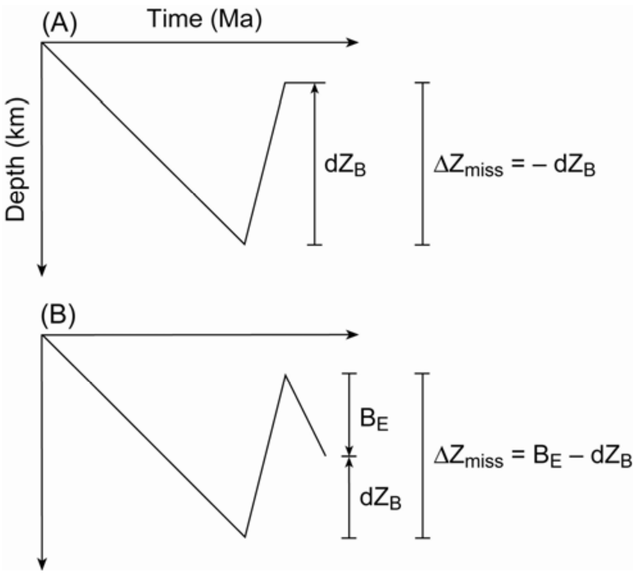

Figure 3-2. *Burial diagrams illustrating that the magnitude of the missing (or removed) section (Δz_{miss}) will be less than the magnitude of the measured burial anomaly (dZ_B) in the case of post-exhumational burial (B_E) (Eq. 3-2). (A) Exhumation followed by no deposition; (B) exhumation followed by burial.*

3.2 Overpressure-prediction using shale and chalk sonic data

Overpressure in the central North Sea was successfully predicted from velocity-depth anomalies for the Cenozoic succession relative to a normal velocity-depth trend for shale close to that given by Eq. (4-2) (Japsen 1999; Fig. 3-1). The overpressure results from a balance between the load of the upper Cenozoic deposits, and the draining determined by the thickness and sealing quality of the lower Cenozoic sediments. The overpressure of an undercompacted rock, ΔP_{comp}, is proportional to the burial anomaly, dZ_B, if the effective stress is increasing with time (cf. Magara 1978; Japsen 1998). We get $\Delta P_{comp} = \Delta \rho_{up} \cdot g \cdot dZ_B$ where $\Delta\rho_{up}$ is the density contrast (wet bulk density minus pore fluid density) of the upper Cenozoic and g is the gravitational acceleration (9.807 m/s2). The equation is based on Terzaghi's principle and states that if a rock is buried at a greater depth by dZ_B without change in the effective stress (indicated by unchanged velocity), the effective stress of the added load is carried by an increase in pore pressure. If we substitute $\Delta\rho_{up} \approx 1.02 * 10^3$ kg/m^3, and dZ_B is in meters, we find that the overpressure of an undercompacted rock, ΔP_{comp} [MPa], is proportional to the burial anomaly, dZ_B [m] (Fig. 3-1):

$$\Delta P_{comp} \approx dZ_B/100 \text{ [MPa]}, \tag{3-3}$$

which means that a burial anomaly of 1000 m may reflect overpressure due to undercompaction of 10 MPa (Japsen 1998). From the above expression we can define the effective depth, Z_{eff}, for a unit at measured depth, Z, as the depth where the same effective stress would occur during normal compaction. In the case of overpressure (ΔP) we get

$$Z_{eff} = Z - \Delta P \cdot 100 \tag{3-4}$$

where ΔP is measured in MPa and depths are in metres (cf. Japsen 1998).

In Figure 3-3 we compare the degree of undercompaction of the lower Cenozoic succession in the North Sea expressed by its burial anomaly, dZ_B^{low}, with pressure data from the underlying Chalk, ΔP_{Ch}, because pressure measurements from the lower Cenozoic shales are rare in the central North Sea. We observe that ΔP_{Ch} is proportional to dZ_B^{low}, and in the order of the overpressure predicted by Eq. (3-3). This indicates that the burial anomaly for the lower Cenozoic succession relative to the shale trend given by Eq. (4-2) is a measure of overpressure due to undercompaction. Investigation of interval velocities from almost a thousand wells revealed basin-wide differences in the physical properties of the Cenozoic deposits related to disequilibrium compaction below the mid-Miocene unconformity in the central North Sea (cf. Osborne and Swarbrick 1997).

Japsen (1998) demonstrated that positive burial anomalies for the chalk in the central North Sea were proportional to measured values of overpressure in the chalk and that the overpressure was in the order of magnitude given by Eq. (3-3).

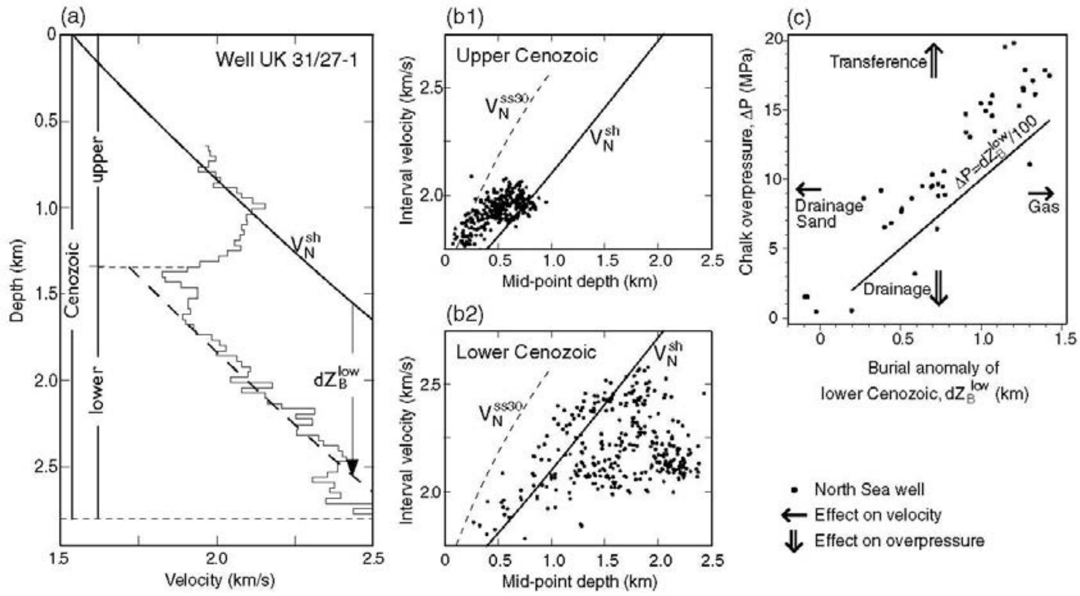

Figure 3-3. *Prediction of overpressure in the North Sea from interval velocities of the Cenozoic deposits (excluding the Danian) (cf. Figure 3-1).*

(a) Sonic log where low velocities reveal undercompaction of the lower Cenozoic sediments corresponding to measured overpressure in the underlying chalk.

(b1) and (b2) Interval velocity versus depth to the midpoint of the upper and lower Cenozoic deposits, respectively, for 322 North Sea wells.

(c) Burial anomalies for the lower Cenozoic sediments (dZ_B^{low}) versus Chalk formation overpressure (ΔP) in North Sea wells.

The upper Cenozoic deposits are close to normal compaction whereas velocity-depth anomalies for the lower Cenozoic sediments outline a zone of undercompaction in the central North Sea. The deviations from the trend line in figure (c) is due to the non-compactional sources that add to the Chalk overpressure from below (transference; cf. Osborne and Swarbrick 1997), the easier drainage from the more shallow Cenozoic section and sandy lithology; $\Delta P = dZ_B/100$- see equation 3-3). The burial anomalies are calculated relative to the shale trend given by equation (5). Depths below top of sediments. V_N^{ss30}: modified Voigt model for sandstone, 30% clay content. V_N^{sh}: marine shale (Eq. 4-2). Modified after Japsen et al. (2007b).

4. Normal velocity-depth trends for different lithologies

4.1 Baselines for chalk

4.1.1 Published baselines for North Sea chalk (Japsen 1998, 2000)

Japsen (1998) published a normal velocity–depth trend for the Chalk Group based on an analysis of 845 wells throughout the North Sea Basin and ODP data. For the shallowest part of the trend, no data representing normal compaction were found for the Chalk of the North Sea Basin, so sonic log data from Eocene to Recent ooze and chalk deposits from the stable Ontong Java Plateau in the Pacific Ocean were used to guide the trend (cf. Urmos 1993). At intermediate depths, Japsen (1998) applied qualitative arguments to identify North Sea data representing normal compaction along the lower bound for velocity–depth data for which the effect of overcompaction due to erosion is minimum. At greater depths, data representing normal compaction were identified along the upper bound where the effect of undercompaction due to overpressuring is a minimum.

Japsen (2000) found additional geological constraints that refine the identification of reference data at intermediate depths where the influence of erosion and overpressuring is difficult to ascertain. Because the sonic method identifies deviations from maximum burial, post-erosional reburial of a formation will reduce its observable burial anomaly; e.g. a pre-Quaternary erosion of 500 m will be masked by a subsequent Quaternary reburial of 500 m. This implies that, where the Quaternary is thick, even minor deviations from maximum burial due to Neogene erosion may correspond to a substantial missing section. Deep erosion is, however, not likely where the base-Quaternary hiatus is minor, e.g. where the Quaternary is underlain by late Neogene sediments.

Normally–compacted Chalk is thus likely to be found in areas where the Quaternary is thick, late Neogene deposits are present and pressure is hydrostatic. Consequently, the normal velocity–depth trend for the North Sea Chalk should follow the upper bound for data from such areas, whereas data representing undercompaction due to overpressuring should plot below the trend. A revised baseline has been defined by such maximum velocity data for $900<z<1700$ m. The revised trend lines up with the maximum velocity data used to define the original trend for $z>2000$ m, and with a velocity at the surface of 1550 m/s.

4.1.2 A revised baseline for North Sea chalk

The sonic data plotted in Figure 4-1 show that the velocity-depth gradient is significantly higher than predicted by the normal trend suggested by Japsen (2000) for velocities above

c. 4 km/s. Sonic data from a number of wells presented in this report can be used to investigate the increase of chalk sonic velocity for velocities higher than 4 km/s:

Wells 8/9-1, 9/2-2, 9/4-1, 9/4-4, 9/8-1 and 17/11-2.

These wells have thick chalk sections over which the sonic velocity increases steadily to almost 5 km/s (wells 8/9-1, 9/4-4 and 9/8-1).

Whereas Japsen (2000) predicted a gradients of 1.3 1/s for 3862 < V < 4875 m/s, and one of 1 1/s for 4875 < V < 5500 m/s (the trend was undefined for V> 5500 m/s), the trend in the data shows a better match for a gradient of 5 1/s for 3862 < V < 5000 m/s (the minimum value of V chosen to fit the Japsen (2000) trend for slower velocities). We get the following revised normal velocity-depth trend for chalk:

$$\begin{aligned} V_N^{Ch} &= 1550 + 1.3 \cdot z, && z < 900\,\mathrm{m}\,(\mathrm{V} < 2720\,\mathrm{m/s}) \\ V_N^{Ch} &= 920 + 2 \cdot z, && 900 < z < 1471\mathrm{m}\,(2720 < \mathrm{V} < 3862\,\mathrm{m/s}) \\ V_N^{Ch} &= -3493 + 5 \cdot z, && 1471 < z < 1700\,\mathrm{m}\,(3862 < \mathrm{V}\ 5000\,\mathrm{m/s}) \end{aligned} \tag{4-1}$$

This revision is good agreement with the observation of a ‘compaction front’ in chalk for velocities above c. 4 km/s, corresponding to effective depths above c. 1.8 km (Japsen et al. 2005; see Appendix C). It was observed that for effective depths (Eq. 3-4) less than c. 1.8 km, the chalk data plotted along the V–Z and V–φ reference curves for normally compacted chalk of Japsen (1998) and Sclater & Christie (1980) (if depths are referred to sea bed rather than sea level, there is agreement between the data and the chalk trend of Japsen (2000)). Below that depth a pronounced porosity drop and a corresponding velocity increase is observed over a short depth interval for both data sets. These observations imply that porosity reduction and velocity increase for chalk is governed by the effective stress also for porosities less than c. 40% and that below some 20% a rapid increase in pore-filling cementation takes place (corresponding to velocities higher than 4 km/s).

The implication of this revision is that the predicted effective depth of a chalk unit with a sonic velocity of e.g. 4.7 km/s is reduced with c. 500 m from c. 2100 m to 1600 m. Correspondingly, for a unit with that velocity buried below 1 km of sediments, the estimated burial anomaly will be reduced from -1.1 to -0.6 km (estimated exhumation reduced by 500 m) and for a chalk unit buried below 3 km of sediment, the estimated burial anomaly will be increased from 0.9 to 1.4 km (estimated overpressure increased by 5 MPa).

The increased overpressure that the revised model predicts for overpressured chalk with high velocities is an improvement relative to the previous model which explained only 92% of the observed overpressure in the Chalk for 40 wells located away from diapirs and where the overpressure exceeded 4 MPa (Japsen 2000).

The corresponding percentage of predicted relative to measured overpressure based on the revised baseline is 103% for the same wells. This demonstrates that the revised baseline is a better model for the relation between velocity and depth for chalk than the model of Japsen (2000). The improvement is particularly clear for data from relatively high overpressure (15–20 MPa); e.g. well 2/7-2 where chalk overpressure is 20.0 MPa, and for which the overpressure prediction from velocity data has been increased from 13.1 to 16.1 MPa a result which is 3 MPa closer to the measured value than the previous estimate.

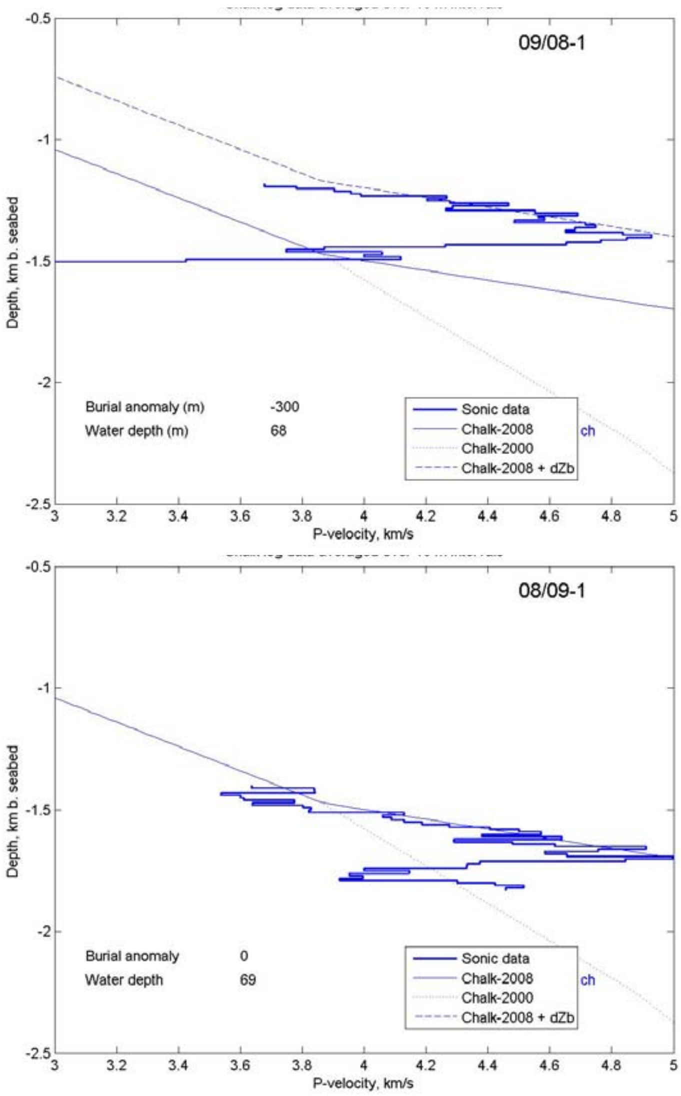

Figure 4-1. *Plot of sonic log data for chalk compared with the baselines for chalk of Japsen (2000) and the revision presented in this report (eq. 4-1); 'Chalk-2000' and 'Chalk-2008', respectively (wells 8/9-1 and 9/8-1). Furthermore, the revised trend is plotted corrected for the estimated burial anomaly ('Chalk-2008+dZb').*

Table 4-1. *Comparison of measured overpressure and overpressure estimated from chalk sonic data relative to the chalk baseline of Japsen (2000) and that presented here in Equation 4-1. Data for 40 wells located away from diapirs and where the overpressure exceeded 4 MPa.*

(MPa)	mean	std	min	max
Overpressure, dP	13.7	3.8	7.5	20.1
dP_2000	12.4	3.2	6.2	17.9
dP_2008	13.9	3.9	6.2	19.8
error_2000	1.3	2.3	-4.3	7.0
error_2008	-0.3	2.1	-5.9	4.0

Overpressure: Calculated overpressure based on pressure measurement in the chalk.
dP_2000, dP_2008: Overpressure estimated from chalk interval velocities relative to the chalk baselines of Japsen (2000) and that presented here (Eq. 4-1). The overpressure is estimated from Eq. 3-3.
error_00, error_08: dP – error_00, dP-error_08, respectively.

4.2 A baseline for marine shale

Japsen (2000) formulated a constrained baseline, V_N^{LJur}, for marine shale dominated by smectite/illite based on velocity-depth data for the Lower Jurassic F-1 Member of the Fjerritslev Formation from 31 Danish wells of which 28 have sonic data for the Chalk (Fig. 6):

$$tt = 460 \cdot e^{-z/2175} + 185 \qquad (4\text{-}2)$$

where transit time, *tt*, is the inverse of velocity. The baseline was reconstructed by correcting present formation depths for the effect of late Cenozoic erosion as estimated from the velocity of the overlying Chalk in these wells relative to the Chalk baseline of Japsen (2000). The corrected depths correspond to the burial of the formation prior to erosion when the sediments were at maximum burial at more locations than today. The baseline can thus be traced more easily in a plot of velocity versus the corrected depths, and is well defined at great depth where velocity-depth data for normally compacted shale at maximum burial can be difficult to identify (2.1<z<3.8 km). This formulation is a constrained, exponential transit time-depth model that fulfils reasonable boundary conditions at the surface (1500 m/s) and at infinite depth (5405 m/s); maximum velocity-depth gradient 0.6 1/s for z=2.0 km. The shale trend given by Eq. 4-2 corresponds closely to baselines for marine shale found by other workers (Scherbaum 1982, Hansen 1996; see discussion in Japsen 1999 and in Japsen et al. 2007b.

4.3 A baseline for the Lower Triassic Bunter 'Shale'

Japsen (2000) formulated a segmented, linear baseline, V_N^{BSh}, for the Lower Triassic Bunter Shale based on velocity-depth data from 142 British and Danish wells of which 91 have velocity-depth data for the Chalk:

$$
\begin{aligned}
V_N^{BSh} &= 1550 + z \cdot 0.6, & 0 < z < 1393\,\mathrm{m} \\
V_N^{BSh} &= -400 + z \cdot 2, & 1393 < z < 2000\,\mathrm{m} \\
V_N^{BSh} &= 2600 + z \cdot 0.5, & 2000 < z < 3500\,\mathrm{m} \\
V_N^{BSh} &= 3475 + z \cdot 0.25, & 3500 < z < 5300\,\mathrm{m}
\end{aligned}
\qquad (4\text{-}3)
$$

The trend indicates a pronounced variation of the velocity gradient with depth. The gradient is only 0.5 1/sin the upper part, and increases to 1.5 1/s for depths around 2 km, from where it decreases gradually with depth to 0.5 and then 0.25 1/s. The decline of the gradient with depth reflects that velocity approaches an upper limit.

The Bunter Shale baseline was reconstructed by applying the same procedure as for the Lower Jurassic shale by correcting present formation depths for the effect of late Cenozoic erosion as estimated from Chalk velocities. The trend was constructed to predict likely values near the surface (1550 m/s), and is based on reference data with corrected depths from 1600 to 5600 m (Japsen 2000). Rather than proposing a specific baseline for the Lower Triassic Bunter Sandstone, Japsen (2000) found that the trend derived for the Bunter Shale was a reasonable approximation for a data set from 133 British and Danish wells of which 87 have velocity-depth data for the Chalk. Burial anomalies for the Bunter Sandstone can thus be used to place an upper limit on estimates of erosion based on Bunter Shale data.

The dominance of smectite/illite in the distal parts of the Fjerritslev Formation, and of kaolin in the continental Bunter Shale was suggested by Japsen (2000) to be a possible explanation why baselines for these formations diverge, and why those for Bunter Shale and Bunter Sandstone converge at depth. Alternatively, the similarity of the baselines for the Bunter Shale and the Bunter Sandstone may be due to the dominance of quartz in both formations.

4.4 A revised baseline for sandstone

Japsen et al. (2007b) found *V-z* trends for sandstone by eliminating porosity from an exponential porosity-depth relation by assuming a so-called modified Voigt relation between sonic velocity and porosity for sandstone with different clay content. The resulting modified Voigt velocity-depth model for sandstone has a *V-z* gradient that decreases monotonously from values greater than 1 s^{-1} for z<0.4 km and 30% clay content. Reduction of the clay content leads to higher velocity and velocity gradient.

If we compare the modified Voigt model with the normal trend for the Bunter Shale and Sandstone, we find that the Bunter trend plot between the sandstone models for 0% and 10% clay content for depths below *c*. 2 km. The match between the modified Voigt model and the Bunter Sandstone trend supports the application of the modified Voigt model for sandstone as well as the estimation of the amount of exhumation by means of chalk velocities (because burial anomalies based on chalk velocities were used to derive the Bunter baseline). The match between the modified Voigt model and the data points for the Bunter Shale suggests that the lithology of the Bunter Shale is dominated by quartz in the wide area covered by the data set (southern and eastern North Sea Basin). Consequently, the term ‘Shale’ seems to be an indication of grain size rather than of mineralogy.

The modified Voigt model can be approximated by a modified velocity-average equation:

$$V = V_m - (V_m - V_c)e^{-z/b} \qquad (4\text{-}4)$$

where V_m is the matrix velocity of the sediment, V_c is the sonic velocity of the sediment at critical porosity (the porosity limit above which a particular sediment exists only as a suspension) and b is a decay parameter (Nur et al. 1998). Japsen et al. (2007b) estimated the parameters in equation (4-4) as an approximation to the modified Voigt trend for z<4 km taking V_c=1600 m/s. Since that study, datasets that extend to much greater depths have become available and it is thus possible to adjust the parameters in the modified velocity-average equation (Eq. 4-4) so that they are in better agreement with velocity-depth data for very deep sandstone units:

0% clay: V_m = 5400 m/s, b_3 = 2500 m. (4-5)
5% clay: V_m = 5400 m/s, b_3 = 2800 m.

If we compare this model with the normal trend for the Bunter Shale and Sandstone, we find that the model for 5% clay corresponds to the Bunter trend. Very pure sandstone units are thus likely to plot in the interval defined by the 0 and 5% clay models.

5. Discussion of lithological indicators and identification of velocity-depth trends

Plots of the log data for each well are found in Appendix A:

- Composite plot of the caliper, sonic, density, neutron porosity (where available) and gamma logs.
- Comparison of the gamma and sonic logs for the Shetland Group.
- Plot with interpretation of burial anomaly based on a comparison of the sonic log and the baselines for chalk, shale and sandstone.

Comments to the characteristics of the log data for each well are also given in Appendix A, whereas the estimation of the burial anomaly for the drilled section in the wells is discussed in Chapter 6. Note that depths are given in round numbers in km below sea bed to facilitate references between the text and the figures.

5.1 Sonic data for the chalk of the Shetland Group

5.1.1 Identification of impure chalk based on gamma response and drop in sonic velocity

Analysis of numerous wells from the Danish sector of the central North Sea shows that the typical level for gamma readings in pure chalk in the Tor Formation is around 10 API. Impure chalk intervals in this formation may have maxima up to 20 API. Bad calibration of the gamma tool may be the reason why the same relative variations are found for chalk in other wells, only with a much higher base level. The true variation of the gamma radiation in the chalk may also be obscured by potassium content of the drilling mud. Moreover, there is a clear tendency that relatively high gamma readings correspond to a drop in sonic velocity for the chalk.

Plots of the gamma response for the chalk sections in this study show the same tendencies. For example as shown in the plots of sonic velocity and gamma vs depth for the chalk in well 8/9-1 where minimum gamma is around 10 API and maximum values are around 20 API (Figure 5-1). High gamma readings are found in an interval above the base of the chalk, between 1.7 and 1.8 km. The higher GR values correlate with a pronounced minimum for the sonic velocity for this well. Such a drop in sonic velocity in an interval above the base of the chalk corresponding to impure chalk intervals can be recognised in many wells in this study; e.g. 3/5-2, 8/9-1, 9/2-3, 9/4-1, 9/8-1, 10/8-1, 11/10-1. The minimum gamma level for the chalk in these wells is not much above 10 API, but in other wells the gamma tool seems to have been uncalibrated or erroneous, since the minimum level is much higher (than in neighbouring wells); e.g. 8/3-2, 11/10-1, or simply shows an erratic gamma pattern; e.g. 9/3-1, 9/4-4, 10/5-1, 10/7-1. In most of these cases the sonic log shows the typical drop in velocity at a level above the base of the chalk that probably is indicative of impure chalk despite the failure of the gamma log to support this interpretation.

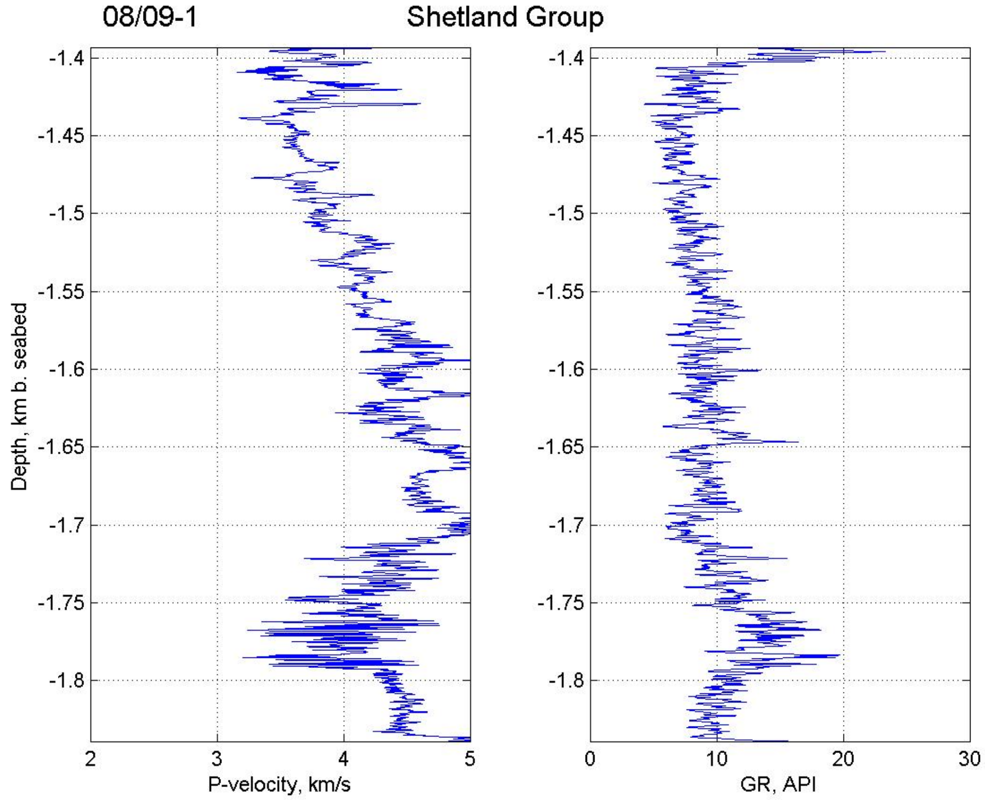

Figure 5-1. *Plot of sonic velocity and gamma vs depth for the chalk for well 8/9-1. Minimum gamma around 10 API and maximum values up to 20 API. High gamma readings are found in an interval above the base of the chalk, between 1.7 and 1.8 km. The higher GR values correlate with a pronounced minimum for the sonic velocity.*

5.1.2 Porosity-preservation in chalk on the Yme field due to hydrocarbons?

Anomalously low velocities are found in the uppermost part of the chalk below high-velocity carbonates with bryozoans, in several wells on the Yme field (Fig. 5-2). This is clearly expressed in the log data for wells 9/2-1, 9/2-2 and 9/2-4s as well as in well 25/12-1 for which mineral fluorescence in the chalk is reported in the completion log. There is no correlation between the gamma response and the low velocities in these intervals.

It is a possible explanation that these low velocities (high porosities) can be caused by the presence of hydrocarbons in the chalk at an early stage during the compaction of the chalk. Presence of hydrocarbons is known to have a porosity-preserving effect in chalk where coating of the grains with hydrocarbons prevents pressure solution of the carbonates (e.g. Fabricius et al. 2008). The above mentioned wells are located on the Yme field where generation of hydrocarbons in the Mesozoic section below the chalk has taken place.

Note that there is a clear velocity-depth trend for the low-velocity chalk in well 9/2-2 and that this trend is parallel to chalk baseline. The burial anomaly for this interval is about 100 m whereas that of the lower part of the chalk is estimated to c. 400 m. A possible interpretation of this observation is that hydrocarbon migration into the upper part of the chalk occurred when the chalk was c. 300 m less deeply buried than during maximum burial; i.e. 300 m 'prior to' maximum burial.

In some wells two factors may make identification of maximum velocities corresponding to pure chalk difficult: Porosity-preservation due to early hydrocarbon migration and impure chalk intervals where high gamma reflects increased shale content. Both factors may cause the absolute velocity-depth level for the chalk in a well to be lower than the level corresponding the theoretical level for pure chalk and thus potentially to exhumation being underestimated; e.g. wells 9/2-1 and 18/11-1.

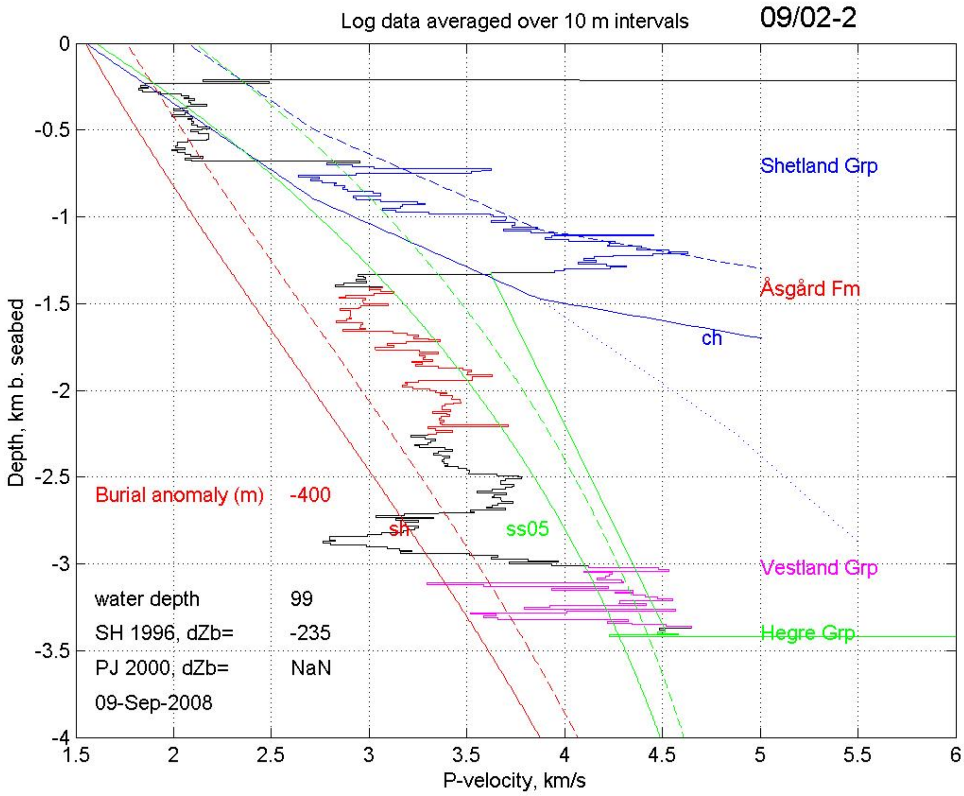

Figure 5-2. *Plot of the sonic log for well 9/2-2 illustrating the pronounced low velocities of the upper part of the chalk, 0.75-0.95 km (below the high-velocity Ekofisk Formation where bryozoans were encountered).These relatively low velocities (high porosities) may be caused by porosity-preserving effect of hydrocarbons that may have migrated into the chalk at an early stage of the compaction process (i.e. prior to maximum burial). Legend in App. A.*

5.2 Sonic data for the shales above and below the chalk

5.2.1 Velocity-depth trend for the Palaeogene shales

A well-defined velocity-depth trend can be observed for the Palaeogene shales in many wells; e.g. in well 9/4-4 where there is a general increase of velocity with depth interrupted by low-velocity excursion over thin intervals, 0.3-1.1 km below sea bed (cf. wells 8/3-2, 9/12-1, 11/10-1, 17/11-2). In some wells there are only data for a relatively thin Palaeogene shale section, but often with a clear indication of the level of the sonic velocity for these units (e.g. 17/12-1R). In some wells the sonic data reveal increasing overpressure towards the base of the Cenozoic section. A clear example of this is well 3/5-2 where the sonic log follows a clear shale trend between 0.5 and 1 km and thus indicates that this section is by normally compacted. Below 1 km, there is no general increase of velocity with depth which is indicative of overpressure build-up.

5.2.2 Log response of the Tau Formation

The Tau Formation is clearly marked in the log data by a significant drop in sonic velocity and an increase in gamma response (Fig 5-3).

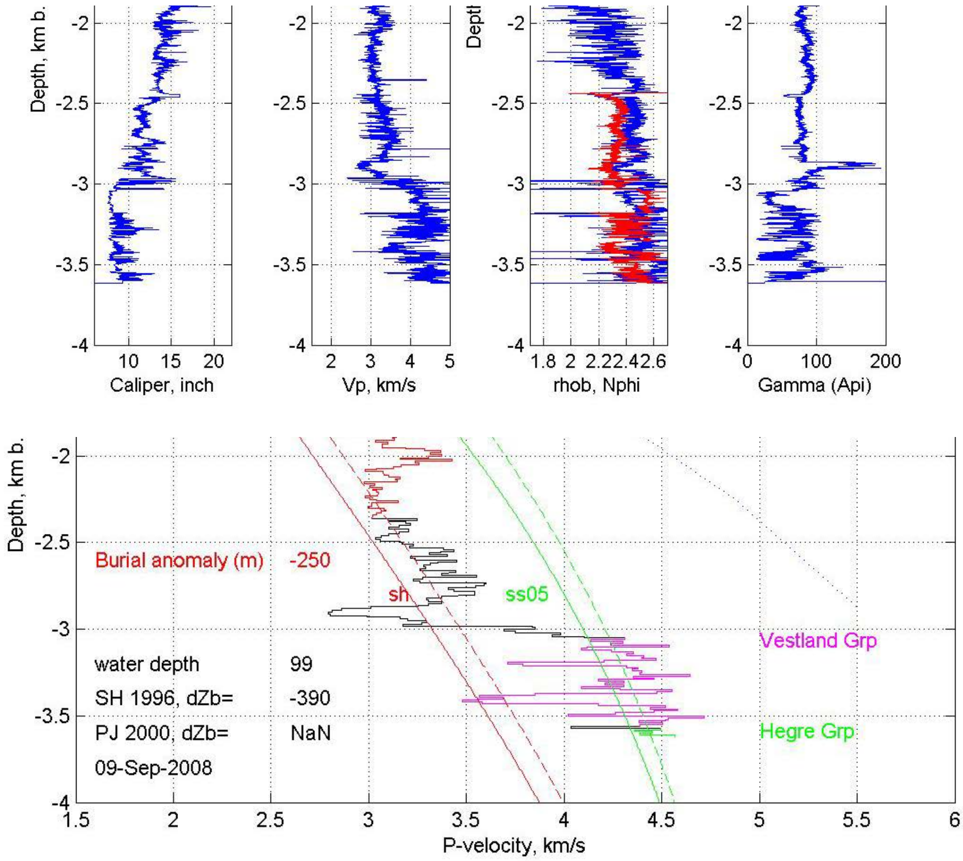

Figure 5-3. *Log response of the Tau Formation illustrated with the lower parts of the plots for well 9/2-1 in Appendix A. The Tau Formation at c. 2.9 km below sea bed is characterized by a drop in sonic velocity and a pronounced gamma peak.*

5.2.3 Velocity-depth trend for the shales below the chalk

In many of the studied wells there is no velocity-depth trend in the sonic data for the shales of the Cromer Knoll and Boknfjord Groups (above the Middle Jurassic sand-rich units of the Vestland and Hegre Groups); e.g. wells 8/1-1, 9/4-4, 10/5-1, 7-1, 8-1.

The sonic data from well 9/4-4 reveals a characteristic sonic pattern for the Lower Cretaceous interval with two pronounced peaks in the shale-dominated interval above the Vestland Group. The most shallow sonic trough corresponds to the Rødby and Sola Formations, 1.8-1.9 km and the underlying moderate peak to the Åsgård Formation. The second peak corresponds to the Flekkefjord and Sauda Formations, 2.2- 2.5 km. The deepest of the sonic troughs corresponds to the Tau Formation, c 2.5 km, for which it is to be expected that the sonic velocity plots below the shale trend in this interval. The shale baseline inferred from the chalk data in these wells is consistently found to correspond to a level just below the max values of two sonic peaks below the chalk.

There is less scatter in the sonic data for the shales below the chalk in other wells; e.g. well 8/3-2 where a level close to the upper bound for the sonic data seems to define a consistent level that lines up with the Palaeogene shale trend. In contrast to this well, the data for well 9/2-1 seem to vary around an intermediate level with pronounced peaks in the sonic log above (in the Åsgård Formation) and below (the Tau Formation) the trend (cf. 9/2-3, 9/3-1). There are no major variations in the gamma log for these intervals above the Tau Formation. Further studies will benefit from a better way of identifying shale intervals below the chalk.

5.2.4 Sonic data for Triassic–Jurassic sandstone units

Data for the sand-rich Hegre Group are only used as a secondary support for the interpretation of the burial anomalies in this study. However, for future studies it is of interest to note that the Hegre Group is thick in a number of wells, and that studies of velocity-depth data for this unit may be useful for putting limits on the possible range of the burial anomaly. The following wells penetrate formations of the Hegre Group and the details are described in the NPD publications in some cases:

10/8-1	Skagerrak Formation / Smith Bank Formation	NPD 26
11/9-1	Skagerrak Formation	
11/10-1	Skagerrak Formation	NPD 23
17/3-1	Smith Bank Formation	
17/10-1	Skagerrak Formation / Smith Bank Formation	NPD 21
17/12-1R	Skagerrak Formation	

Well 10/8-1 penetrates thick sandstone sequence of the Skagerrak Formation including a 200 m thick high-velocity unit above the base of the Skagerrak Formation, c. 2.3-2.5 km (cf. 11/9-1). According to NPD report 26 anhydrite is present throughout the basal 500 m of the Skagerrak Formation including limestone units and it is thus possible that the highest velocities in this interval reflect these lithologies. The absolute level for the sonic velocity of pure sandstone is thus not easily established and these aspects could be studied in more detail.

6. Estimation of burial anomalies

6.1 Quantitative estimation

The burial anomalies are estimated qualitatively for the Mesozoic–Palaeogene succession in each well and they are primarily based on a comparison between (1) the sonic data for the chalk of the Shetland Group and the chalk baseline (Eq. 4-1) and (2) the sonic data for the Palaeogene shales and the shale baseline (Eq. 4-2). Furthermore, the interpretation may be supported by a comparison between the sonic data below the chalk and the shale baseline; typically in the interval above the Tau Formation. Finally, a comparison is made between the sonic data for Triassic-Jurassic sandstone intervals and the baseline for relatively pure sandstone (5% clay, Eq. 4-5).

The qualitative estimation of the burial anomaly is based on depth-shifting all three baselines by the same amount until a match is obtained with the data for the intervals of the identified lithologies that are considered more reliable; typically the chalk and the Palaeogene shale. The match is primarily based on the absolute level of the sonic velocities in these intervals, but also on identification of velocity-depth trends for these intervals. The benefit of this qualitative approach is that whereas the velocity-depth trend for one of the above mentioned intervals may be difficult to identify, the comparison of sonic data for two or more lithologies with their respective baselines effectively limits the range of the possible burial anomalies. This is clearly illustrated by the interpretation of well 9/8-1 shown in Fig. 6-1.

6.2 Results

The estimated burial anomalies and their range of uncertainty is given in Table 6-1. The results are shown on a map in Figure 6-2. that reveals a consistent trend of negative anomalies (indicating exhumation) increasing in magnitude in direction of the Norwegian coast (not shown!) and a narrow belt of burial anomalies near 0 m (indicating maximum burial) towards the central North Sea where overpressure is reflected in positive anomalies in one well shown on the map and in one well south of the map limit (3/5-2).

For 20 wells the Mesozoic-Palaeogene succession is found to have been more deeply buried. The maximum burial anomaly is estimated to 2500 m for a well drilled on a salt structure, but this is not very well constrained because only data for the Hegre Group is penetrated by this well. Burial anomalies for the other wells range from -200 and -700 m with maximum values in Block 9 of -600 m (well 9/3-1) and -700 m in Block 10 (well 10/7-1).

For 9 wells the Mesozoic-Palaeogene succession is found to be near maximum burial (absolute value of the burial anomaly equal to or less than 150 m) whereas the succession was found to be overpressured in two wells.

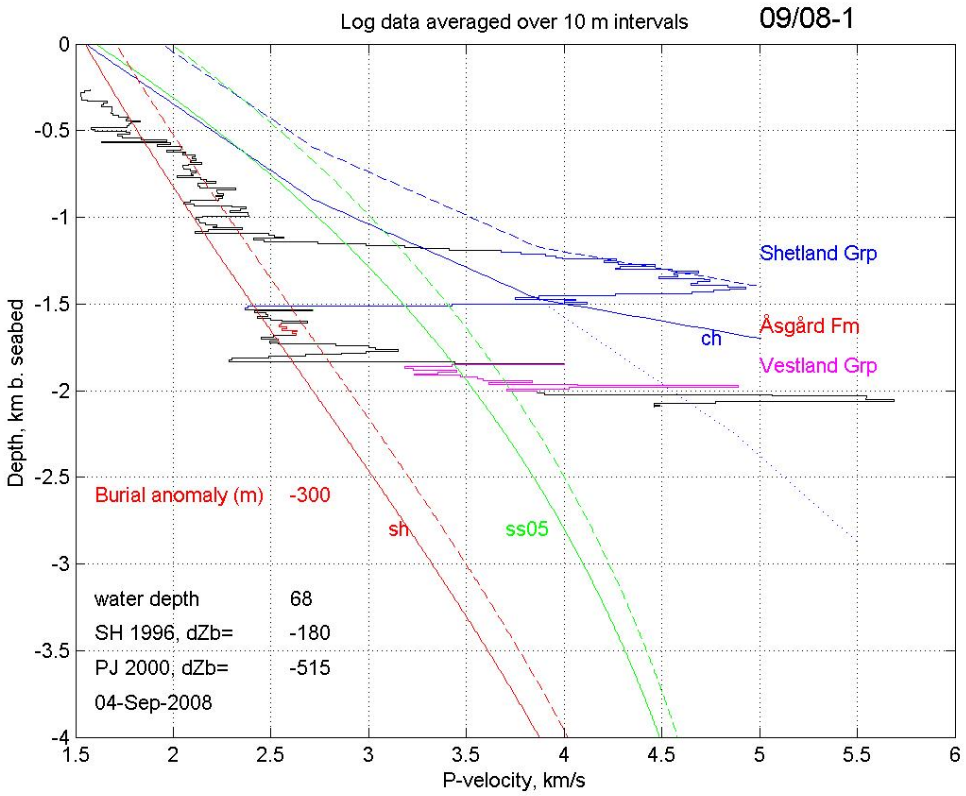

Figure 6-1. *Plot of the sonic log for well 9/8-1 compared to baselines for three lithologies and to the baselines shifted by a burial anomaly of -300 m (legend see Appendix A). The chosen value of the burial anomaly is based on the good agreement between the sonic data for the Paleogene shale and for the Upper Cretaceous-Danian chalk and the respective baselines. The match is primarily based on the absolute level of the sonic velocities in these intervals, but also on identification of velocity-depth trends for these intervals. The interpretation is supported by the sonic data for the shales of the Åsgård Formation and in agreement with the sonic data for the sandstone of Vestland Group, 1.8-2.0 km (disregarding the high-velocity peak).*

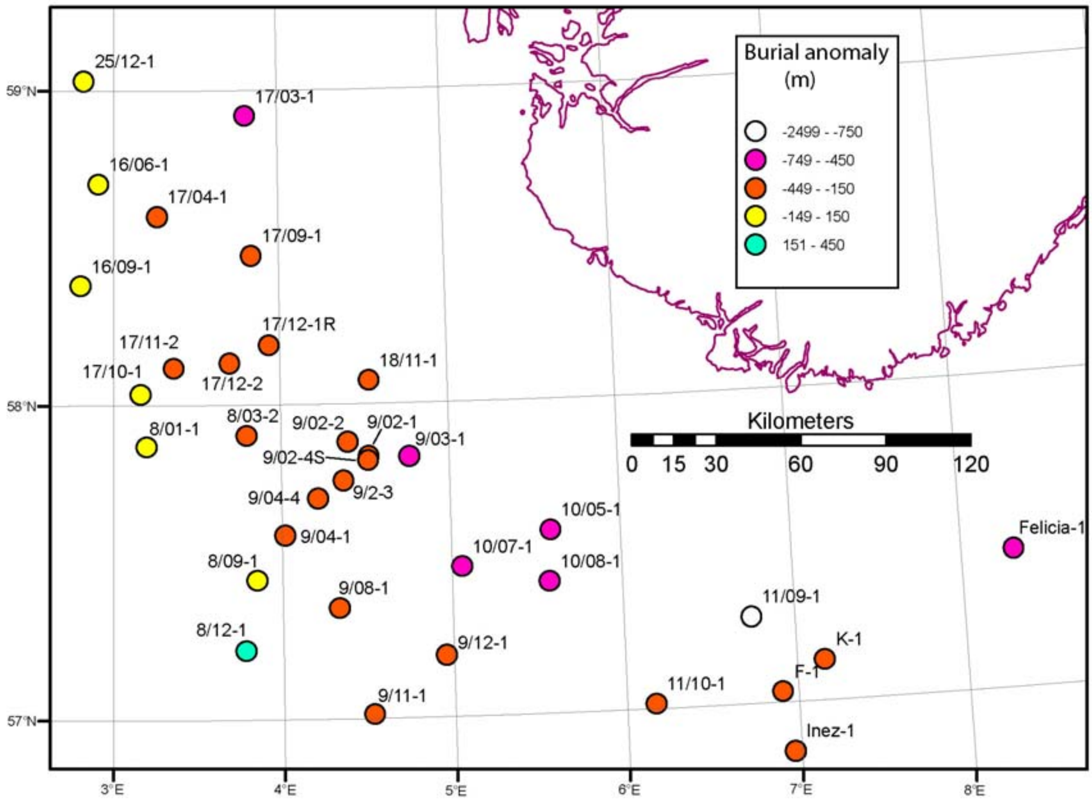

Figure 6-2. *Map of the estimated burial anomalies based on Norwegian wells investigated in this report together with results from Danish wells (Japsen & Bidstrup 1999; Japsen et al. 2007a).*

Table 6-1. *Estimation of the burial anomaly for the drilled section in individual wells. The estimate is based on comparison between the normal velocity-depth trends for shale, chalk and sandstone and sonic log data for the relevant intervals. Depths below sea bed.*

Well	Burial anomaly (m)	Estimate based on	Shale	Chalk	Sandstone
03/05-02	1000 ±200 Overpressure	Interpretation based on chalk data, but broadly consistent with data for the basal part of the Palaeogene shales.	Shale trend not defined in the overpressured section below 1.2 km, but normal compaction defined fairly well above, 0.4-1.2 km.	Chalk trend defined by upper bound (high-velocity Ekofisk Fm). Chalk clearly overpressured.	The data for the Hegre Group supports the interpretation
08/01-01	100 ±100 Near max burial	Interpretation based on chalk data and supported by data for the Palaeogene shales.	Shale trend loosely defined by the data for the Palaeogene section, but not the absolute level (within 200 m).	Chalk trend defined by uniform increase, 1.5-1.7 km.	The data for the Hegre Group supports the interpretation
08/03-02	-200 ±100 Exhumation	Good agreement between shale and chalk trend	Well-defined level for the Palaeogene shale trend, 0.4-0.8 km, that lines up with the upper bound for the Åsgård Fm.	Well-defined upper bound, 1.0-1.4 km	-
08/09-01	0 ±100 Near max burial	Mainly based on chalk trend	Significant variations above the chalk. Ffit with shale trend, 0.3-0.5 km.	Chalk trend well-defined by upper bound between 1.5 and 1.7 km	-
08/12-01	300 ±200 Overpressure	Agreement between chalk trend and shale data above the chalk.	Shale trend defined by lower bound for intervals above and below chalk. Normal compaction, 0.5-1.0 km. Velocity inversion below 1.2 km indicative of overpressure.	Chalk trend defined by upper bound over narrow interval, 1.8-1.9 km. Velocity-depth level clearly indicative for overpressuring.	The upper bound for the Vestland and Hegre Groups supports the interpretation.
09/02-01	-250 ±200 Exhumation	Agreement between the chalk trend and the shale trend. Exhumation could be underestimated.	Shale trend defined by the lower bound for the section between the chalk and the Tau Fm, 2.1-2.8 km.	Chalk trend defined by the data for the lower part of the chalk, 1.1-1.3 km.	The mean level of upper bound for the Vestland Group supports the interpretation.
09/02-02	-400 ±200 Exhumation	Shale trend is 200 m more shallow than chalk trend (preferred).	Shale trend below (?) the lower bound for the section between the chalk and the Tau Fm and the average level for Palaeogene shales.	Chalk trend well defined by the upper bound between 1.0 and 1.2 km.	The upper bound for the Vestland Group supports the interpretation.
09/02-03	-250 ±200 Exhumation	Agreement between the chosen shale and chalk trends.	Shale trend chosen near lower bound for the section between the chalk and the Tau Fm (Åsgård Fm) (disregarding velocity inversion below 2.5 km).	Chalk trend difficult to define, trend chosen close the upper bound.	The upper bound for the Vestland Group supports the interpretation.

Well	Burial anomaly (m)	Estimate based on	Shale	Chalk	Sandstone
09/02-4s	-300 ±200 Exhumation	Agreement between the chosen shale and chalk trends.	Shale trend defined by lower bound for the section below the chalk, 1.5-2.5 km.	Chalk trend loosely defined by the upper data bound (Ekofisk Fm and thin unit at 1 km).	-
09/03-01	-600 ±200 Exhumation	Agreement between the chosen shale and chalk trends.	Shale trend defined by lower bound for the section below the chalk, 0.7-1.5 km, in agreement with the upper bound for the Palaeogene shales.	Chalk trend defined by upper data bound (disregarding sharp velocity peak), 0.4-0.6 km.	The upper bound for the Vestland Group supports the interpretation.
09/04-01	-150 ±100 Near max burial	Good agreement between chalk trend and shale data above the chalk	Well-defined trend, 0.5-0,7 km. Low velocities at 1 km may be due to overpressure. Velocities for Åsgård Fm agrees with the interpretation.	Well-defined upper bound, 1.3-1.5 km.	Max. velocities for Hegre Group agrees with interpretation.
09/04-04	-200 ±100 Exhumation	Good agreement between shale and chalk trend	Well-defined level of shale velocities, 0.2-1.0 km, above the chalk. The trend lines up with values for the Åsgård Fm.	Upper bound (1.2-1.5 km) defines general trend.	-
09/08-01	-300 ±100 Exhumation	Good agreement between shale and chalk trend	Well-defined level of shale velocities, 0.5-1.0 km, above the chalk that matches the sonic data for the Åsgård Fm. Marked drop in velocity above 0.5 km	Well-defined upper bound, 1.2-1.4 km	-
09/11-01	-250 ±200 Exhumation	Based on the trend for the Palaeogene shales.	Well-defined shale trend above the chalk, 0.6-1.3 km. Scattered data below the chalk. Data for the Åsgård Fm lines up with the trend for the Palaeogene shales.	Very thin chalk section, 137 m. Maximum velocities plot on chalk trend indicating maximum burial, But the section is probably too thin to give reasonable data.	-
09/12-01	-350 ±100 Exhumation	Good agreement between shale and chalk trend	Well-defined trend above the chalk (0.3-1 km) supported by intervals below (at c. 1.7 km)	Upper bound defined between 1.1 and 1.3 km	Scattered sonic pattern for Hegre Group. Overall level in agreement with the interpretation.
10/05-01	-500 ±100 Exhumation	Primarily based on the chalk trend. Supported by data above and below the chalk	No trend defined, but data above and below the chalk line up.	Upper bound defined over thick chalk section, 0.2-0.9 km. Well-defined within some scatter.	-
10/07-01	-700 ±200 Exhumation	Based on the chalk data. Exhumation could be overestimated.	No trend defined. The baseline inferred from the chalk data corresponds to a level below the max values of two peaks below the chalk.	Level of the chalk trend not well defined, but chosen as typical velocity values around 0.8 km.	-

Well	Burial anomaly (m)	Estimate based on	Shale	Chalk	Sandstone
10/08-01	-600 ±250 Exhumation	Based on a combination of data for shale and chalk.	No shale trend identified. The baseline inferred from the chalk data corresponds to a level below the max values of the sonic peak below the chalk.	Large velocity variations over thin chalk intervals and partly erroneous data. Chalk trend is defined by the upper bound around 0.7 km.	Uniform high velocities in the lower part of the Hegre Group, 2.2-2.5 km.
11/09-01	c. -2500 ±500 Exhumation	Assuming that the velocity maximum is affected by anhydrite and that a level below the maximum reflects pure sand unit. Drilled on a salt structure, not representative for the regional level of exhumation.	No shale identified	No chalk section	Only Hegre Group penetrated. Uniform velocity maximum, 1.2-1.4 km, coincides with gamma low indicative for both pure sandstone and anhydrite
11/10-01	-350 ±200 Exhumation	Primarily based on the Palaeogene shale trend and not well supported by the chalk data. In agreement with the Hegre data.	Well defined trend for the Palaeogene shales, 0.5-0.9 km; lines up with Åsgård Fm.	No chalk trend defined by the data. Level for the chalk data chosen to be high-velocity peak matching low gamma response.	High velocities over thick Hegre Group, 1.8-2.3 km.
16/06-01	-100 ±200 Near max burial	Reasonable agreement between results based on Palaeogene shale and chalk data. Estimate primarily dictated by chalk data that define a slightly minor magnitude of the burial anomaly than the section below the chalk.	Trend defined by increasing velocities in the Palaeogene shales, 0.3-0.7 km. This trend lines up with minimum velocities for the section below the chalk, c. 1.7 km.	Upper bound defined over thin section, 1.2-1.4 km	-
16/09-01	0 ±150 Near max burial	Primarily based on the chalk trend, but in agreement with the Palaeogene shales.	No clear shale trend. Roughly constant velocity in the Palaeogene shales, 0.4-1.3 km, probably indication of slight overpressure above the chalk. Large velocity variations in the section below the chalk.	Trend defined by upper bound for the upper part of the chalk, 1.3-1.4 km, coincides with the normal trend for chalk.	Thick Hegre Group. The interpretation is in agreement with the Hegre data.

Well	Burial anomaly (m)	Estimate based on	Shale	Chalk	Sandstone
17/03-01	-500 ±100 Exhumation	Good agreement between chalk and shale data.	Shale trend defined below the chalk, 1.1-1.9 km, with some scatter. No data above the chalk.	Chalk trend well defined by upper bound, 0.7-1.0 km.	High velocities for the Hegre Group, 2.3-2.4 km.
17/04-01	-150 ±150 Near max burial	Good agreement between chalk and shale data.	Shale trend defined by upper bound for lower part of Palaeogene shales, 0.5-1.1 km, and for the section between the chalk and the Vestland Group, 1.3-2.2 km	Chalk trend broadly defined by upper bound, 1.1-1.25 km.	Hegre Group data supports the interpretation.
17/09-01	-400 ±150 Exhumation	Good agreement between chalk and shale trends.	Shale trend defined by upper bound for the Palaeogene shales, 0.2-0.5 km, and for section between the chalk and the Vestland Group, 1.0-2.1 km, disregarding peak velocity for Åsgård Fm	Chalk trend broadly defined by upper bound following data for Ekofisk Fm and high-velocity chalk between 0.7 and 0.9 km.	-
17/10-01	0 ±150 Near max burial	Agreement between shale and chalk trends.	Scattered sonic log pattern above and below the chalk. Overall trend loosely defined.	Upper bound defined, 0.9-1.1 km.	High velocities in lower part of the Hegre Group, 3.3-3.4 km supports the interpretation.
17/11-02	-150 ±100 Near max burial	Good agreement between shale and chalk trends.	Shale trend defined by upper bound for Palaeogene shales data, 0.3-0.8 km. This trend corresponds to intermediate sonic values in the section between the chalk and Tau Fm, 1.7-2.3 km	Chalk trend well defined by upper bound, 1.25-1.45 km.	-
17/12-1R	-400 ±150 Exhumation	Agreement between chalk and shale trend.	Shale trend defined by limited data for the Palaeogene section, 0.4-0.6 km, and intermediate sonic values above Tau Fm.	Chalk trend defined by upper bound over the deeper part of the chalk, 0.8-1.0 km	The upper bound for the Hegre Group supports the interpretation (disregarding peaks).
17/12-2	-250 ±100 Exhumation	Good agreement between chalk and shale trend.	Shale trend well defined by upper bound for Palaeogene shales. Supported by intermediate values in section between the chalk and the Vestland Group.	Chalk trend well defined by upper bound, 1.0-1.24 km.	-
18/10-01	-	Erroneous log data			
18/11-01	-400 ±200 Exhumation	Agreement btw shale and chalk trends. Shale trend may be too deep, if so chalk level is masked due to porosity preser-	Level for shale trend defined by lower bound for section below the chalk.	Chalk trend poorly defined by upper bound determined by Ekofisk and basal chalk peaks.	The upper bound for the Vestland Group supports the interpretation.

Well	Burial anomaly (m)	Estimate based on	Shale	Chalk	Sandstone
		vation			
25/12-1	100 ±200 Near max burial	Overall agreement between the chalk and shale trend, but no well-defined solution.	Intermediate trend for Palaeogene shales above 1.0 km defines normal compaction, above velocity inversion due to overpressure.	Chalk trend defined by thin interval, 1.43-1.5 km.	(High velocities in sandstone of ?Devonian age, 2.3-2.5 km, possibly due to km-scale exhumation during pre-mid Jurassic times)

6.3 Comparison with previous studies

Hansen (1996) estimated burial anomalies for Norwegian offshore wells based on sonic data for shale intervals by comparing the data with a normal velocity-depth trend for shale which is very close to trend applied in this study; for depth less than 2.4 km the two trends are less than 100 m apart, but the difference increases with depth and is 800 m for a shale velocity of 4 km/s. The overlap between this study and that of Hansen (1996) consists of 18 wells as indicated on the plots in Appendix A. A comparison of the results of Hansen (1996) with those of this study shows that the mean difference between the results of the two studies is 160 m which means that this study finds burial anomalies that are 160 m less that Hansen (1996) did and thus indicating less exhumation or more overpressuring (Table 6-2). The main cause for the difference is probably in the identification of the shale intervals and on the integration with chalk sonic data in this study (e.g. well 8/12-1 where the chalk data clearly indicate minor overpressure whereas data for the shale intervals are more indicative of the present depth being close to maximum burial).

Japsen (2000) estimated burial anomalies for Norwegian offshore wells based on interval velocities for chalk of the Shetland Group by comparing the interval velocity with a normal velocity-depth trend for chalk which is almost identical to the trend applied in this study for velocities less than 4 km/s. For higher velocities, the difference can be significant; e.g. 500 m for a velocity of 4.7 km/s (se section 4.2). The overlap between this study and that of Japsen (2000) consists of 17 wells as indicated on the plots in Appendix A. A comparison of the results shows that the mean difference between the results of the two studies is 38 m which means that the results from two studies finds are broadly identical (Table 6-2). The similarity of the results are of cause not so surprising because they are based both based on chalk data and on almost the same chalk baseline. However, two differences appear to have effects that cancel each other: The more shallow baseline for higher velocities tend to reduce the estimated exhumation (increase in estimated overpressure; e.g. well 3/5-2) whereas the use of chalk trends defined by the upper bound for the sonic data tend to increase the estimated amount of exhumation compared to estimates based on interval velocities.

Table 6-2. *Comparison between the results of this study with those of previous studies.*

	Number of overlapping wells	Lithology	Correlation with results in this study	Mean difference (m)*	Max difference (m) / well	Min difference (m) / well
Hansen (1996) **	18	Shale	0.71	160	300 8/12-1	-223 10/7-1
Japsen (2000)	17	Chalk	0.94	38	245 3/5-2	-350 10/7-1

* Difference between present study and previous study (positive numbers: less exhumation or more overpressure estimated in the present study)
** Including wells assumed to be normally compacted.

7. Suggested future work

The interpretation of maximum burial depth for the Mesozoic and Palaeogene sediments in the wells studies is mainly based on the sonic data for the chalk of the Shetland Group, the Palaeogene shales (where present) and to some degree on the Lower Cretaceous shales. A better understanding of the causes of the sometimes pronounced velocity variations of the shales below the chalk would improve the interpretation of which intervals that can be identified as representing uniform shale. Furthermore, the deeper intervals of sand-rich sediments of Jurassic and Triassic age need to be studied in more detail for a reliable identification of intervals dominated by relatively pure shale and sandstone lithologies. Here it is important to be able to discriminate if sonic velocities in such intervals are affected by e.g. presence of anhydrite. A further investigation of the well data available in this study will benefit from the well-defined velocity-depth relations for the Palaeogene shales and the Upper Cretaceous chalks and this may be of importance in future studies in areas where e.g. the chalk of the Shetland Group is not present.

8. References

Al-Chalabi, M. & Rosenkranz, P.L. 2002. Velocity-depth and time-depth relationships for a decompacted uplifted unit. *Geophysical Prospecting* **50**, 661–664.

Bulat, J. & Stoker, S.J. 1987. Uplift determination from interval velocity studies, UK, southern North Sea. In: *Petroleum geology of north west Europe* (Ed. by J. Brooks and K.W. Glennie), pp. 293–305, Graham & Trotman.

Chapman, R.E. 1983. *Petroleum geology*. Elsevier, Amsterdam.

Corcoran, D.V. & Doré, A.G. 2005. A review of techniques for the estimation of magnitude and timing of exhumation in offshore basins. *Earth-Science Reviews* **72**, 129–168.

Fabricius, I.L., Gommesen, L., Krogsbøll, A. & Olsen, D. 2008. Chalk porosity and sonic velocity versus burial depth: Influence of fluid pressure, hydrocarbons, and mineralogy. *AAPG Bulletin* **92**, 201-223.

Hansen, S. 1996. Quantification of net uplift and erosion on the Norwegian Shelf south of 66ºN from sonic transit times of shale. *Norsk Geologisk Tidsskrift* **76**, 245–252.

Heasler, H.P. & Kharitonova, N.A. 1996. Analysis of sonic well logs applied to erosion estimates in the Bighorn Basin, Wyoming. *AAPG Bulletin* **80**, 630–646.

Hillis, R.R. 1995. Quantification of Tertiary exhumation in the United Kingdom southern North Sea using sonic velocity data. AAPG Bulletin **79**, 130–152.

Japsen, P. 1993. Influence of lithology and Neogene uplift on seismic velocities in Denmark; implications for depth conversion of maps. AAPG Bulletin **77**, 194–211.

Japsen, P. 1998. Regional velocity-depth anomalies, North Sea Chalk: a record of overpressure and Neogene uplift and erosion. AAPG Bulletin **82**, 2031–2074.

Japsen 1999. Overpressured Cenozoic shale mapped from velocity anomalies relative to a baseline for marine shale, North Sea. *Petroleum Geoscience* **5**, 321–336.

Japsen 2000. Investigation of multi-phase erosion using reconstructed shale trends based on sonic data. Sole Pit axis, North Sea. *Global and Planetary Change* **24**, 189–210.

Japsen, P. & Bidstrup, T. 1999. Quantification of late Cenozoic erosion in Denmark based on sonic data and basin modelling. *Bull Geol. Soc. Denm*. **46**, 79–99.

Japsen, P., Green, P.F., Nielsen, L.H., Rasmussen, E.S. & Bidstrup, T. 2007a. Mesozoic-Cenozoic exhumation in the eastern North Sea Basin: a multi-disciplinary study based on palaeo-thermal, palaeo-burial, stratigraphic and seismic data. *Basin Research* **19**, 451–490.

Japsen,P., Mavko,G., Gommesen,L., Fabricius,I.L., Jakobsen,F., Vejbæk,O.V., Rasmussen,R. & Schiøtt,C.R. 2005. Chalk background velocity: Influence of effective stress and texture. EAGE 67th Conference & Exhibition - Madrid, Spain, 13 - 16 June 2005. 4 pp

Japsen, P., Mukerji, T. & Mavko, G. 2007b. Constraints on velocity-depth trends from rock physics models. *Geophysical Prospecting* **55**, 135–154.

Magara, K. 1976. Thickness of removed sedimentary rocks, paleopore pressure, and paleotemperature, southwestern part of Western Canada Basin. *AAPG Bulletin* **60**, 554–565.

Marie, J.P.P. 1975. Rotliegendes stratigraphy and diagenesis. In: *Petroleum and the continental shelf of north-west Europe* (Ed. by A.W. Woodland), pp. 205–211. Applied Science, London.

NPD paper no. 9 by R.C. Olsen (1977): Lithology. Well 16/6-1. 15 pp.

NPD paper no. 11 by S. Frodesen (1977): Lithology. Well 16/9-1. 21 pp.

NPD paper no. 14 by R.C. Olsen (1978): Lithology. Well 17/4-1. 26 pp.
NPD paper no. 21 by R.C. Olsen (1979): Lithology. Well 17/10-1. 17 pp.
NPD paper no. 23 by I. F. Strass (1979): Lithology. Well 11/10-1. 17 pp.
NPD paper no. 26 by I. F. Strass (1980): Lithology. Well 10/8-1. 17 pp.
NPD paper no. 27 by R.C. Olsen (1980): Lithology. Well 9/12-1. 18 pp.
Nur, A., Mavko, G., Dvorkin, J. & Galmundi, D. 1998. Critical porosity; a key to relating physical properties to porosity in rocks. *Leading Edge* **17**, 357–362.
Osborne, M.J. & Swarbrick, R.E. 1997. Mechanisms for generating overpressure in sedimentary basins. A reevaluation. *American Association of Petroleum Geologists Bulletin* **81**, 1023–1041.
Scherbaum, F. 1982. Seismic velocities in sedimentary rocks; indicators of subsidence and uplift. *Geologische Rundschau* **71**, 519–536.
Urmos, J., Wilkens, R.H., Bassinot, F., Lyle, M., Marsters, J.C., Mayer, L.A. and Mosher, D.C. 1993. Laboratory and well-log velocity and density measurements from the Ontong Java Plateau: New in-situ corrections to laboratory data for pelagic carbonates, *in* W.H. Berger, L.W. Kroenke, L.A. Mayer and T.R. Janecek, Proceedings of the Ocean Drilling Program. Scientific results: College Station, TX, Ocean Drilling Program, v. 130, p. 607-622.

Appendix A – Plots and comments to log data

Legend

Depths given in km below sea bed, also in comments where rough depths are indicated for reference in the diagrams. Depth are displayed as negative numbers in order to produce plots where depth increases downwards, but in the calculations of burial anomalies depth is considered to increase in that direction.

Ltihostratigraphic units according to Well Data Summary Sheets at www.npd.no.

Log plots (left hand plots)

Vp, P-velocity: Sonic p-wave velocities
rhob: Bulk density (blue curve)
Nphi: Neutron porosity converted to limestone densities, -1.6667*nphi + 2.71 (red curve)

Plot with interpretation of burial anomaly (right hand plot)

Selected lithostratigraphic units are indicated in the diagram with a colour corresponding to the colouring of that part of the sonic log.

ch – baseline for chalk; full blue line, modified 2008 based on Japsen (2000) (dotted line)
sh – baseline for shale; full red line (Japsen 2000)
ss05 – baseline for sandstone with 5% shale (Japsen et al. 2007, slightly modified 2008)

Dashed line – baseline for respective lithology shifted vertically by the burial anomaly to fit the data trend:

Burial anomaly >0 indicative of overpressure
Burial anomaly =0 normal compaction
Burial anomaly <0 indicative of exhumation

Exhumation = Reburial – burial anomaly

SH 1996 – burial anomaly estimated for shale data (Hansen 1996)
PJ 2000 - burial anomaly estimated for chalk data (based on the chalk trend of Japsen 2000)

NaN – missing value

negative anomaly – upwards, positive anomaly – downwards.

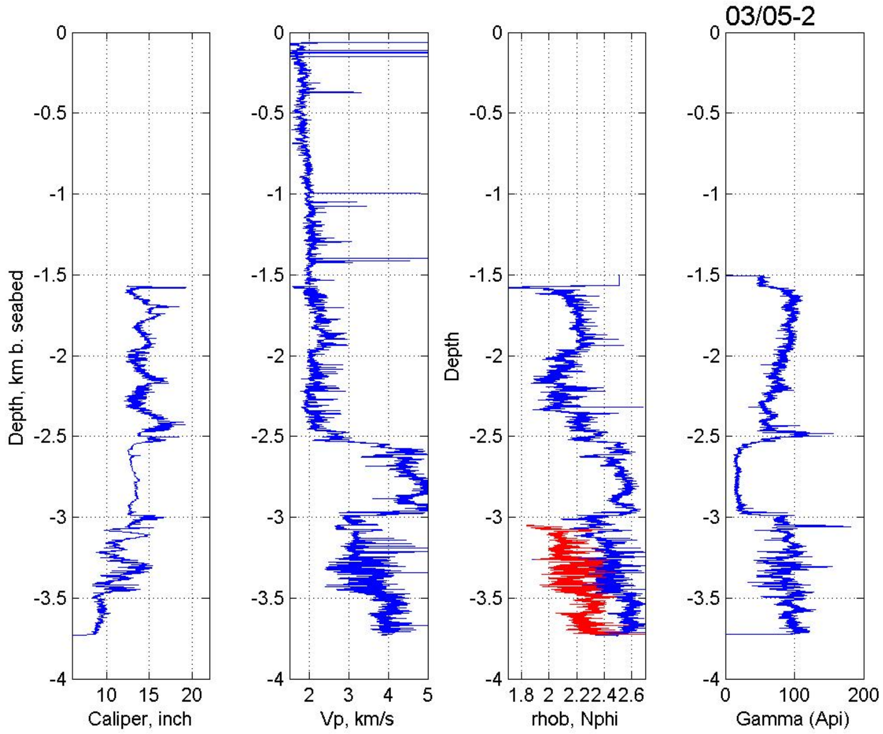
03/05-2
Depth, km b. seabed
Caliper, inch
Vp, km/s
Depth
rhob, Nphi
Gamma (Api)

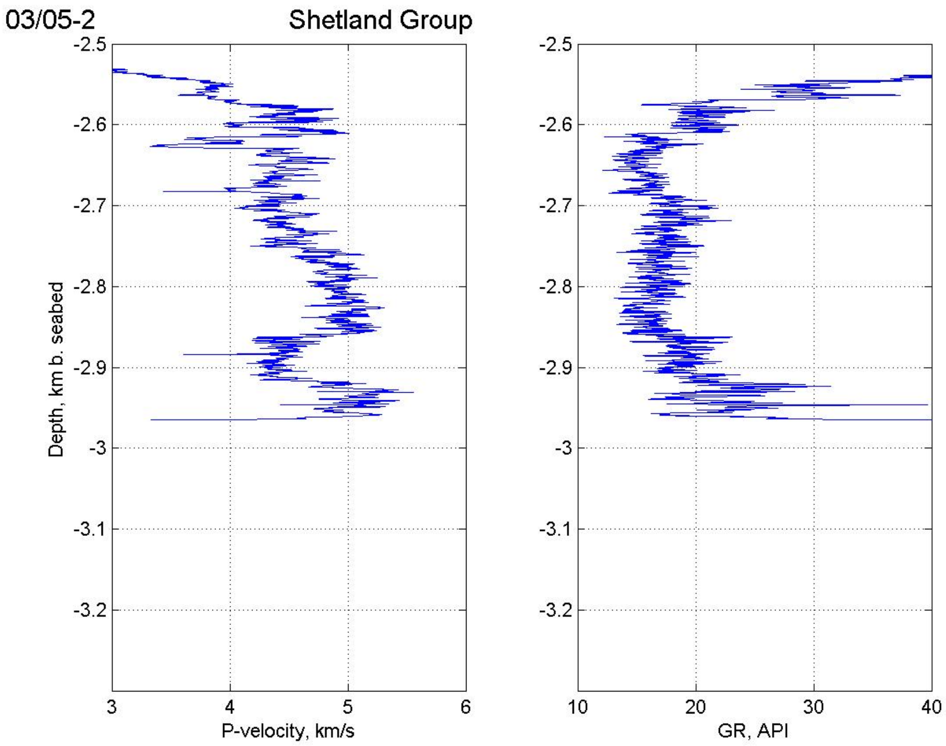
03/05-2
Shetland Group
Depth, km b. seabed
P-velocity, km/s
GR, API

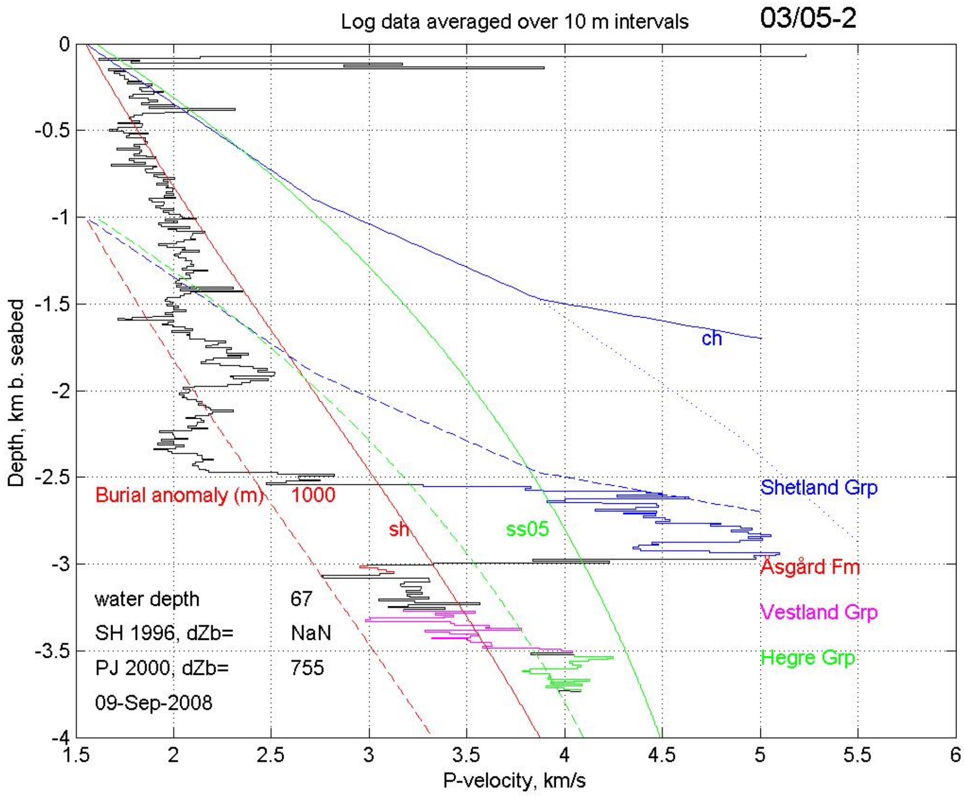

03/05-2

Post-chalk: Normal compaction above 1 km defined by well-defined shale trend, 0.5-1.0 km. No general increase of velocity below 1 km indicative of overpressure build-up.

Chalk: High-velocity Ekofisk Fm corresponding to high gamma (Top Ekofisk probably too shallow, more likely at 2.56 km below very high gamma peak). Low velocity at c. 2.9 km corresponding to high gamma, high-velocity unit below that level also corresponds to high gamma chalk. Pronounced increase of velocity between these levels. Overall low velocities relative to depth indicative of pronounced overpressure.

Pre-chalk: Rapid velocity variations above the Hegre Group, 3.0-3.5 km.

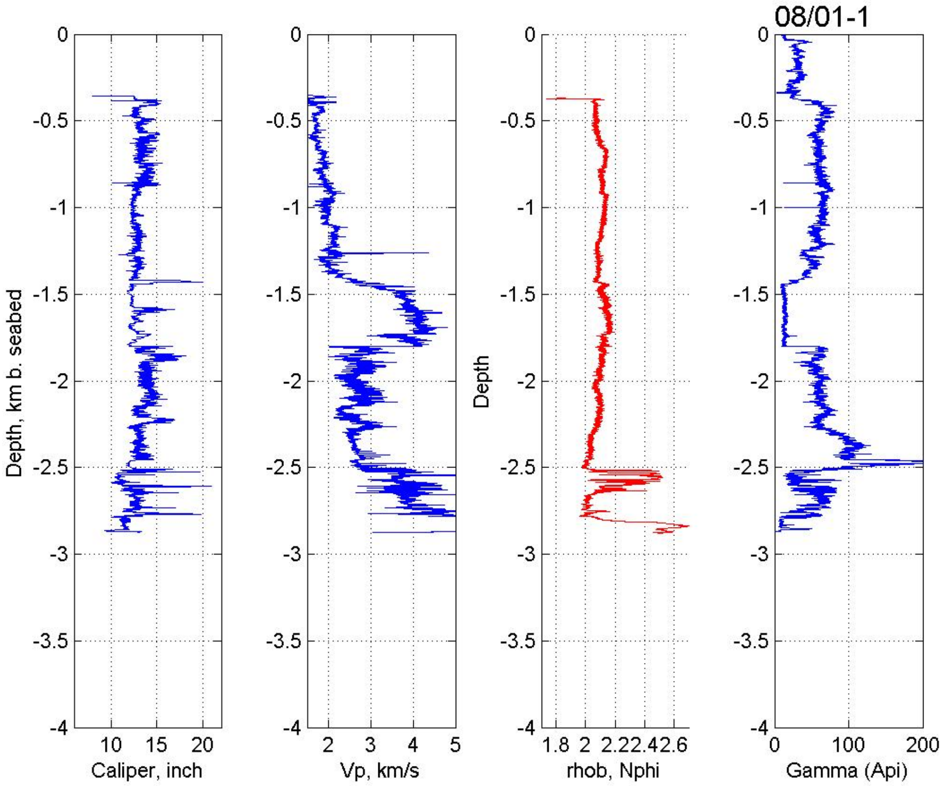
08/01-1
Depth, km b. seabed
Caliper, inch
Vp, km/s
Depth
rhob, Nphi
Gamma (Api)

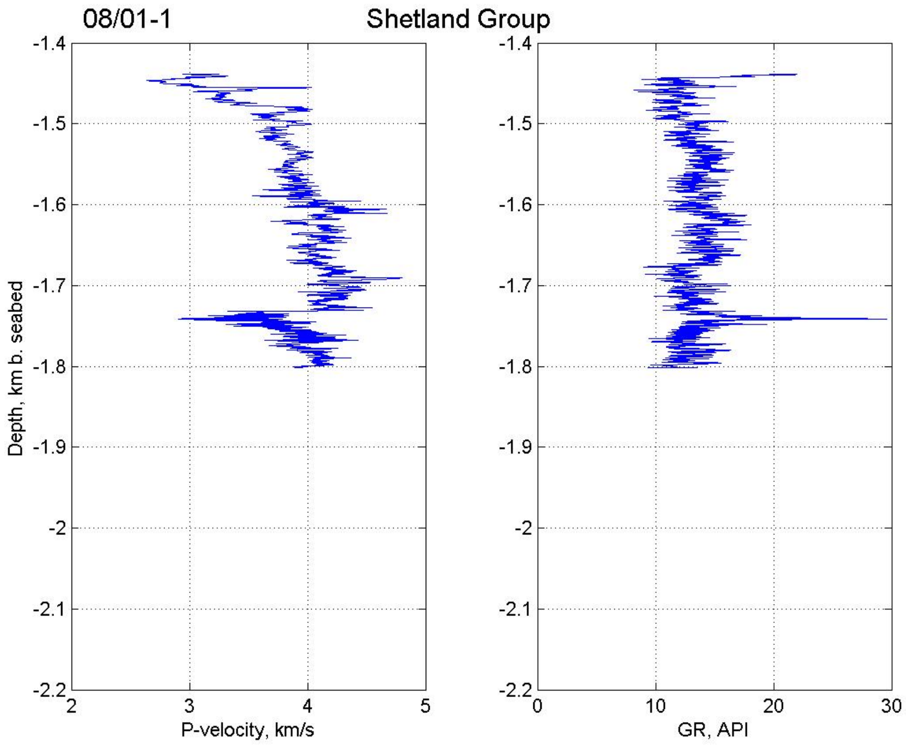
08/01-1
Shetland Group
Depth, km b. seabed
P-velocity, km/s
GR, API

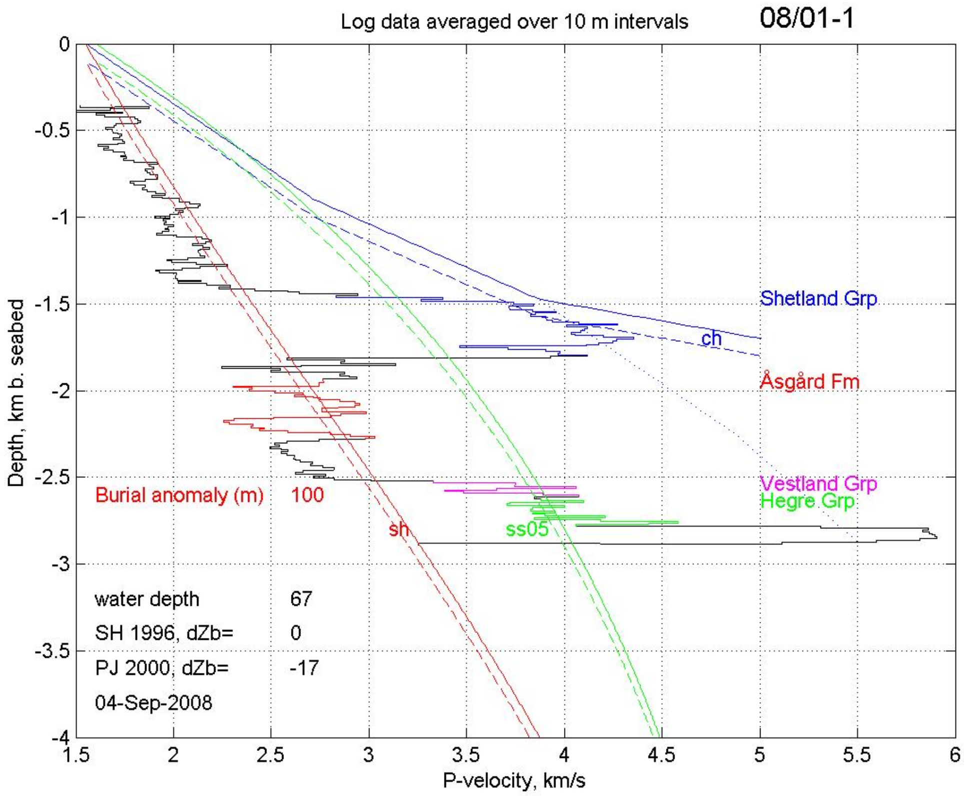

08/01-1

Post-chalk: Minor sonic variations superimposed on general increase of velocity with depth. Upper bound corresponds to shale baseline.

Chalk: General increase of velocity with depth (1.5-1.75 km), small gamma variations.

Pre-chalk: Rapid, major sonic variations above Vestland Group, 1.8-2.5 km. No trend defined.

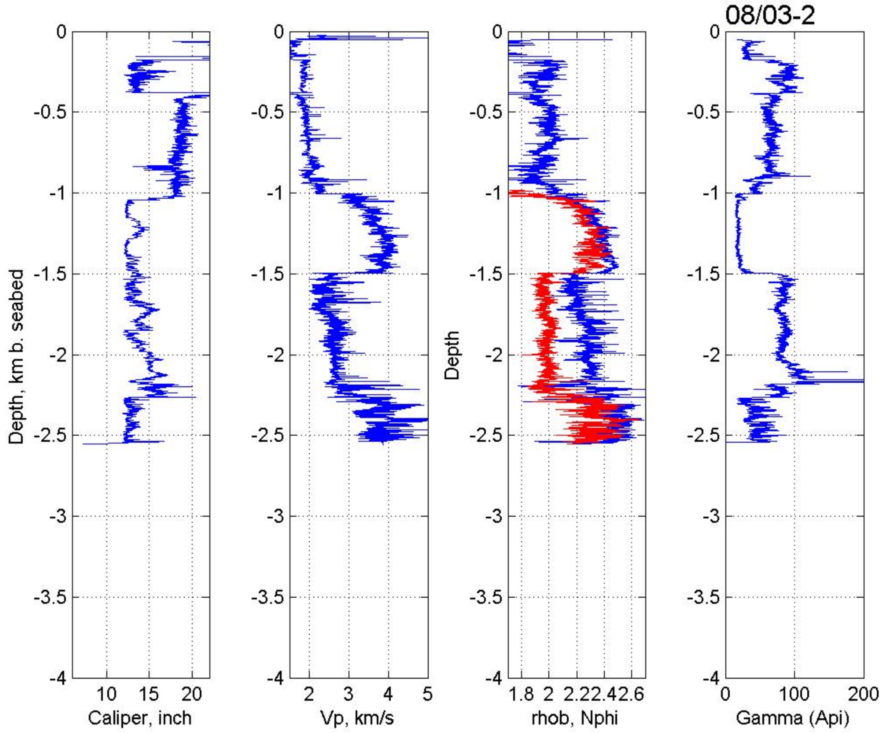
08/03-2
Depth, km b. seabed
Caliper, inch
Vp, km/s
Depth
rhob, Nphi
Gamma (Api)

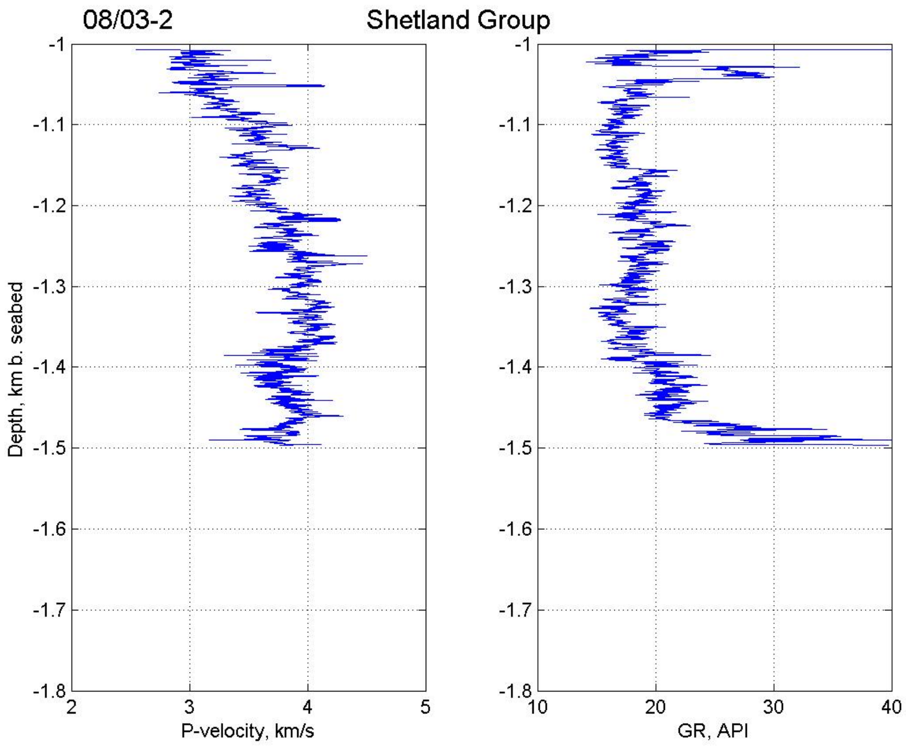
08/03-2
Shetland Group
Depth, km b. seabed
P-velocity, km/s
GR, API

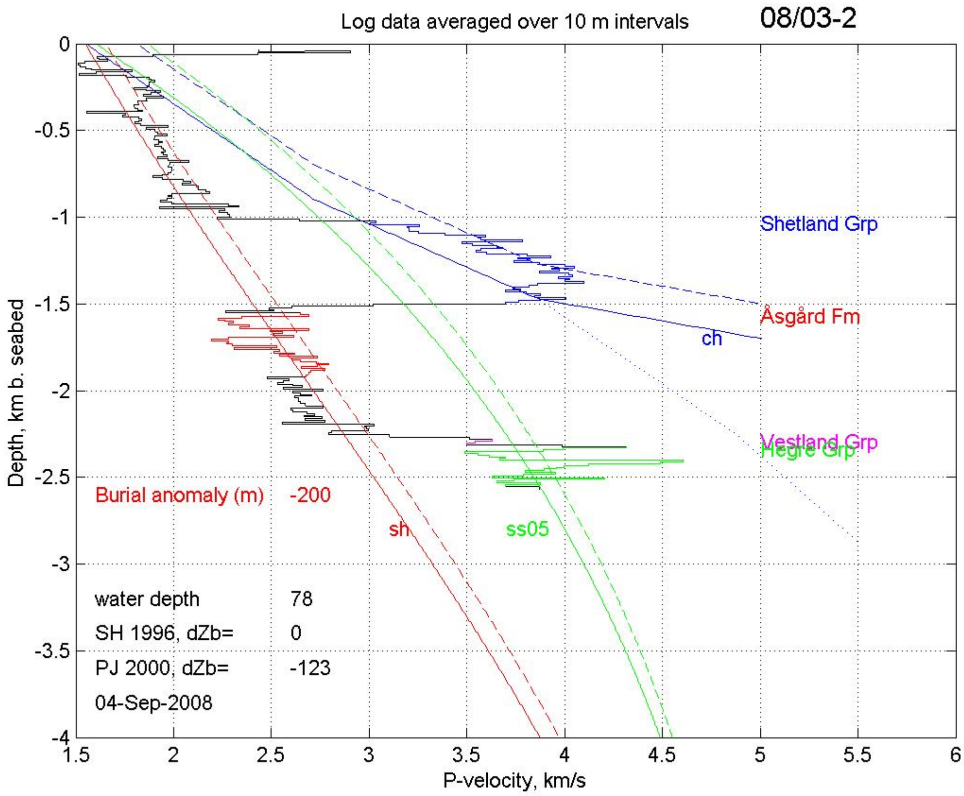

08/03-2
Post-chalk: Fairly uniform sonic pattern below 0.3 km.

Chalk: Pick of top Ekofisk Fm may be too shallow, should probably be below pronounced gamma peak; e.g. c. 1,03 km. High gamma above base chalk, c. 1.44 km, corresponds to drop in velocity. Increase of velocity with depth, 1.0- 1.4 km.

Pre-chalk: Rapid sonic variations (peaks 500 m/s wide) above Hegra Group with upper bound lining up with that of the post-chalk section. Low values may be due to problematic data.

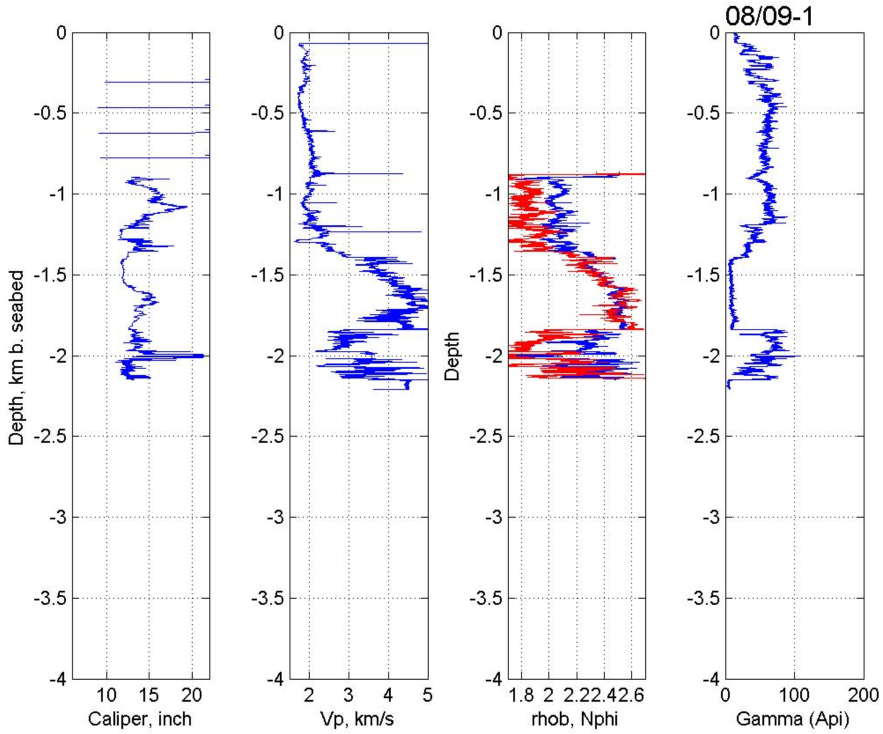
08/09-1
Depth, km b. seabed
Caliper, inch
Vp, km/s
Depth
rhob, Nphi
Gamma (Api)

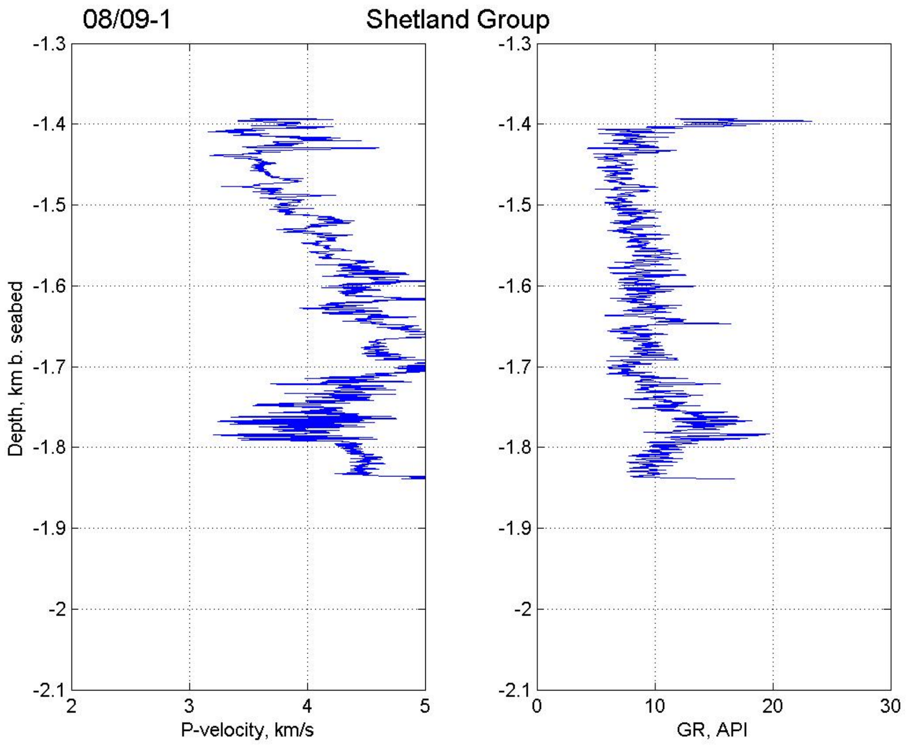
08/09-1
Shetland Group
Depth, km b. seabed
P-velocity, km/s
GR, API

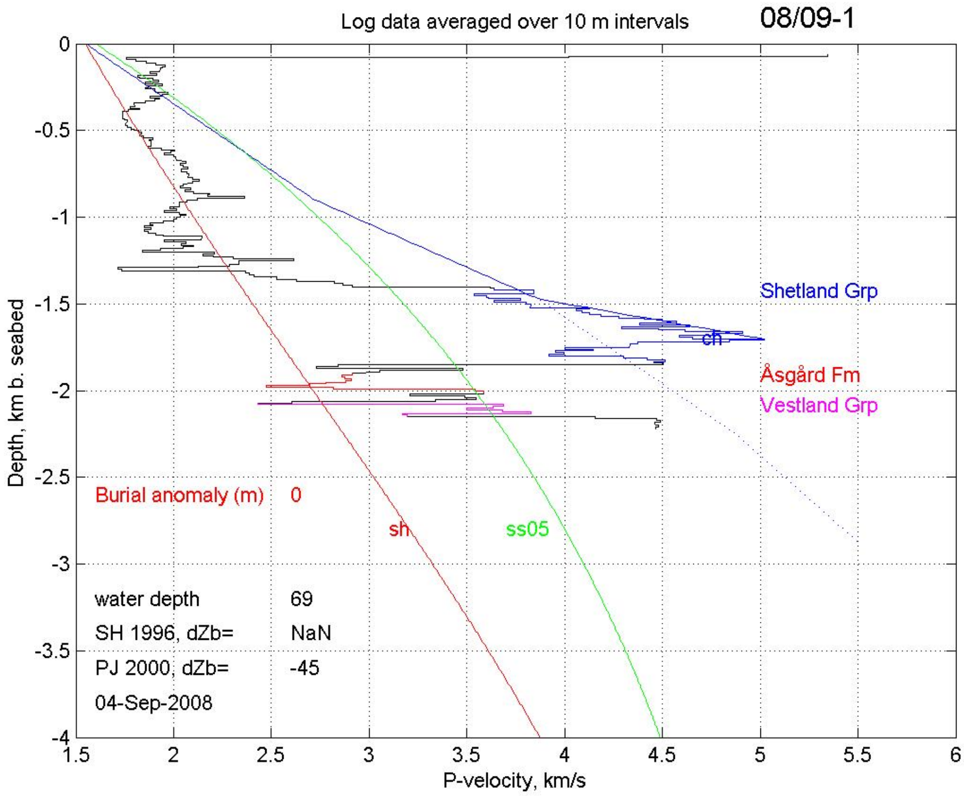

08/09-1
Post-chalk: Broad velocity variations around the level of the shale baseline, 0.1-1.4 km.

Chalk: high-velocity Ekofisk Fm with high gamma response (Top Shetland may be picked too shallow). Low-velocity basal unit with increased gamma response. Steady increase of velocity with depth between these levels, 1.45-1.7 km.

Pre-chalk: Rapid, major sonic variations above the Vestland Group, 1.8-2.1 km.

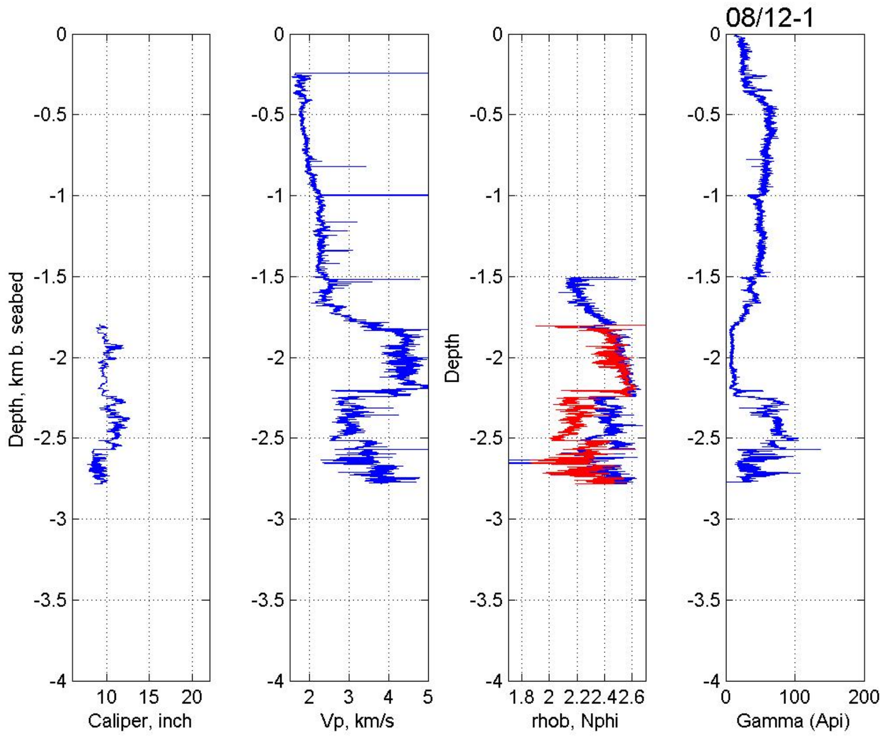
08/12-1
Depth, km b. seabed
Caliper, inch
Vp, km/s
Depth
rhob, Nphi
Gamma (Api)

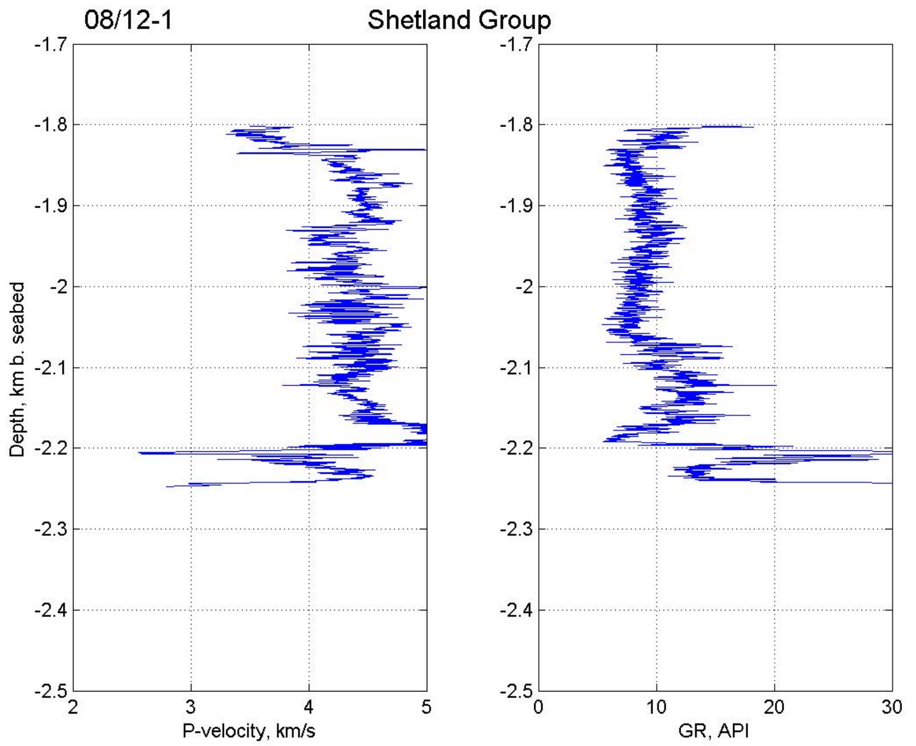
08/12-1
Shetland Group
Depth, km b. seabed
P-velocity, km/s
GR, API

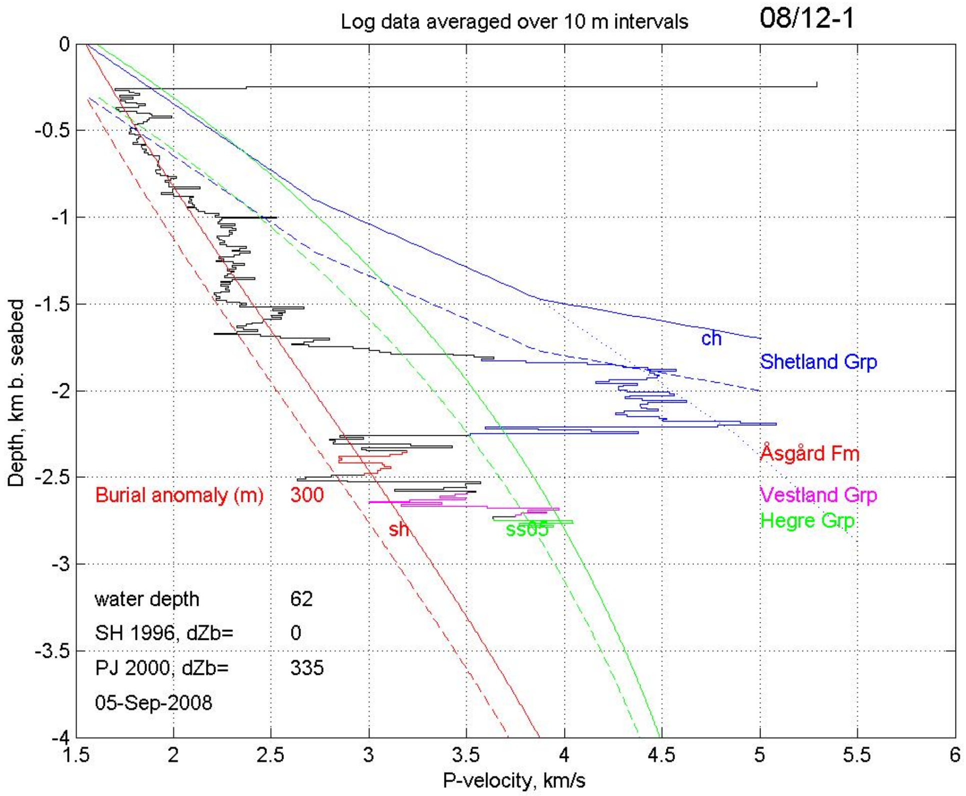

08/12-1

Post-chalk: Uniform sonic and gamma response, 0.3-1.7 km. Data trend follows shale baseline, 0.5-1.0 km, indicating normal compaction. Velocity inversion below 1 km.

Chalk: Low-velocity Ekofisk Fm, but high-velocity chalk below, 1.85-2.2 km, with irregular variations. Drop in velocity, c. 2.1 km, corresponds to increased gamma above pure basal chalk. Interval below 2.2 km is probably not chalk; too high gamma.

Pre-chalk: Rapidly varying sonic above basal part of Vestland Group, 2.3-2.7 km.

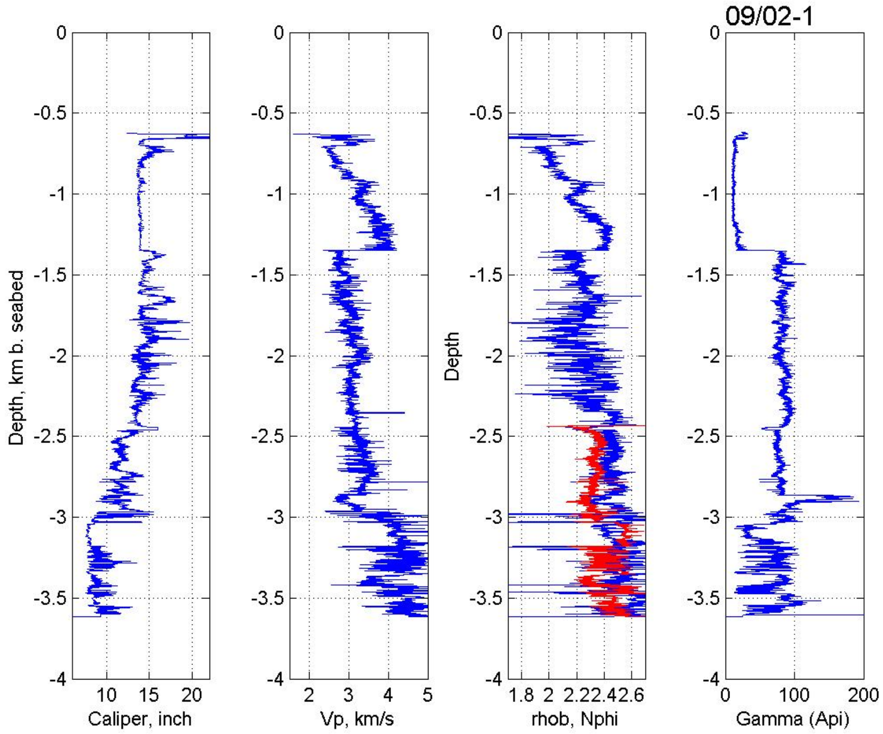
09/02-1
Depth, km b. seabed
Caliper, inch
Vp, km/s
Depth
rhob, Nphi
Gamma (Api)

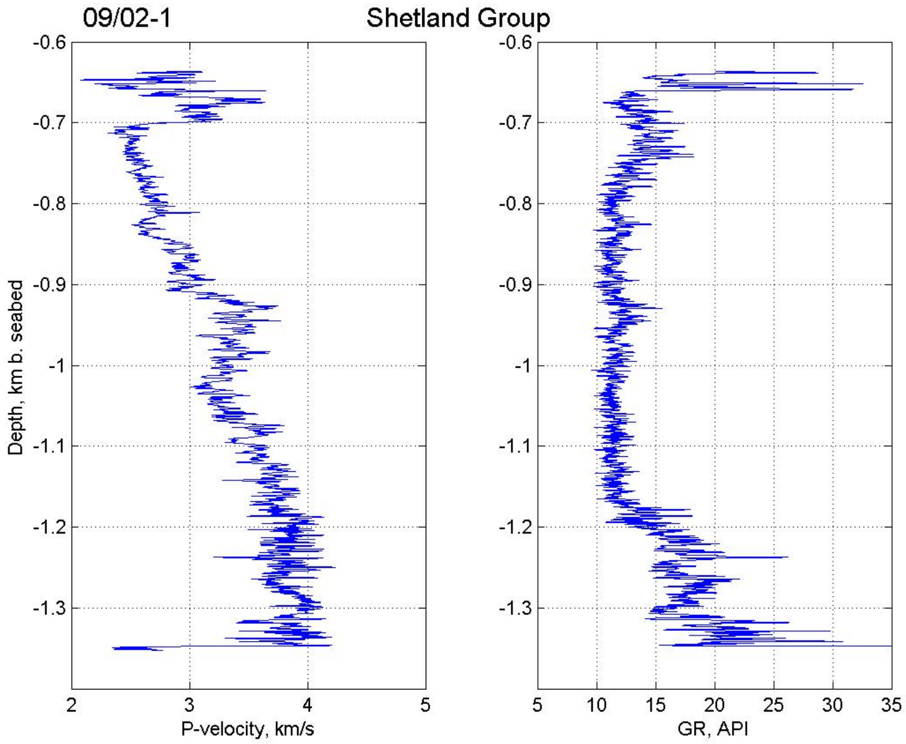
09/02-1
Shetland Group
Depth, km b. seabed
P-velocity, km/s
GR, API

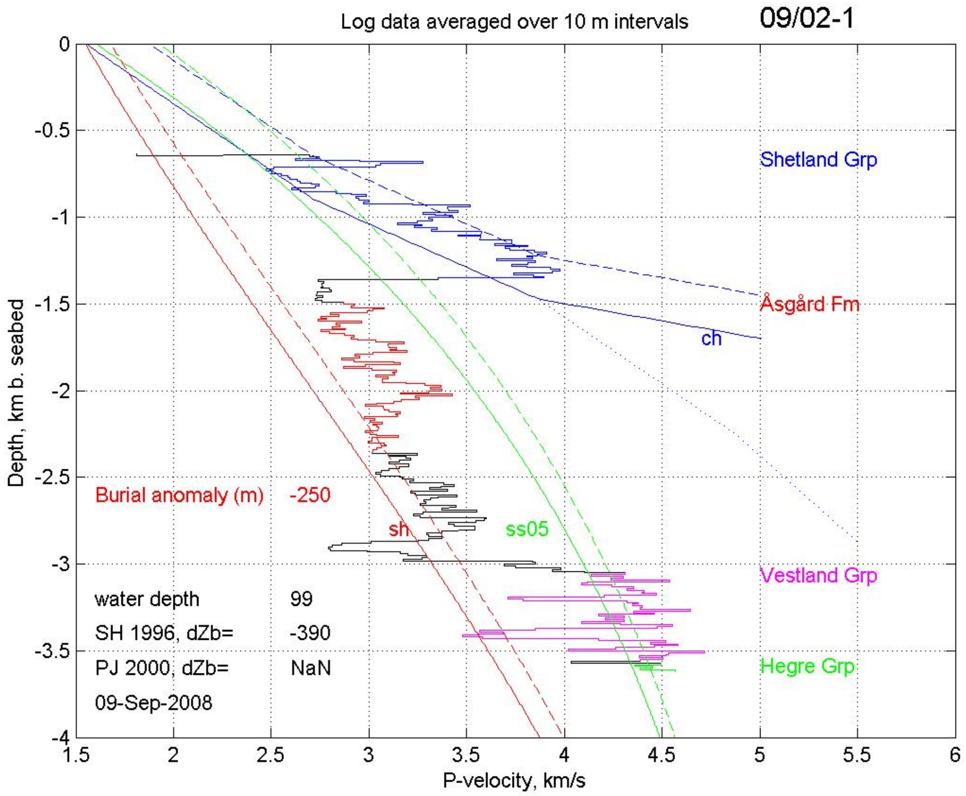

09/02-1
Post-chalk: No data.

Chalk: The high velocities (and corresponding relatively low gamma) in the uppermost unit, 0.65-0.7 km, reflect the presence of bryozoans whereas the high-velocity unit at c. 0.93 km is interpreted to correspond to a hardground (E. B. Nielsen, pers.comm.). High gamma below 1.2 km corresponds to a slow-down in the velocity increase (impure chalk).

Porosity-preservation due to hydrocabons? between the bryozoan unit and the hardground, the sonic velocity is very low between 0.7 and 0.9 km compared to the lower part of the chalk. It is a possible explanation that these low velocities (high porosities) can be caused by the presence of hydrocarbons in the chalk at some stage during the compaction of the chalk. Presence of hydrocarbons is known to have a porosity-preserving effect in chalk where coating of the grains with hydrocarbons prevents pressure solution of the carbonates (e.g. Japsen 1998). Well 9/2-1 is located on the Yme field where there is generation of hydrocarbons in the Mesozoic section below the chalk. Relatively low velocities are also observed at c. 1.02 km without any corresponding gamma peak.

Pre-chalk: Rapid sonic variations (peaks 500 m/s wide) above Tau Fm, 1.3-2.8 km.

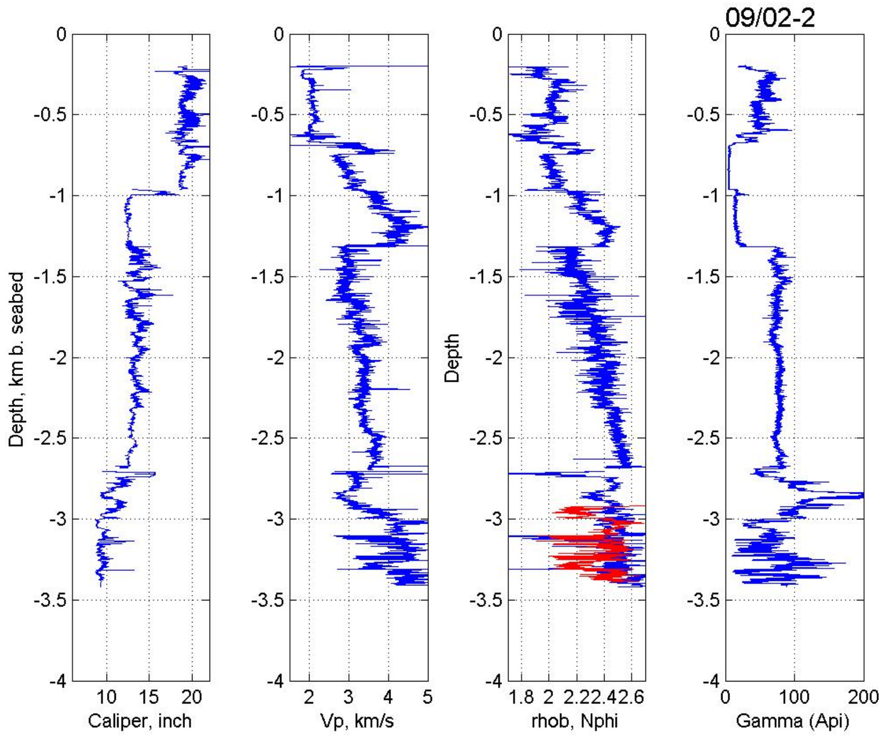

09/02-2
Depth, km b. seabed
Caliper, inch
Vp, km/s
Depth
rhob, Nphi
Gamma (Api)

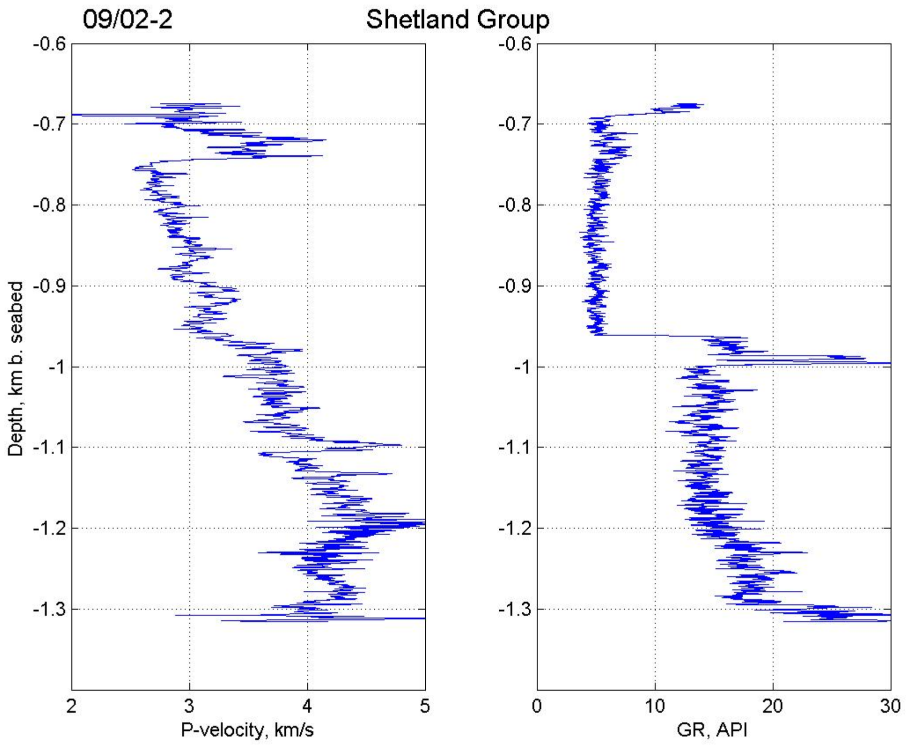

09/02-2
Shetland Group
Depth, km b. seabed
P-velocity, km/s
GR, API

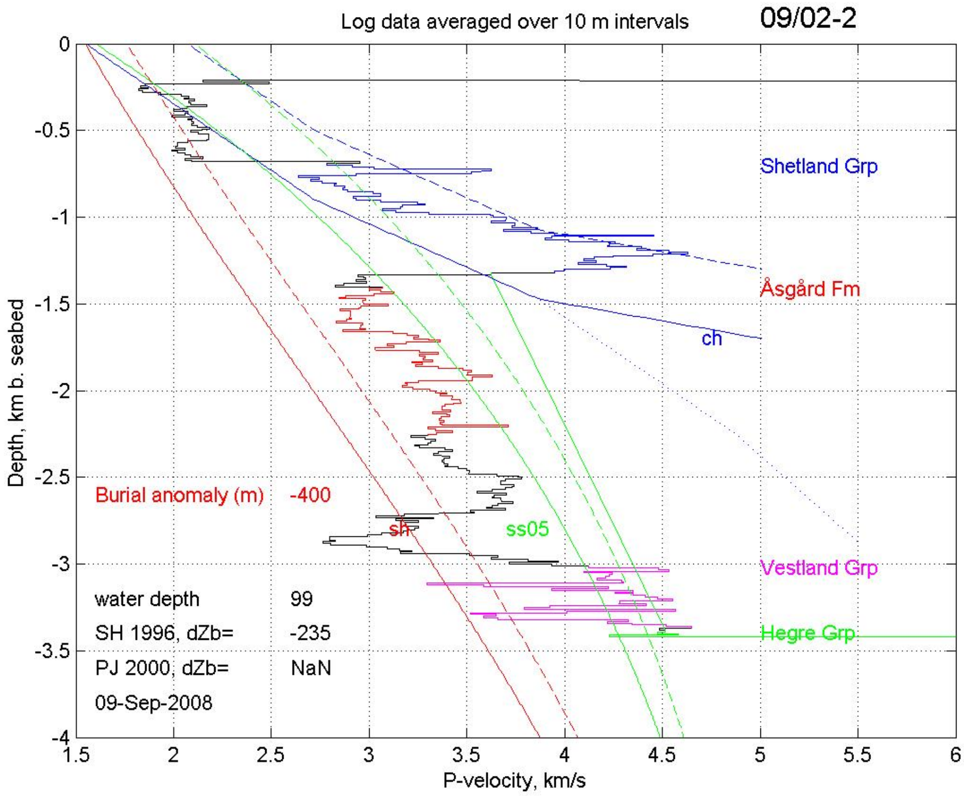

09/02-2

Post-chalk: Moderate variations in the sonic data, 0.3-0.7 km

Chalk: The gamma-log data are clearly affected by the casing at 0.97 km (e.g. the jump in gamma log), but the pattern of the sonic log is very similar to that of 9/2-1. The interpretation of 9/2-2 has to rely on a comparison with 9/2-1 because the depth of the casing also corresponds to the where the sonic increase occurs. High velocity unit in the uppermost chalk corresponds to the presence of bryozoans according to the completion log. Top Shetland may be too shallow (rather below gamma peak above 0.7 km). Relatively low velocities in the upper part of the chalk, 0.75-0.95 km, may be caused by porosity-preserving effect of hydrocarbons. No clear hardground at the top of the lower part of the chalk. High gamma below 1.2 km corresponds to a drop in velocity.

Pre-chalk: Rapid sonic variations (peaks 500 m/s wide) above Tau Fm, 1.3-2.8 km.

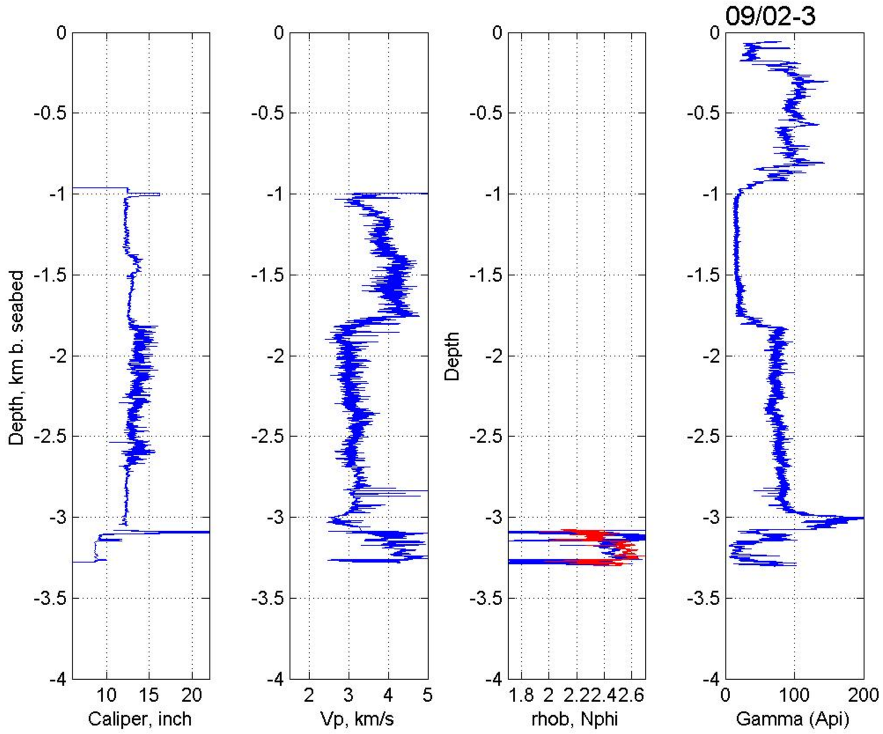
09/02-3
Depth, km b. seabed
Caliper, inch
Vp, km/s
Depth
rhob, Nphi
Gamma (Api)

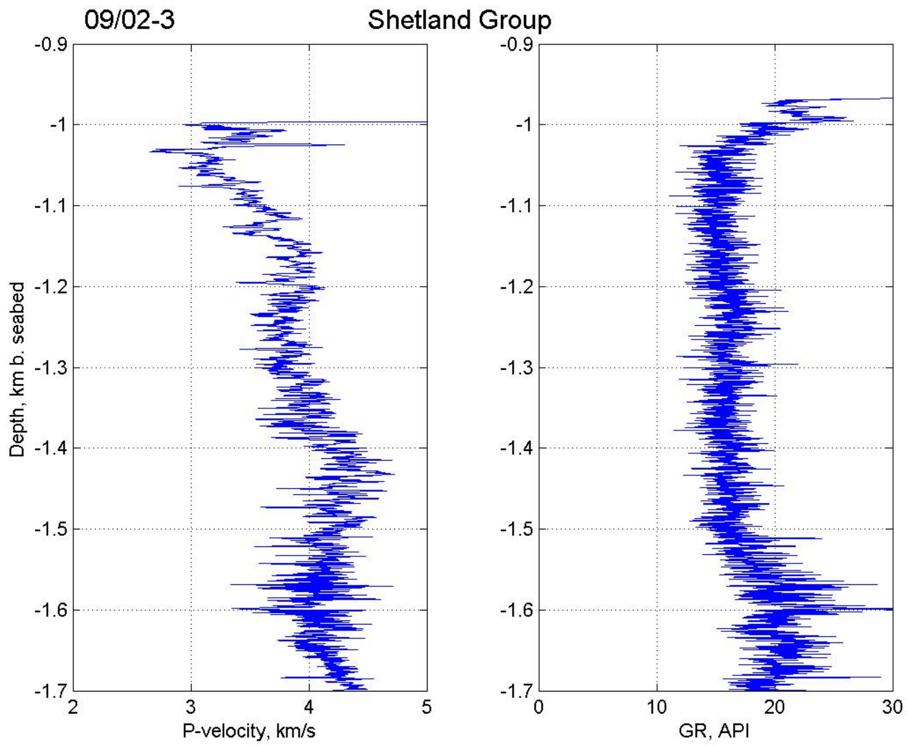
09/02-3
Shetland Group
Depth, km b. seabed
P-velocity, km/s
GR, API

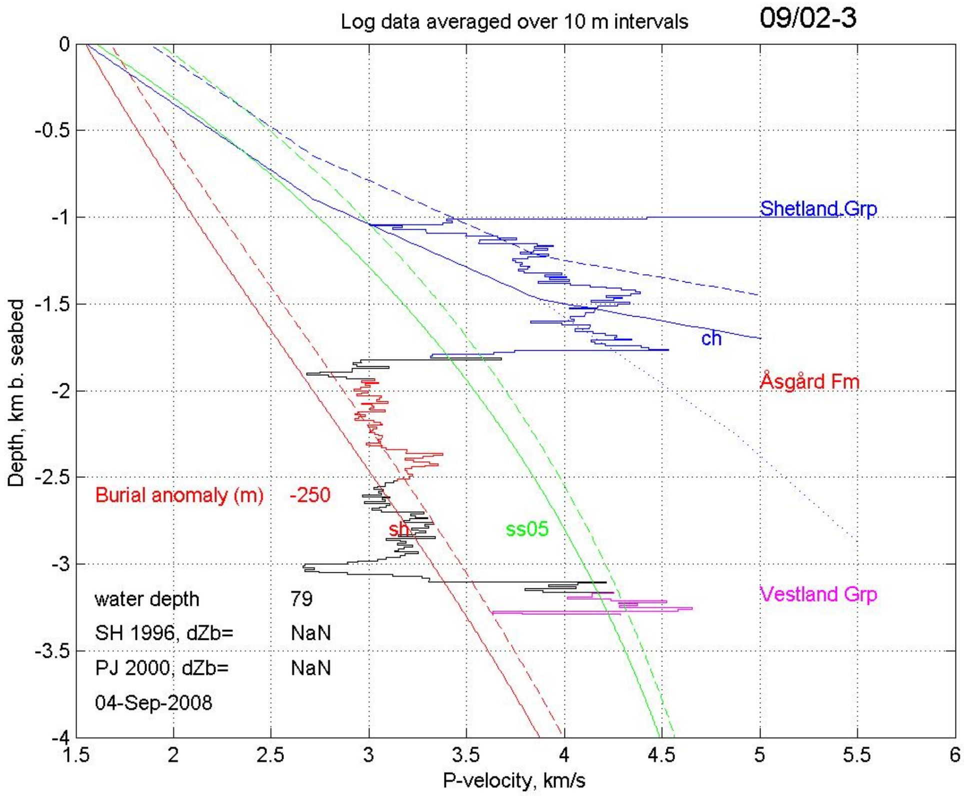

09/02-3
Post-chalk: No data.

Chalk: The sonic pattern for this well is very similar to that of 9/2-1. High velocities in the shallowest part of the chalk (partly data error, bryozoans?), followed by a low-velocity trough (porosity preserved by hydrocarbons?), 1.0-1.1 km, a velocity peak, 1,18 km (hardground?), another low-velocity trough, 1.2-1.35 km, a velocity peak, c 1.43 km, and finally a drop in velocity corresponding to a broad gamma peak below 1.5 km. The main interval of the chalk, 1.15-1.5 km, shows no significant variations in gamma response. This irregular pattern makes it difficult to determine the level of normally compacted chalk.

Pre-chalk: Rapid minor variations above the Tau Fm, 1.8-3.0 km, but velocity inversion below 2.5 km.

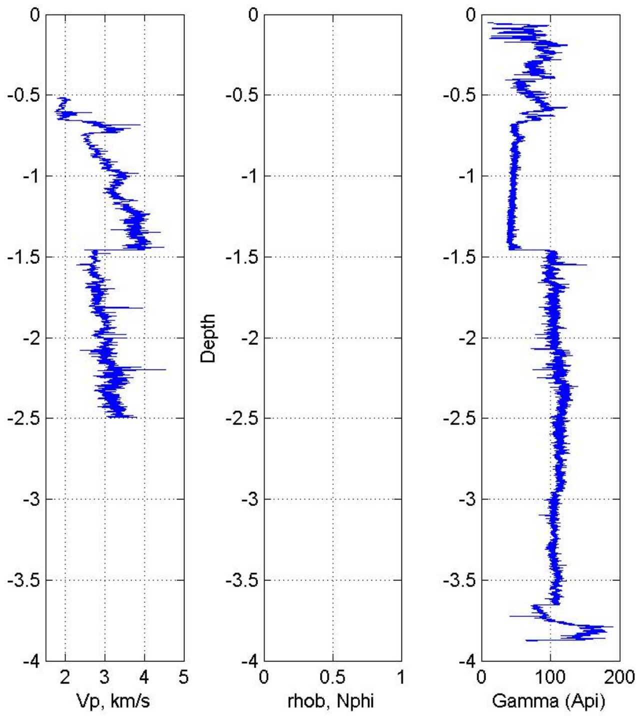

Depth
Vp, km/s
rhob, Nphi
Gamma (Api)

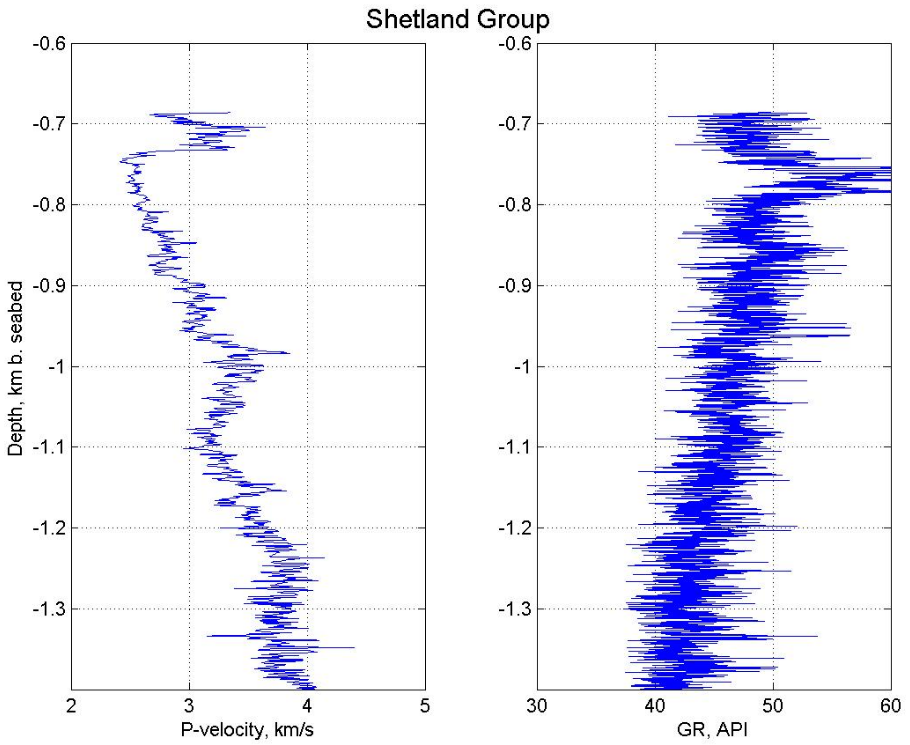

Shetland Group
Depth, km b. seabed
P-velocity, km/s
GR, API

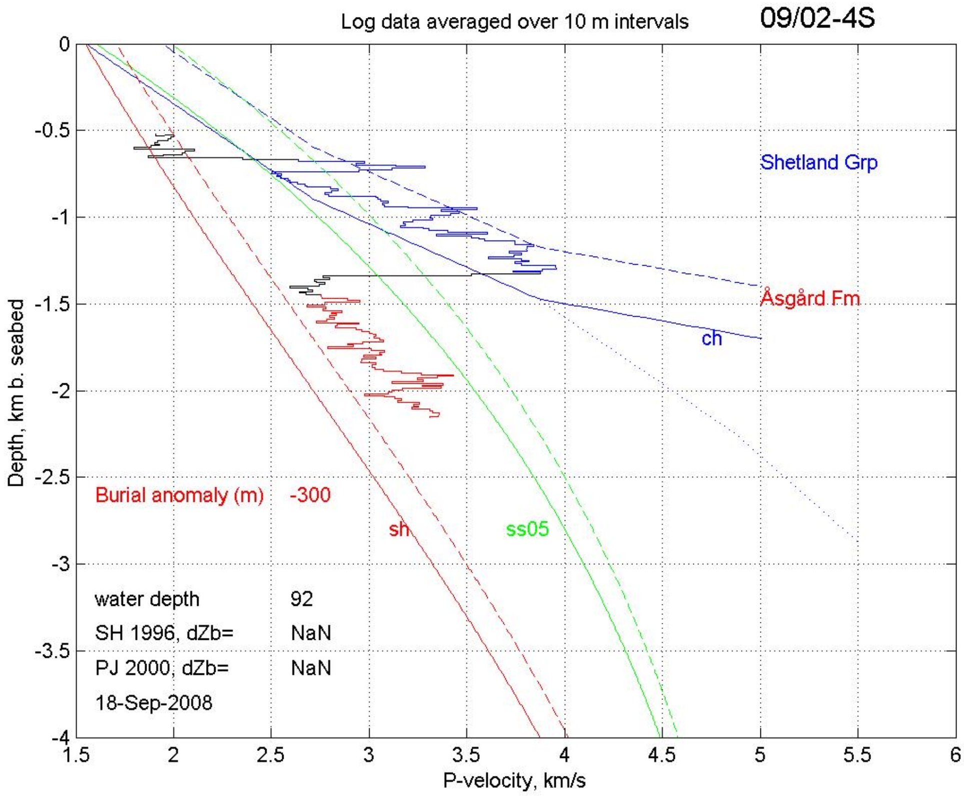

09/02-4S

Post-chalk: Almost no data.

Chalk: The sonic-log pattern is almost identical to that of 9/2-1. However, the gamma log response is completely different (a very high level and a steady decrease throughout the chalk) and probably reflects data errors. High velocities in the shallowest part of the chalk, followed by a low-velocity trough (porosity preserved by hydrocarbons?), 0.74-0.9 km, a velocity peak, 0.99 km, another low-velocity trough, 1.0-1.15 km, a velocity peak, c 1.23 km, and finally a drop in velocity (impure chalk?). The absolute level for the pure chalk velocity-depth trend difficult to estimate.

Pre-chalk: Minor sonic variations relative to a general increase with depth 1.5-2.5 km..

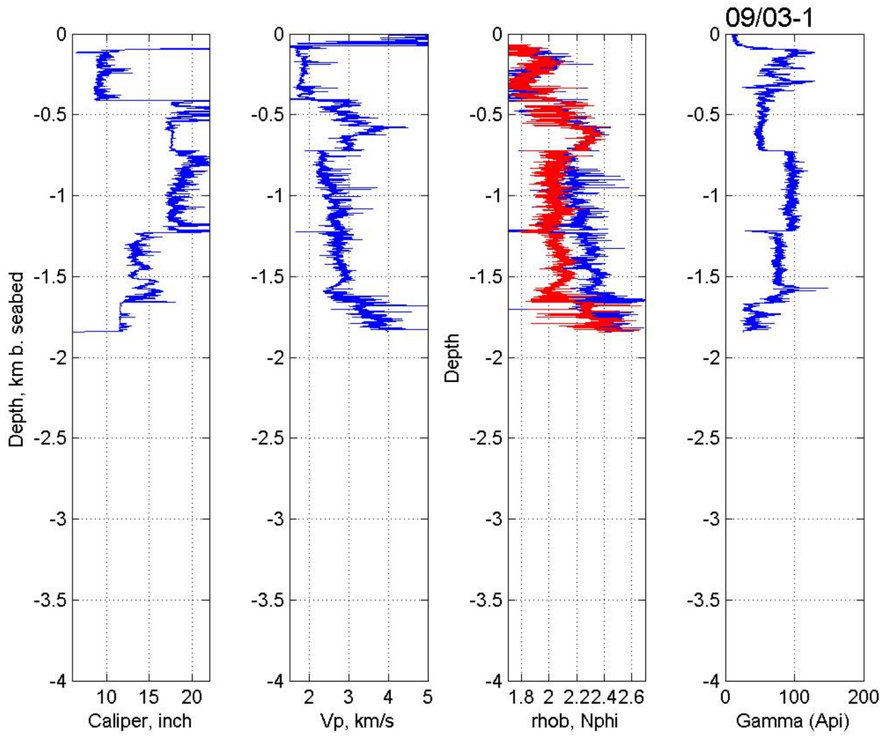
09/03-1
Depth, km b. seabed
Caliper, inch
Vp, km/s
Depth
rhob, Nphi
Gamma (Api)

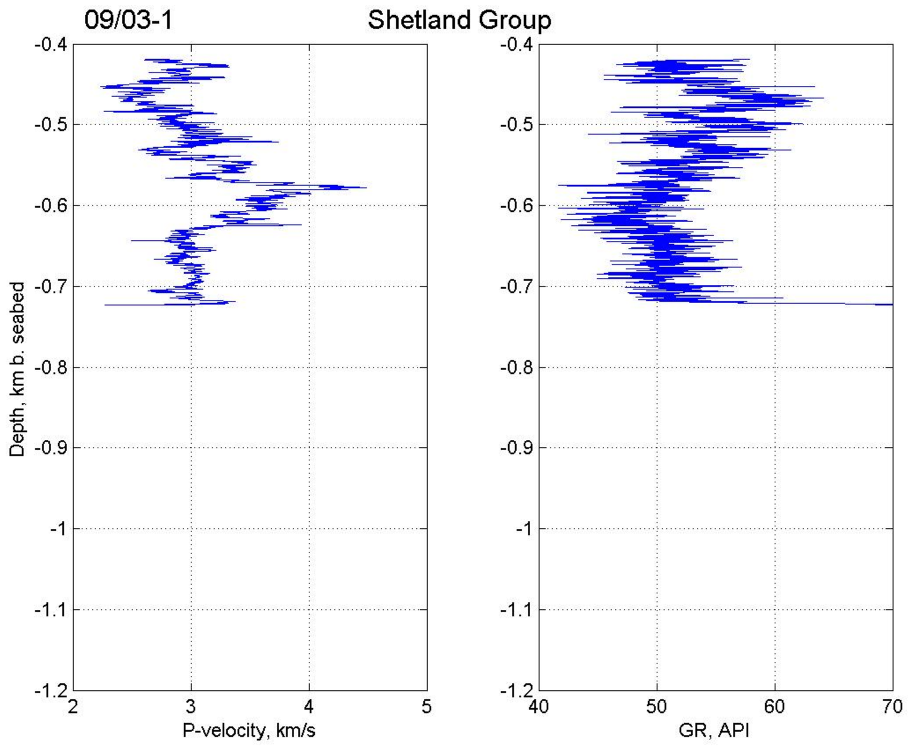
09/03-1
Shetland Group
Depth, km b. seabed
P-velocity, km/s
GR, API

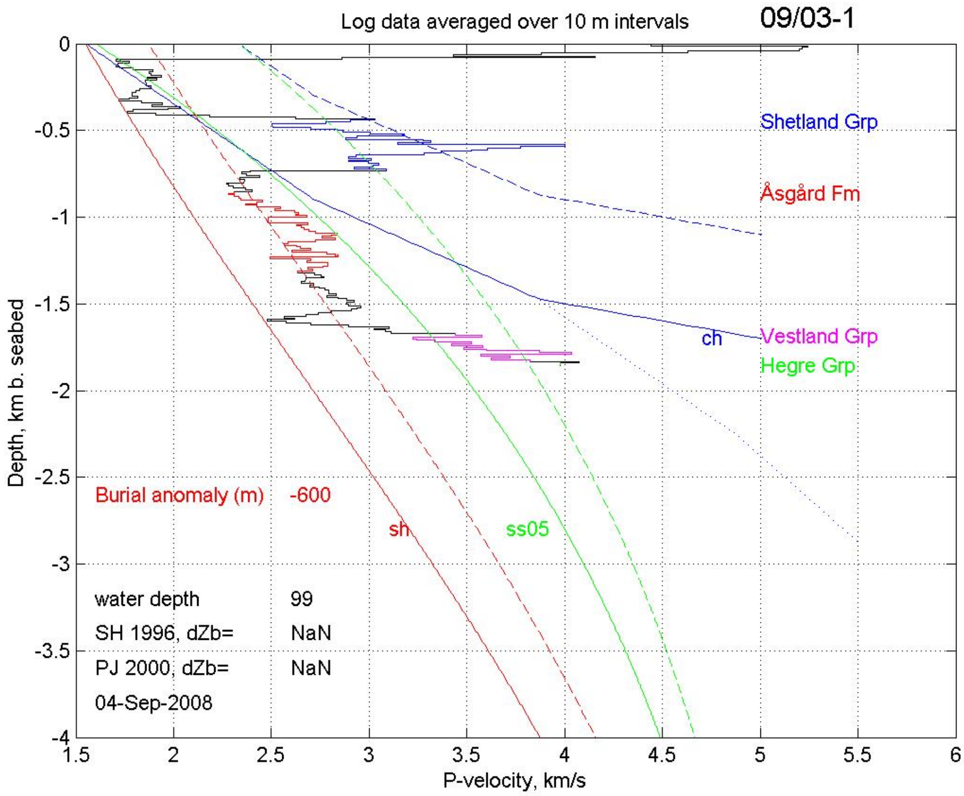

09/03-1

Post-chalk: Thin section, 0.1-0.4 km.

Chalk: Thin chalk interval with velocity variations that are broadly similar to those of 9/2-1. The gamma log response has a very high level and a wide range; data errors? Velocity peak at c. 0.58 km and low velocities below 0.64 km interpreted as deviations from normal compaction.

Pre-chalk: Minor sonic variations relative to a general increase with depth above the Tau Fm, 0.7-1.5 km.

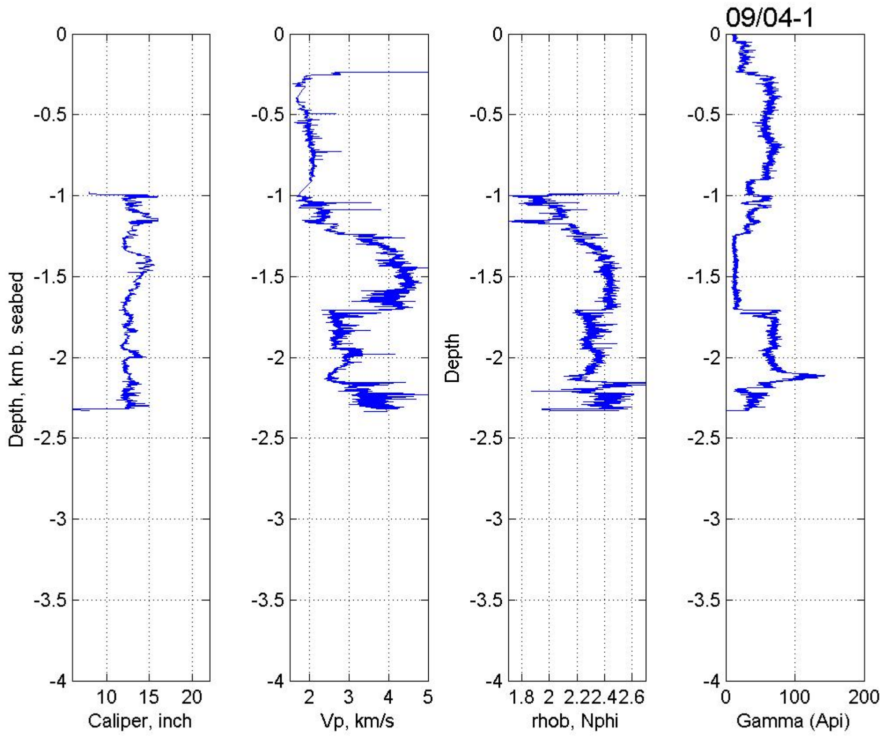
09/04-1
Depth, km b. seabed
Caliper, inch
Vp, km/s
Depth
rhob, Nphi
Gamma (Api)

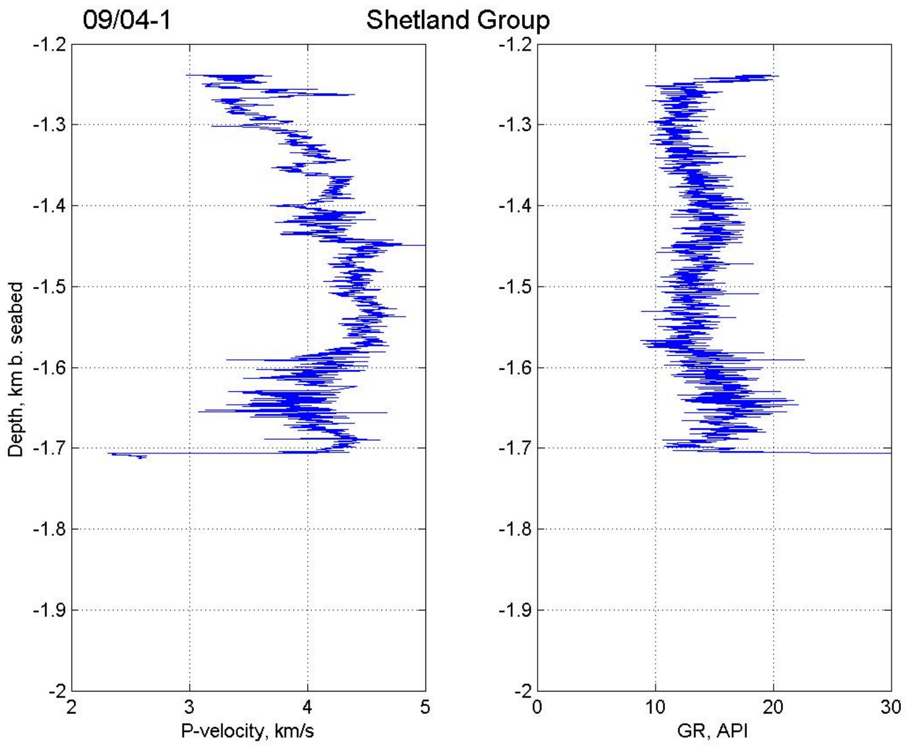
09/04-1
Shetland Group
Depth, km b. seabed
P-velocity, km/s
GR, API

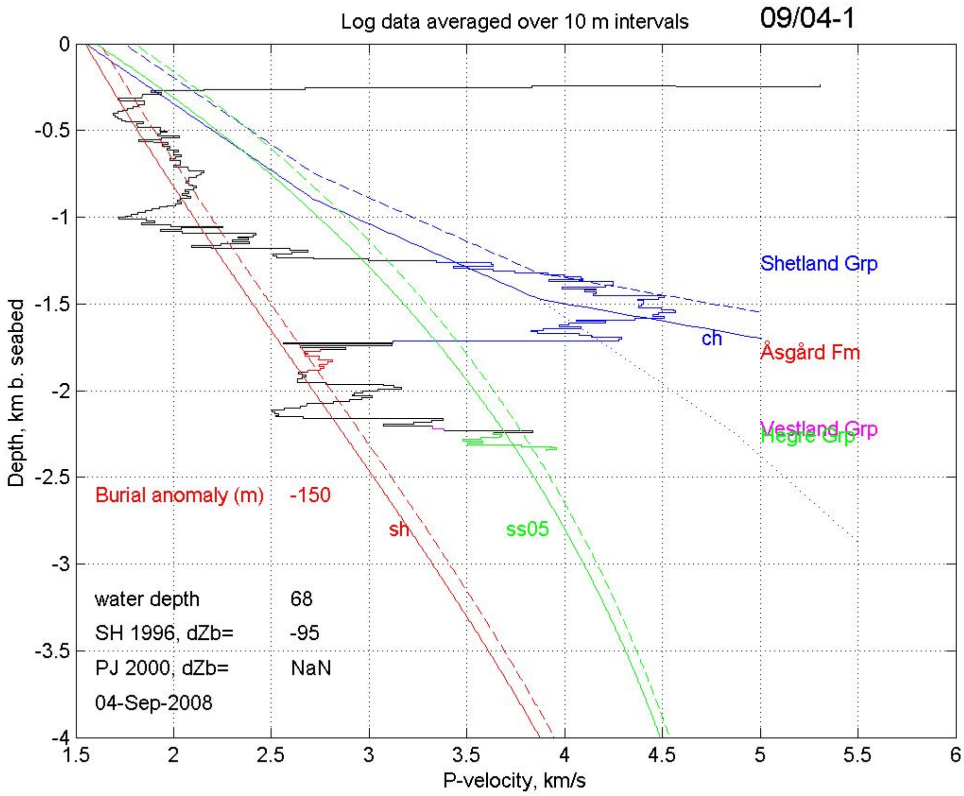

09/04-1

Post-chalk: Increase of velocity with depth 0.5-0.8 km above velocity inversion at c. 1.0 km.

Chalk: General increase of velocity, 1.26-1.6 km above velocity inversion at 1.65 km corresponding to gamma peak.

Pre-chalk: Wide sonic variation over relatively thin interval above Tau Fm, 1.75-2.0 km

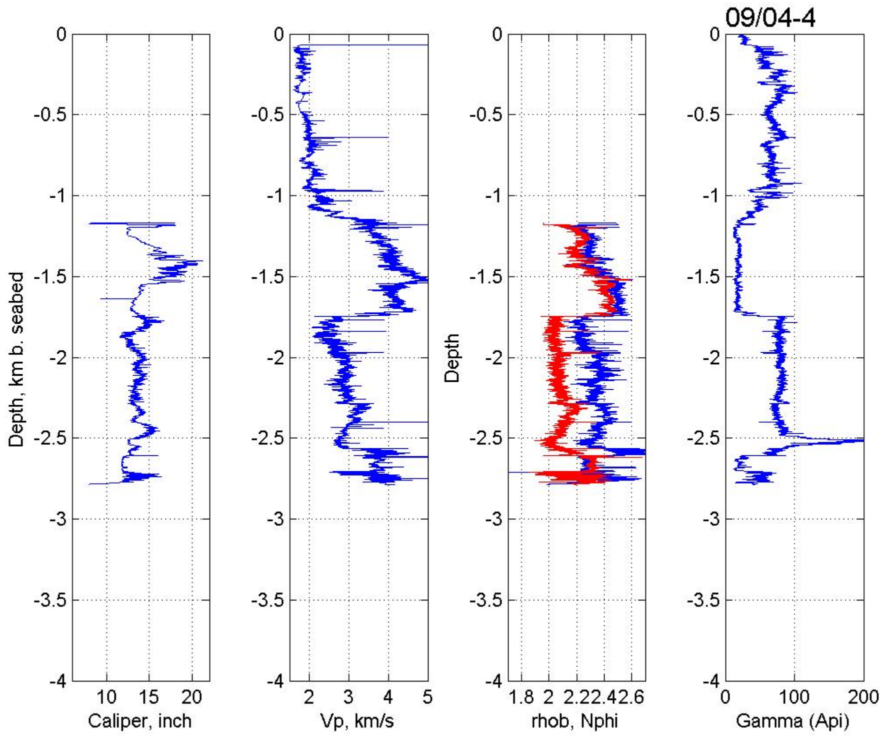
09/04-4
Depth, km b. seabed
Caliper, inch
Vp, km/s
Depth
rhob, Nphi
Gamma (Api)

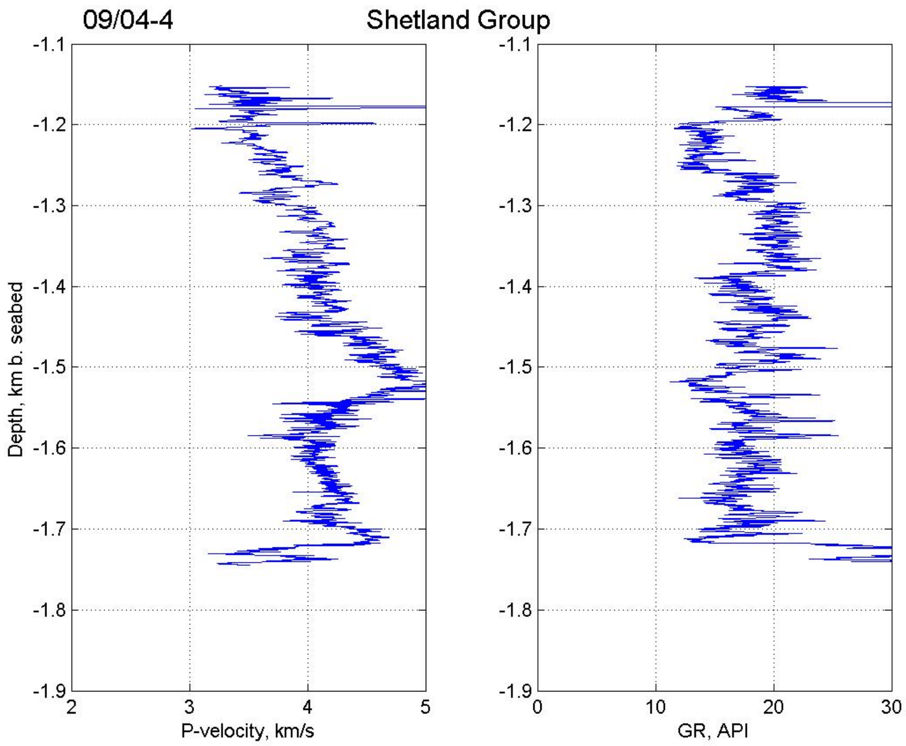
09/04-4
Shetland Group
Depth, km b. seabed
P-velocity, km/s
GR, API

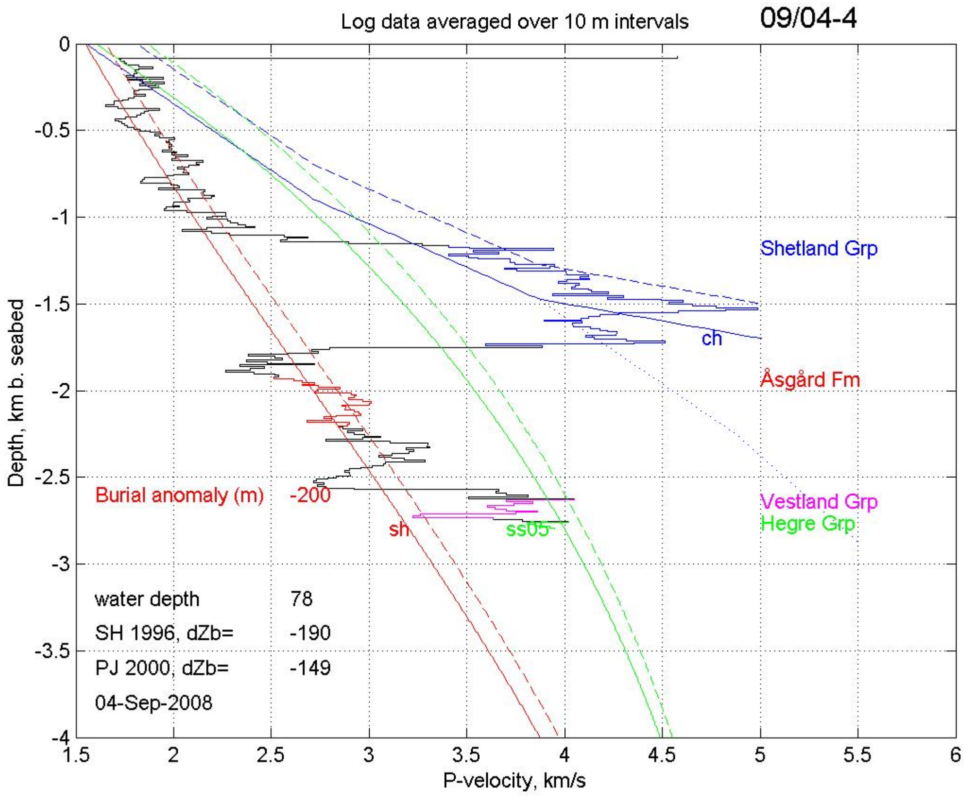

09/04-4

Post-chalk: General increase of velocity with depth interrupted by low-velocity excursion over thin intervals, 0.3-1.1 km.

Chalk: Increase of velocity with depth below uppermost part with high gamma (Top Shetland too shallow?), 1.2-1.53 km. Irregular and rather high gamma readings may indicate data error (cf. 9/4-1). Velocity inversion below 1.53 km probably due to impure chalk. Base Shetland may be too deep.

Pre-chalk: Irregular variations above Tau Fm, 1,78-2.4 km. Separation of Rho_b and N_phi indicative of shale in this interval. Low velocities in the Sola Fm (between Shetland Group and Åsgård Fm); velocity peak across the Sauda Fm (between Åsgård and Tau Fms): sharp increase at the top of Sauda and a gradual decrease over the basal part as a transition to the Tau Fm.

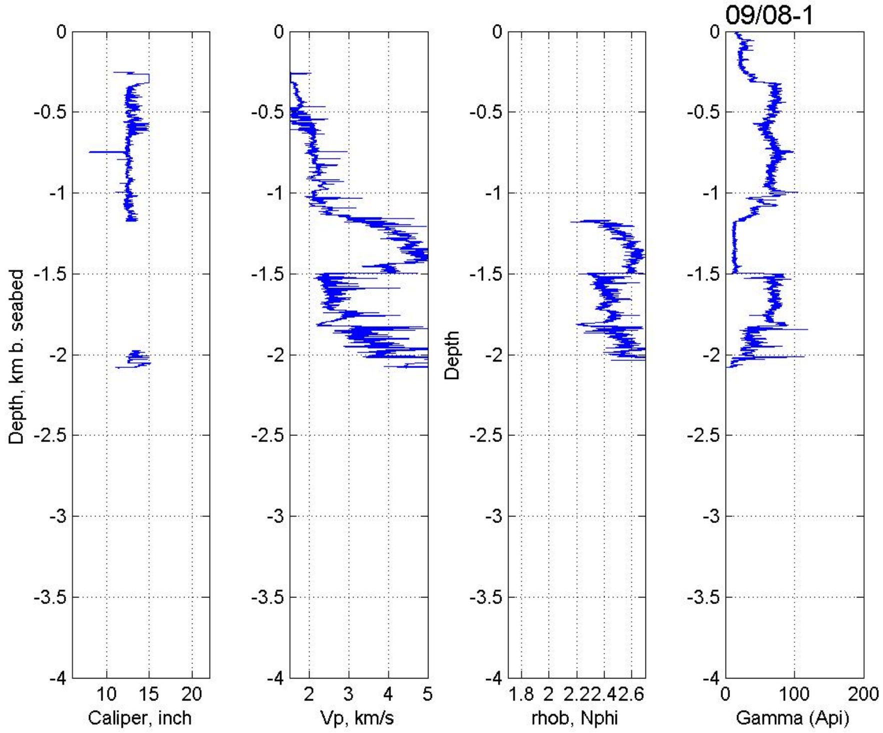
09/08-1
Depth, km b. seabed
Depth
Caliper, inch
Vp, km/s
rhob, Nphi
Gamma (Api)

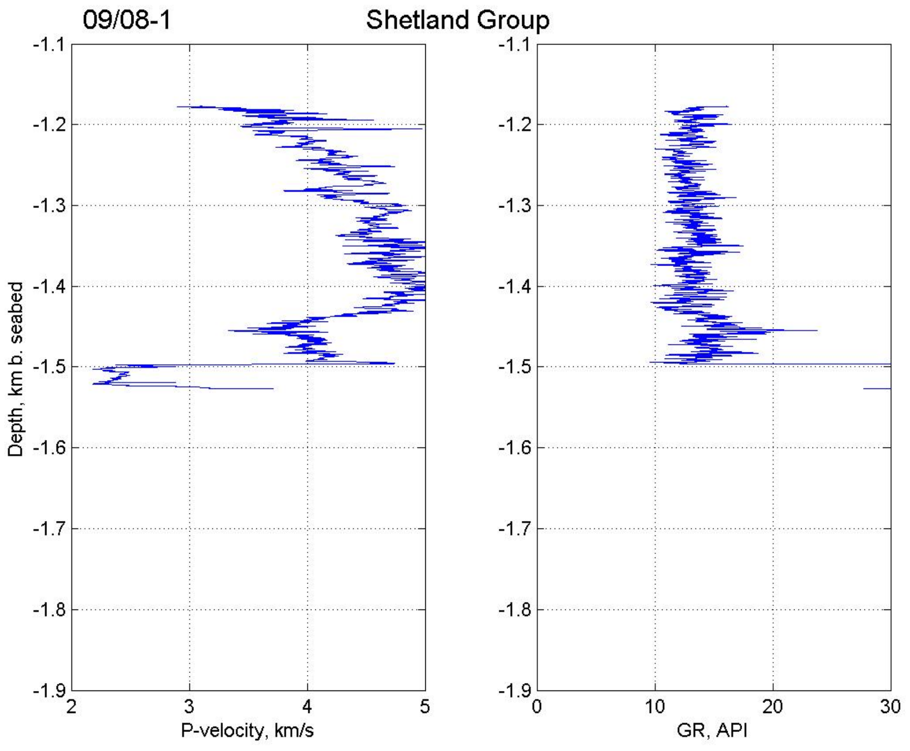
09/08-1
Shetland Group
Depth, km b. seabed
P-velocity, km/s
GR, API

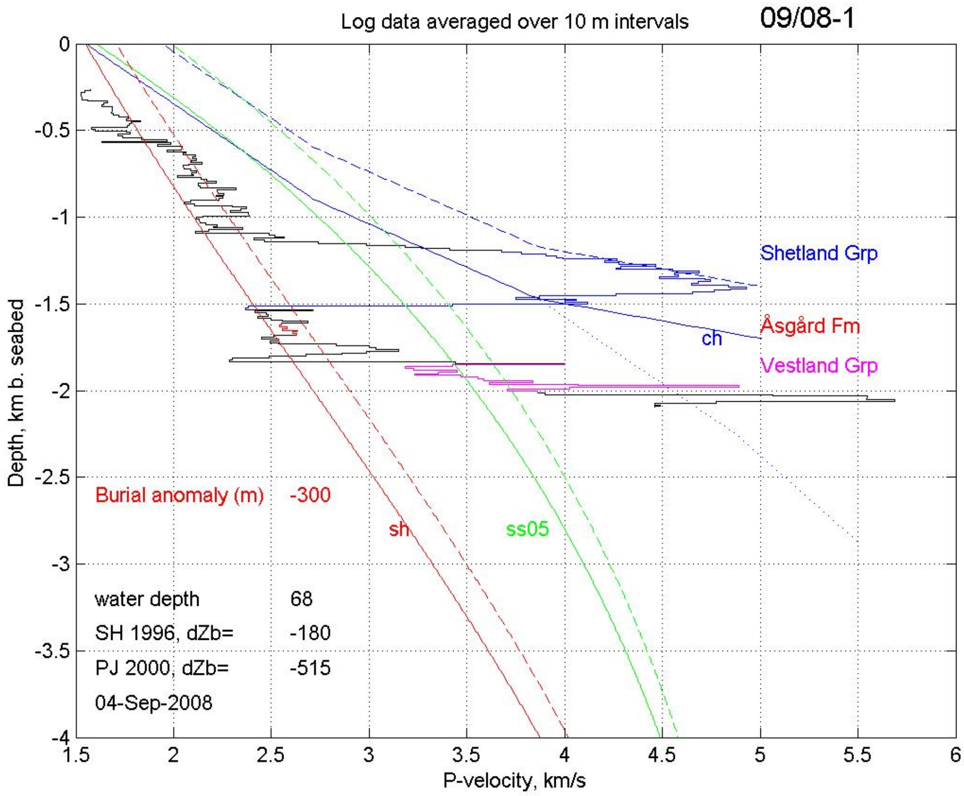

09/08-1

Post-chalk: General increase of velocity with depth interrupted by low-velocity excursion over thin intervals, 0.6-1.2 km. Relatively low velocities above 0.5 km (unconformity?).

Chalk: Increase of velocity with depth over the uppermost part of the chalk, 1.18-1.4 km above velocity inversion correlating with gamma peak at 1.45 km. Base Shetland too deep; should be at 1.5 km above very high gamma peak.

Pre-chalk: Irregular sonic variations above Tau Fm (not indicated in NDP's interpretation), 1.5-1.8 km. High velocities in Zechstein Group below Vestland Group.

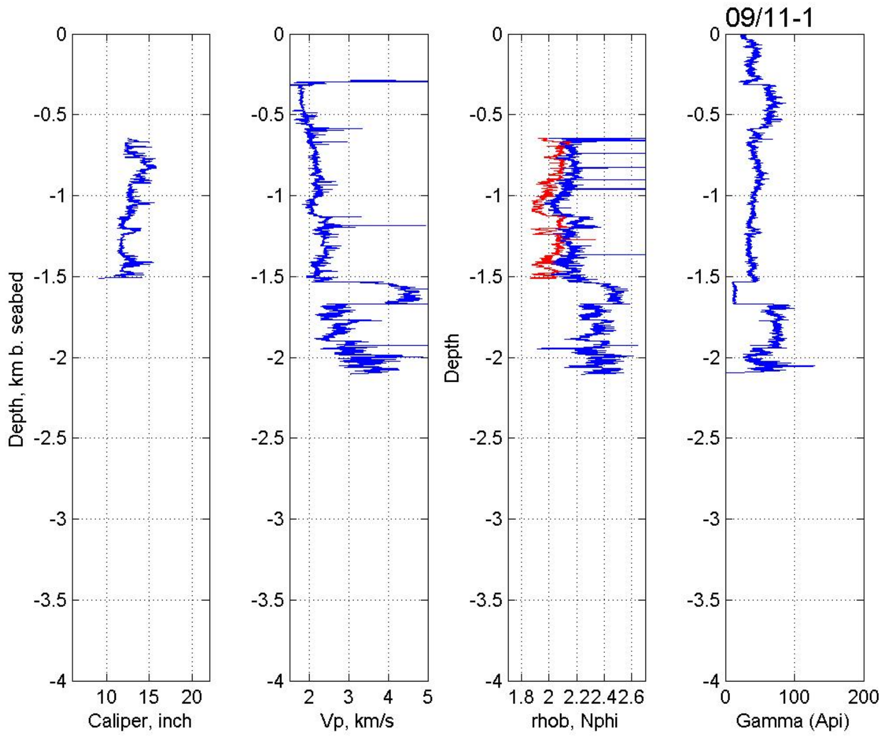
09/11-1
Depth, km b. seabed
Caliper, inch
Vp, km/s
Depth
rhob, Nphi
Gamma (Api)

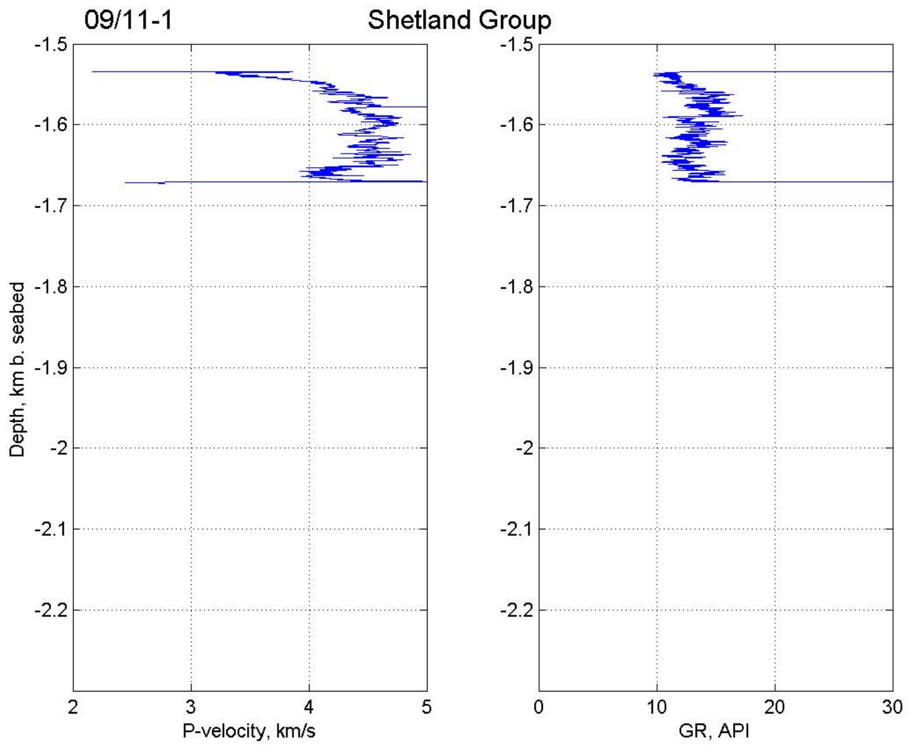
09/11-1
Shetland Group
Depth, km b. seabed
P-velocity, km/s
GR, API

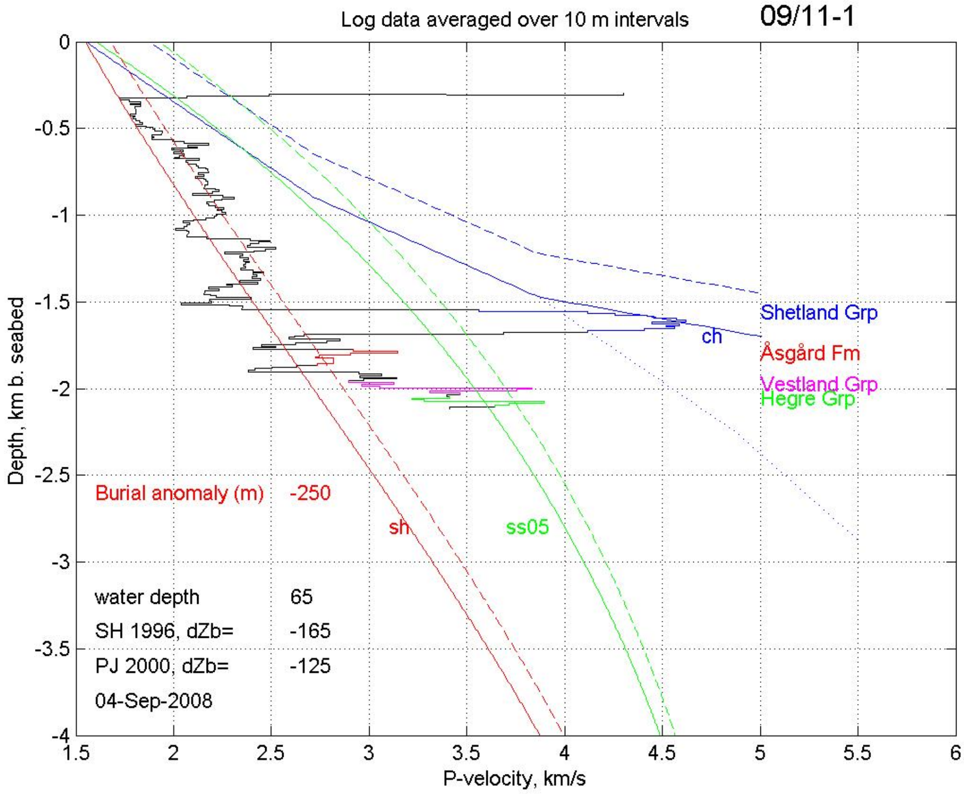

09/11-1

Post-chalk: General increase of velocity with depth interrupted by low-velocity excursion over discrete intervals, 0.6-1.4 km. Relatively low velocities above 0.6 km (unconformity?).

Chalk: Thin Shetland Group (139 m) makes it impossible to evaluate whether the absolute level for pure chalk velocity-depth trend is reached.

Pre-chalk: Wide velocity variations over the thin section above Tau Fm, 1.7-1.9 km.

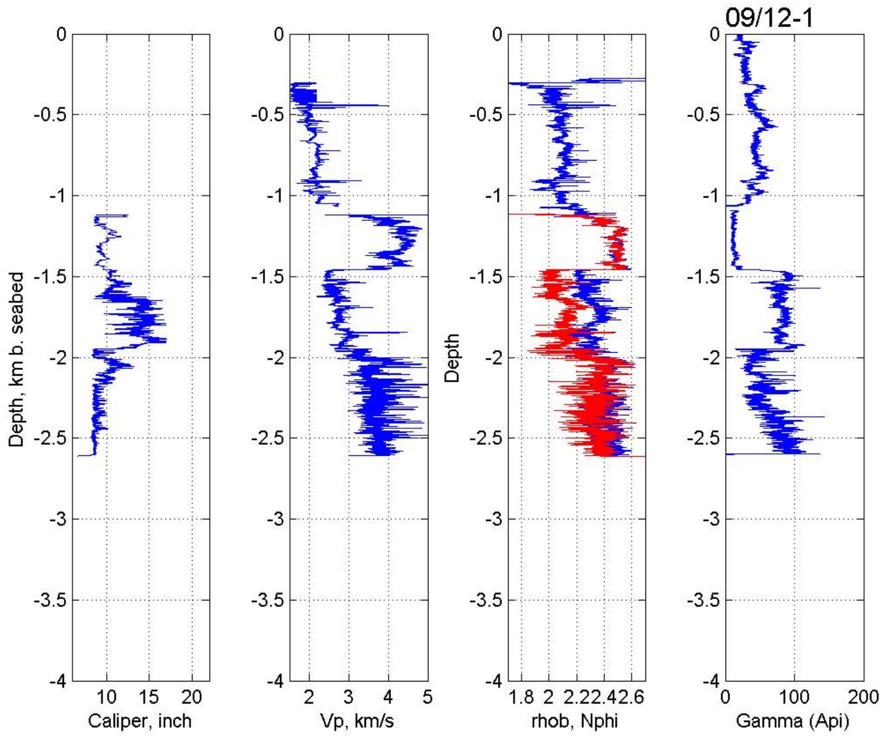
09/12-1
Depth, km b. seabed
Depth
Caliper, inch
Vp, km/s
rhob, Nphi
Gamma (Api)

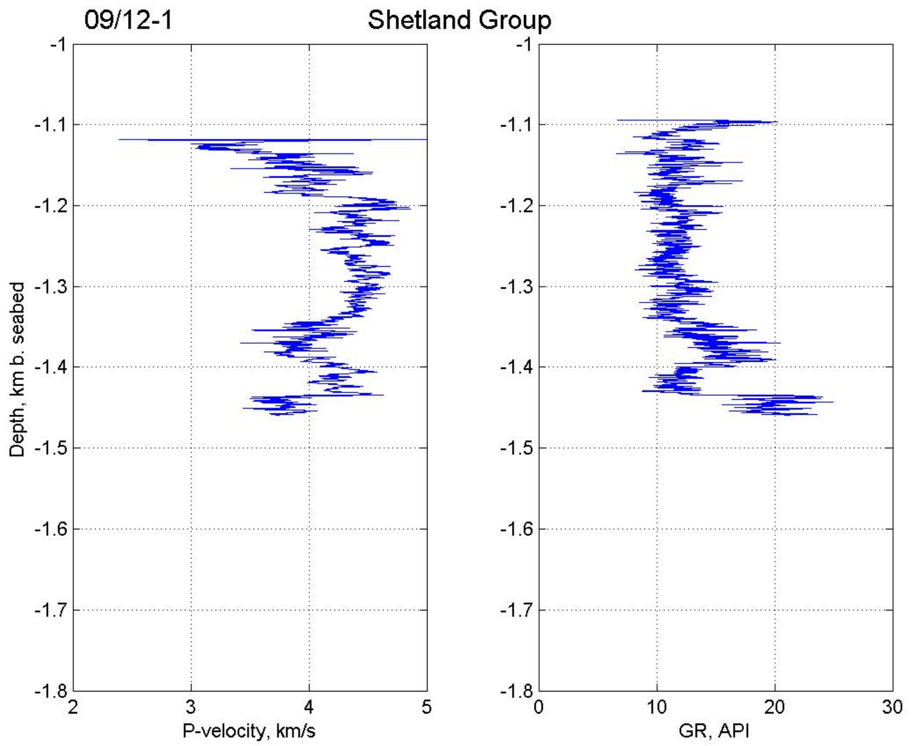
09/12-1
Shetland Group
Depth, km b. seabed
P-velocity, km/s
GR, API

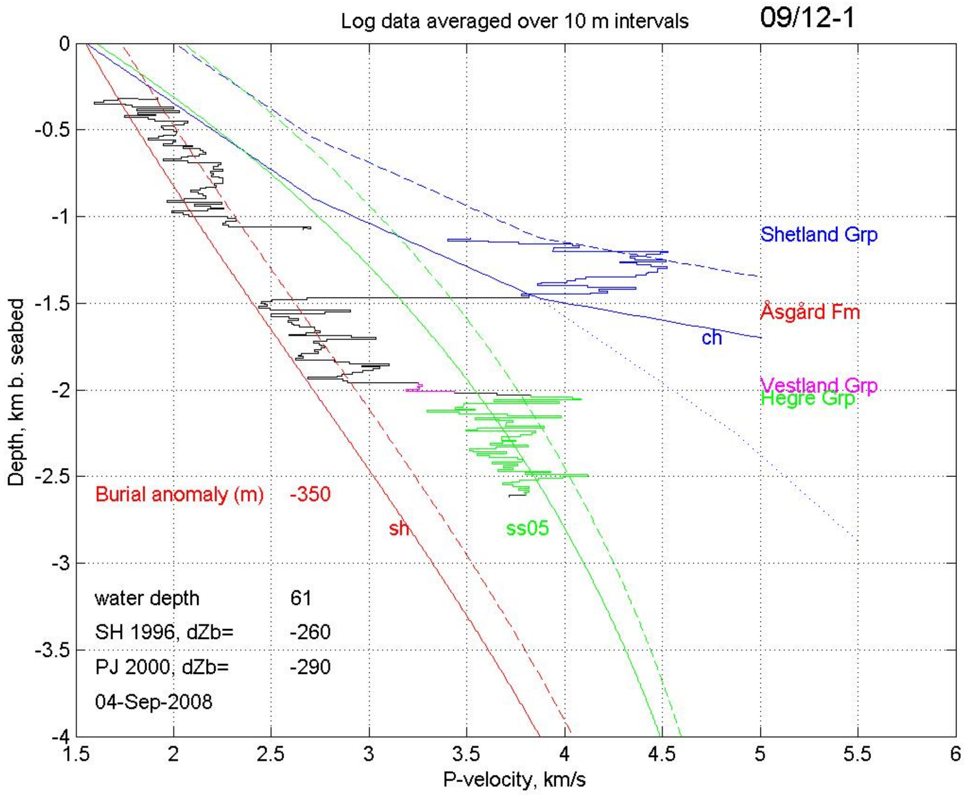

09/12-1

Post-chalk: General increase of velocity with depth interrupted by low-velocity excursion over thin intervals, 0.3-1.1 km.

Chalk: Low-velocity Ekofisk Fm underlain with high-velocity chalk with irregular variations, 1.15-1.33 km. Velocity inversion correlating with gamma peak at c. 1.38 km. Base Shetland too deep; should be at 1.43 km above very high gamma peak.

Pre-chalk: Rapid velocity variations above Vestland Group, 1.4-1.9 km. High-velocity sandstone units in Hegre Group (Skagerrak Fm) below 2 km (cf. NPD paper 27, 1980).

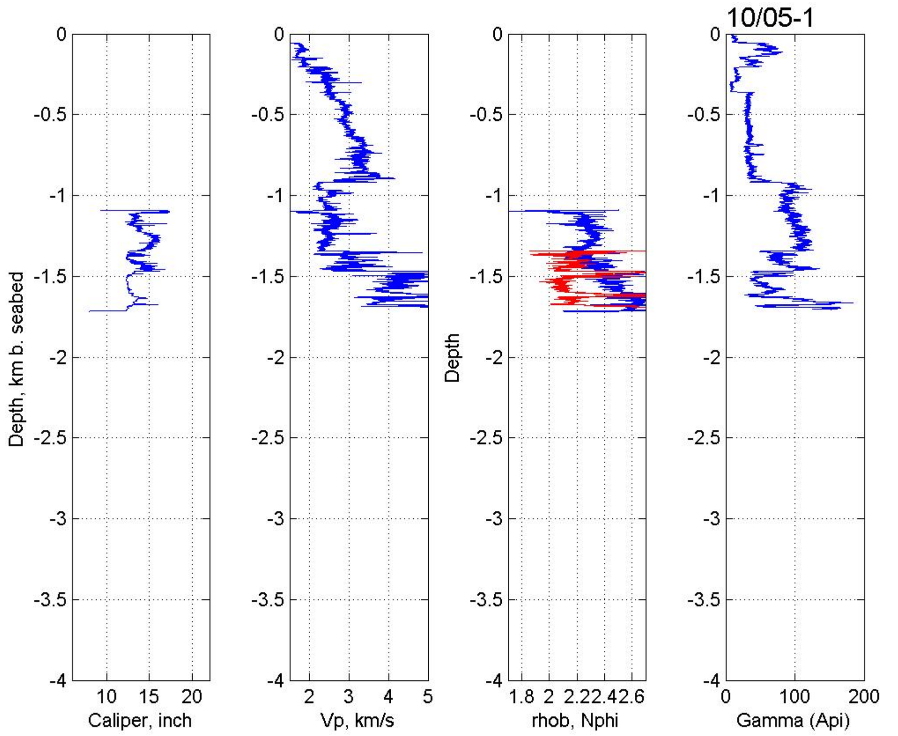
10/05-1
Depth, km b. seabed
Caliper, inch
Vp, km/s
Depth
rhob, Nphi
Gamma (Api)

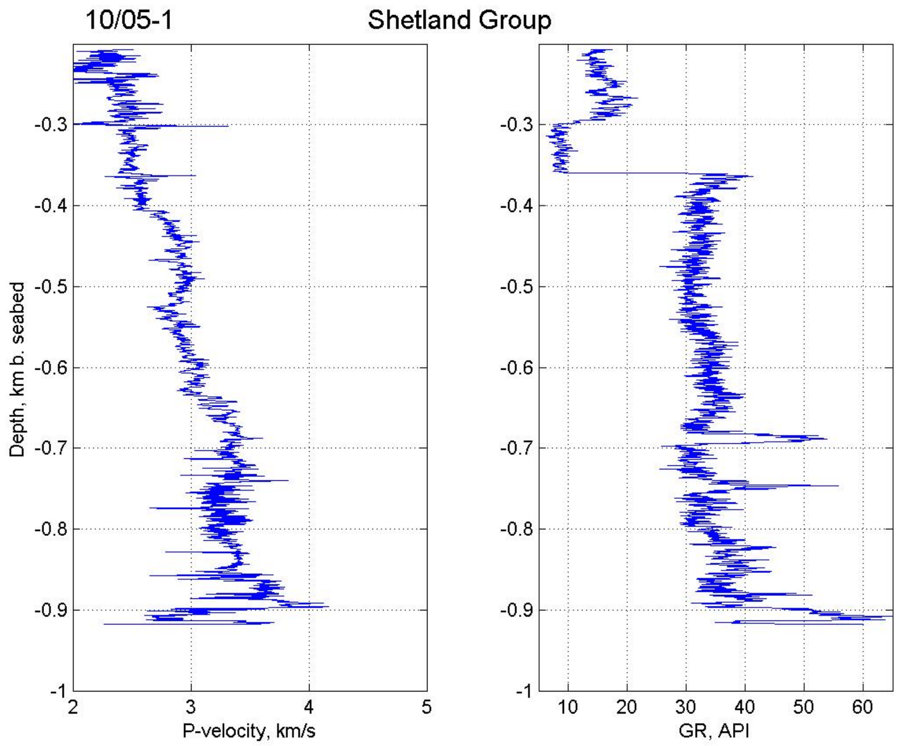
10/05-1
Shetland Group
Depth, km b. seabed
P-velocity, km/s
GR, API

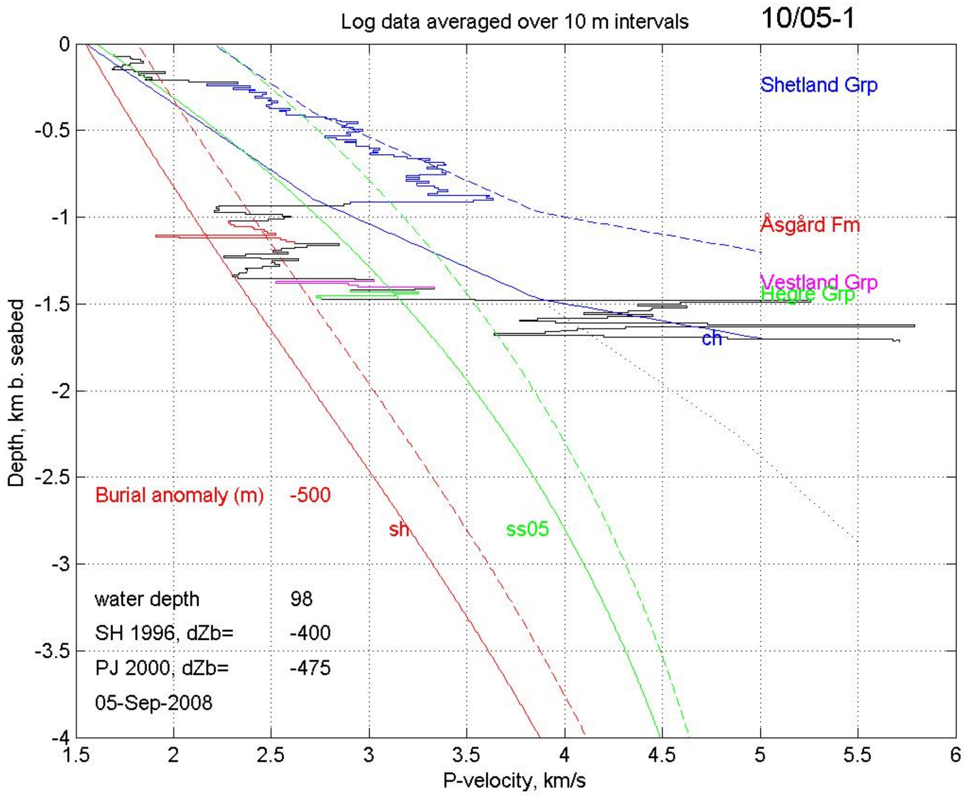

10/05-1

Post-chalk: Almost no data

Chalk: Thick chalk sequence with a general increase of sonic velocity with depth. The gamma log is not properly corrected below the casing at 0.36 km, but it is likely that the gamma level is low over the main part of the drilled interval. Low-velocity Ekofisk Fm with high gamma level and a drop in velocity just above the basal pure chalk, 0.7-0.85 km.

Pre-chalk: Rapidly varying sonic values above the Vestland Group, 0.9- 1.35 km. High velocities in the Zechstein Group below 1.5 km.

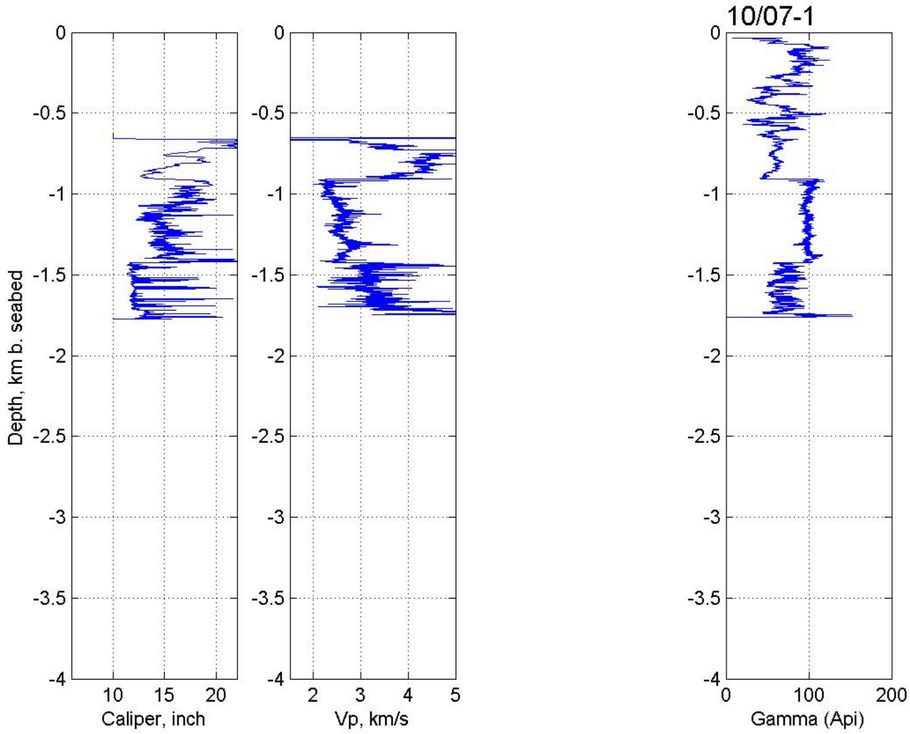
10/07-1
Depth, km b. seabed
0
-0.5
-1
-1.5
-2
-2.5
-3
-3.5
-4
10 15 20
Caliper, inch
2 3 4 5
Vp, km/s
0 100 200
Gamma (Api)

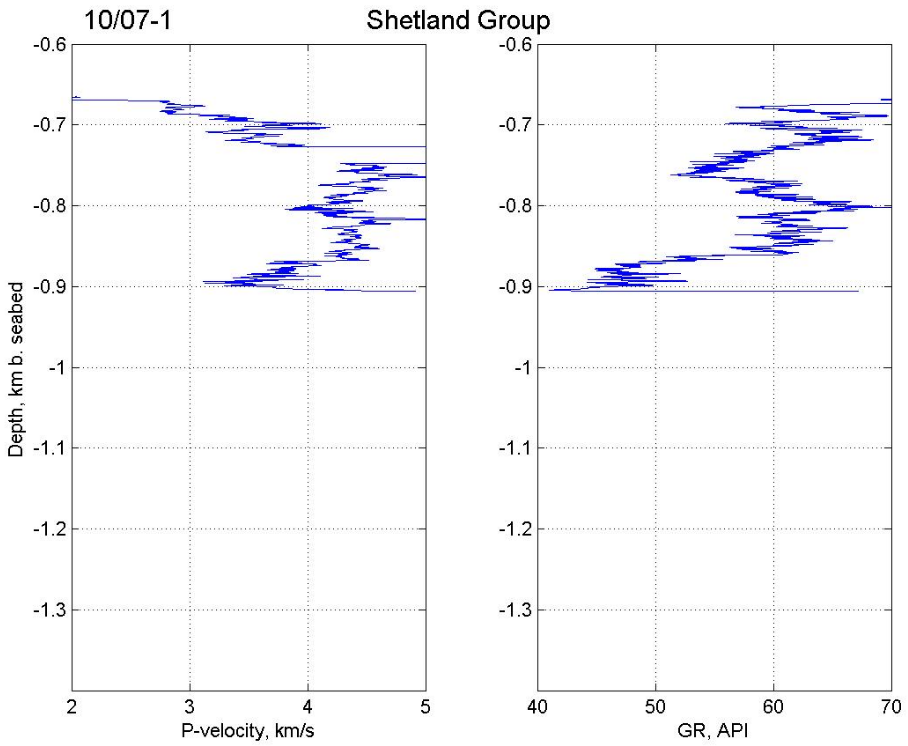
10/07-1
Shetland Group
Depth, km b. seabed
-0.6
-0.7
-0.8
-0.9
-1
-1.1
-1.2
-1.3
2 3 4 5
P-velocity, km/s
40 50 60 70
GR, API

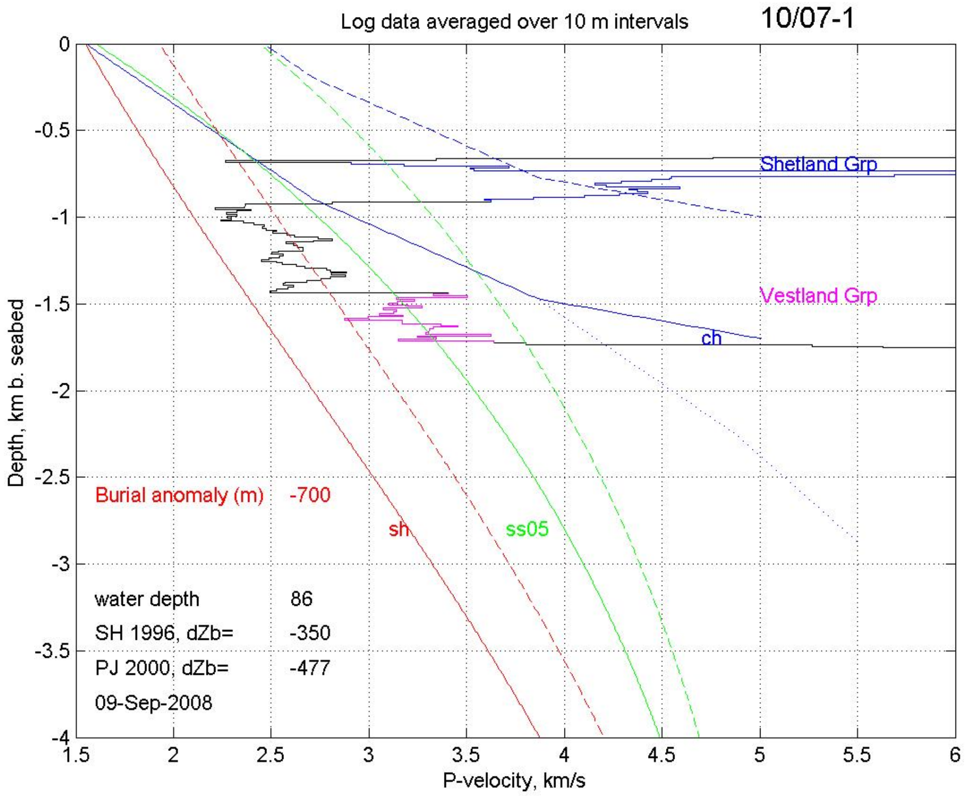

10/07-1

Post-chalk: No data

Chalk: Erroneous sonic data, 0.73-0.75 km, and widely scattered gamma over the entire chalk interval. Stable maximum velocities around 4.25 km/s, 0.75-0.86 km.

Pre-chalk: Two pronounced velocity peaks in the shale-dominated interval above the Vestland Group, 0.9-1.4 km. No correlation with stable gamma log.

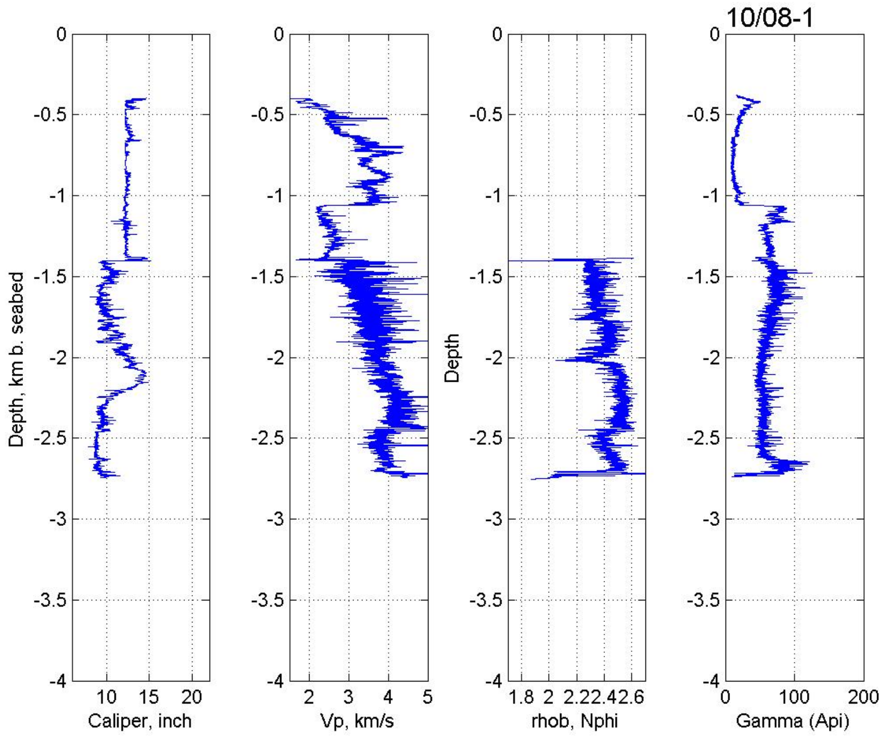
10/08-1
Depth, km b. seabed
Caliper, inch
Vp, km/s
Depth
rhob, Nphi
Gamma (Api)

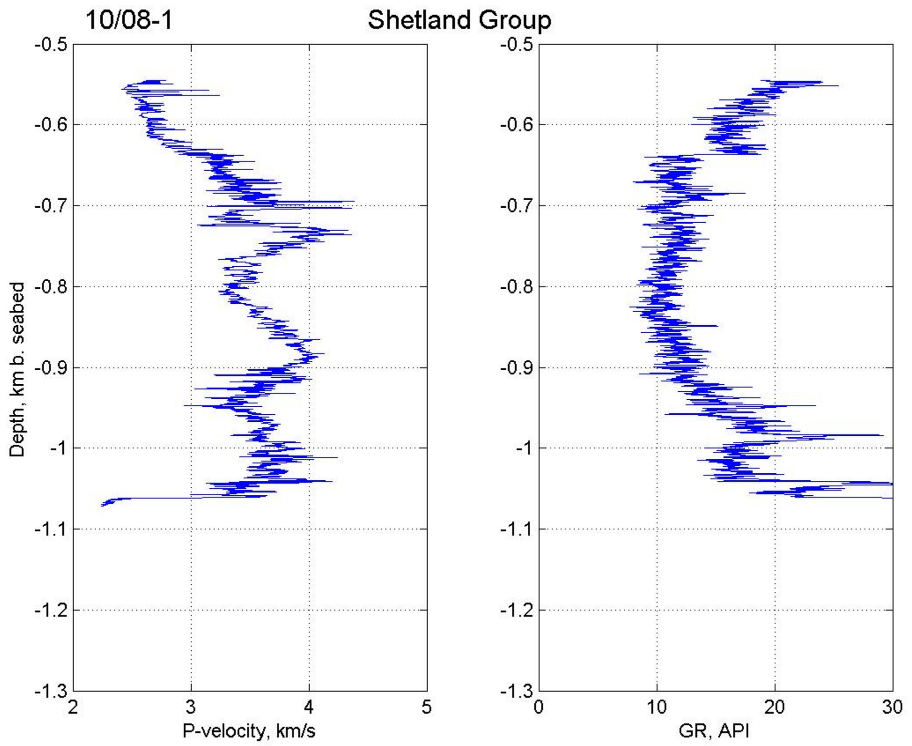
10/08-1
Shetland Group
Depth, km b. seabed
P-velocity, km/s
GR, API

10/8-1

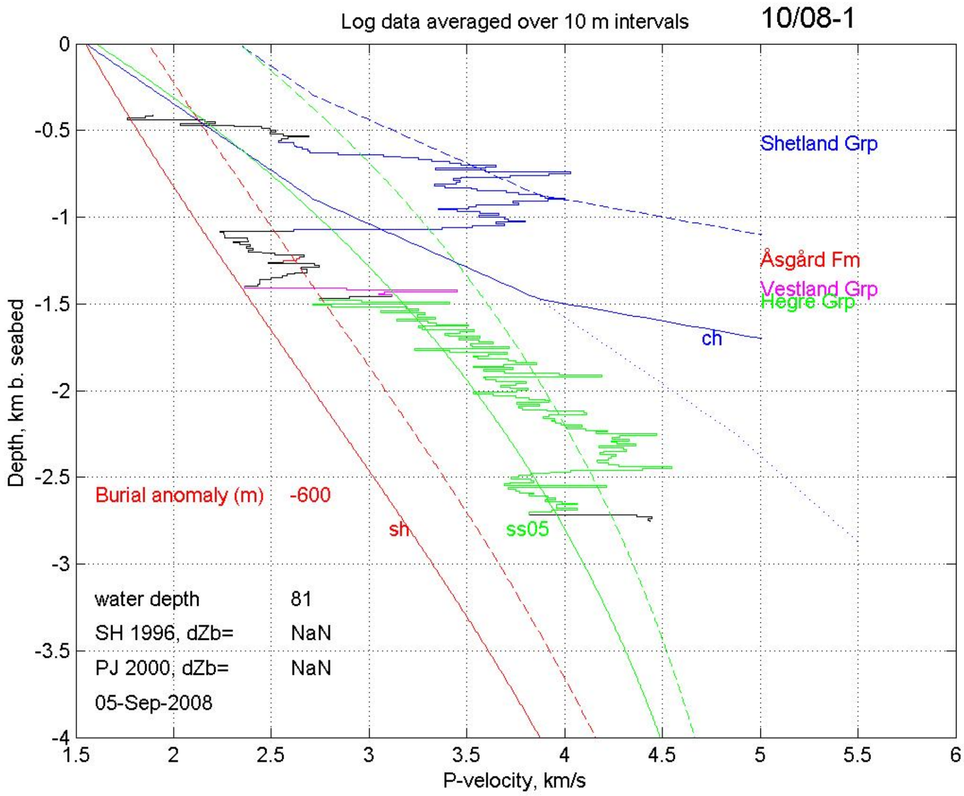

10/08-1

Post-chalk: No data

Chalk: Low velocities for the Ekofisk Fm corresponds to high gamma, above 0.64 km. Velocity inversion below 0.9 km also corresponds to high gamma. Large velocity variations, 0.7-1.0 km, make determination of chalk trend difficult.

Pre-chalk: One pronounced velocity peak in the shale-dominated interval above Tau Fm, 1.1-1.4 km. Thick sandstone sequence of the Hegre Group (Skagerrak Fm) penetrated including a 200 m thick high-velocity unit above the base of the Skagerrak Fm, c. 2.3-2.5 km (cf. 11/9-1). According to NPD report 26 anhydrite is present throughout the basal 500 m of the Skagerrak Fm including limestone units and it is thus possible that the highest velocities in this interval reflect these lithologies. The absolute level for the sonic velocity of pure sandstone is thus not easy to establish.

Cf. NPD paper no. 26

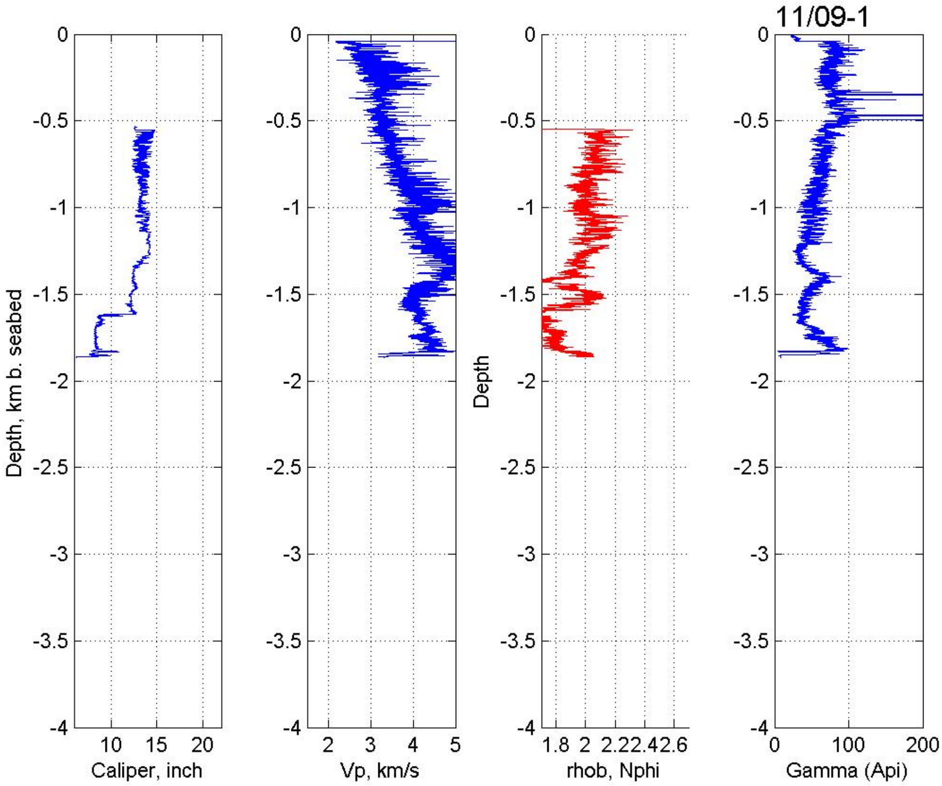
11/09-1
Depth, km b. seabed
Caliper, inch
Vp, km/s
Depth
rhob, Nphi
Gamma (Api)

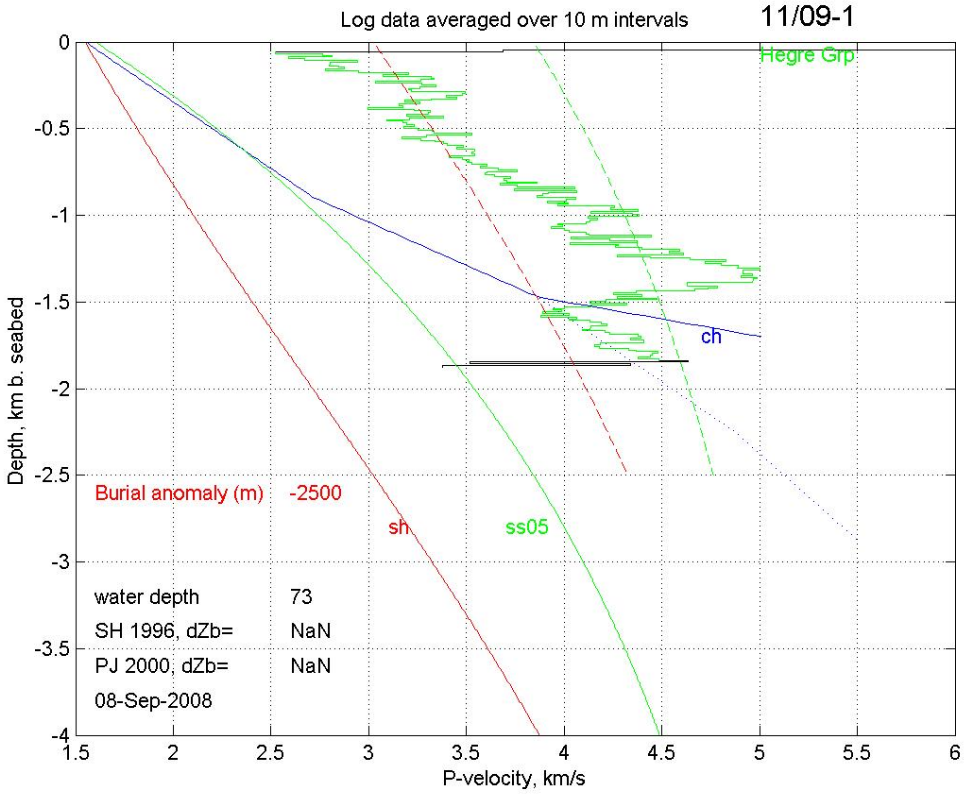

11/09-1
Post-chalk: -

Chalk: -

Pre-chalk: Thick Hegre Group (Skagerrak Fm) penetrated, 0.2-1.8 km. The sonic log shows wide variations across the drilled sequence, 2.5-5 km/s, corresponding to a complex sand-shale lithology probably with stringers of carbonate and anhydrite (cf. 10/8-1).

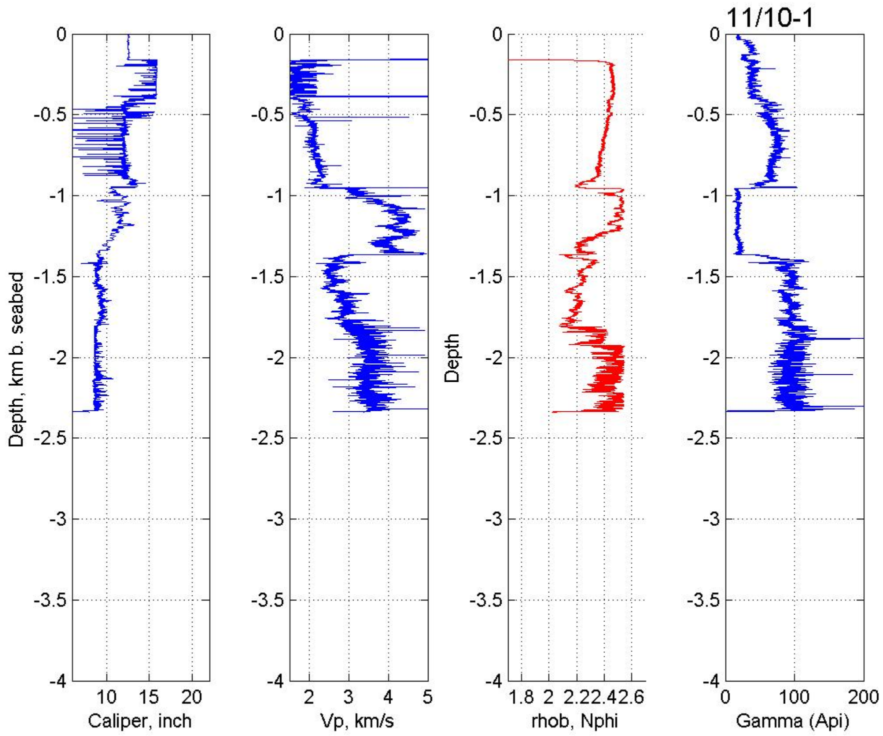
11/10-1
Depth, km b. seabed
Caliper, inch
Vp, km/s
Depth
rhob, Nphi
Gamma (Api)

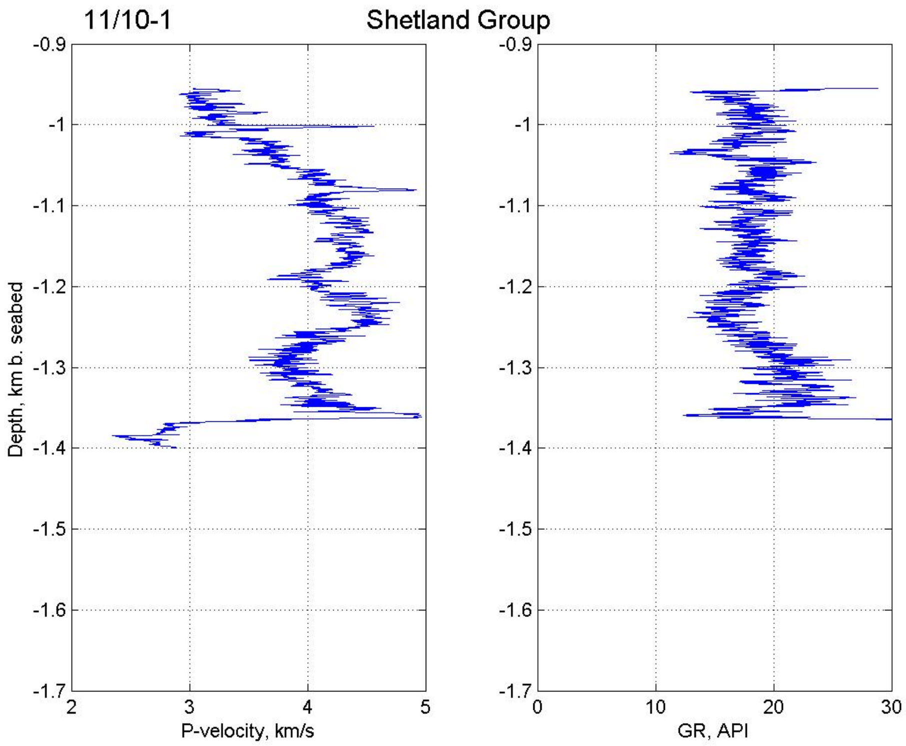
11/10-1
Shetland Group
Depth, km b. seabed
P-velocity, km/s
GR, API

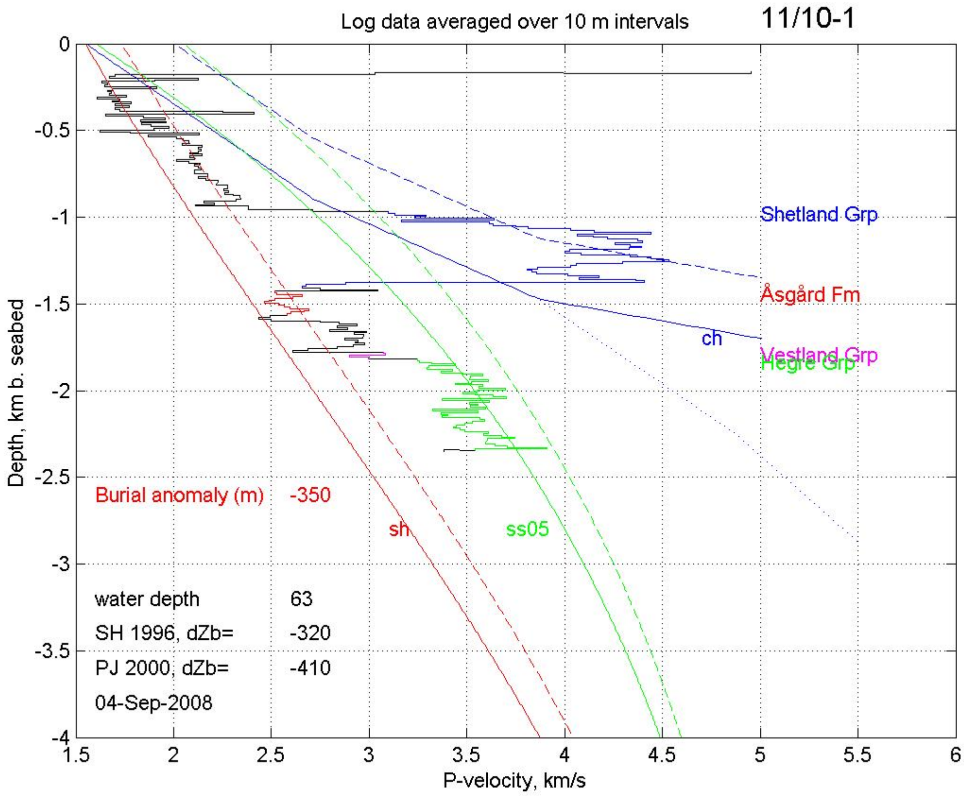

11/10-1

Post-chalk: Increase of velocity with depth, 0.4-0.9 km. Low velocities above this level indicative of unconformity? (coinciding with change in gamma)

Chalk: Large velocity variations over the chalk section, 1.0-1.4 km. Low velocities in the upper part of the chalk and in impure chalk (high gamma) above base chalk. Rapidly varying high velocities, 4.0-4.5 km/s in the intermediate interval, 1.05-1.25 km. Base Shetland too deep; should be at 1.37 km above very high gamma peak.

Pre-chalk: Moderate sonic variations above Vestland Group, 1.4-1.7 km. Relatively high velocities in Saud Fm, between Åsgård Fm and Vestland Group. The Hegre Group (Skagerrak Fm) consists of interbedded shales, sands and clays (NPD 23).

Cf. NPD paper no. 23

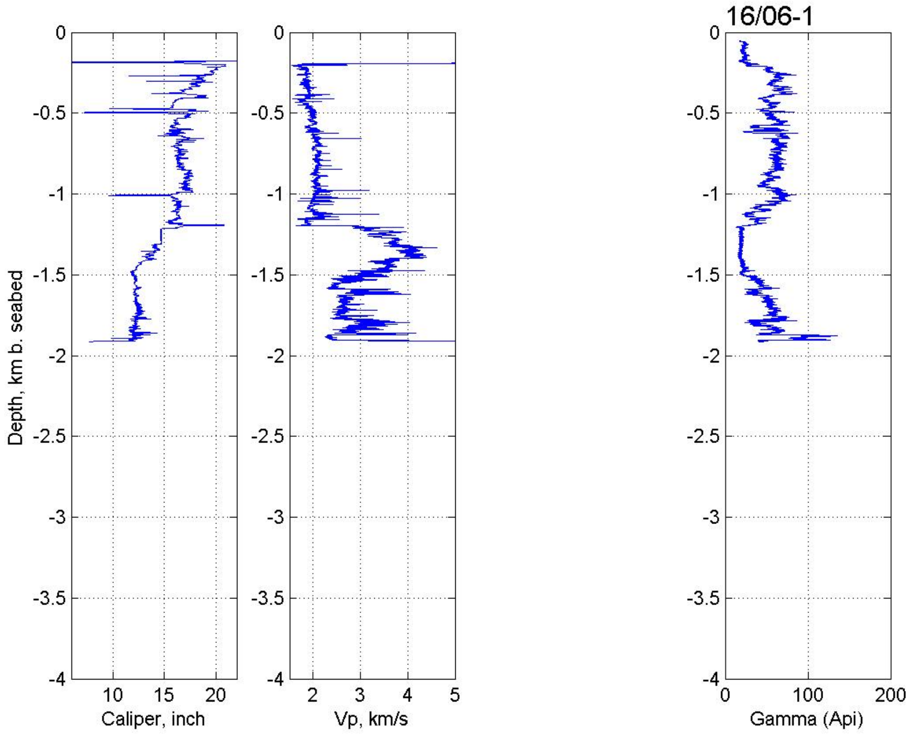
16/06-1
Depth, km b. seabed
Caliper, inch
Vp, km/s
Gamma (Api)

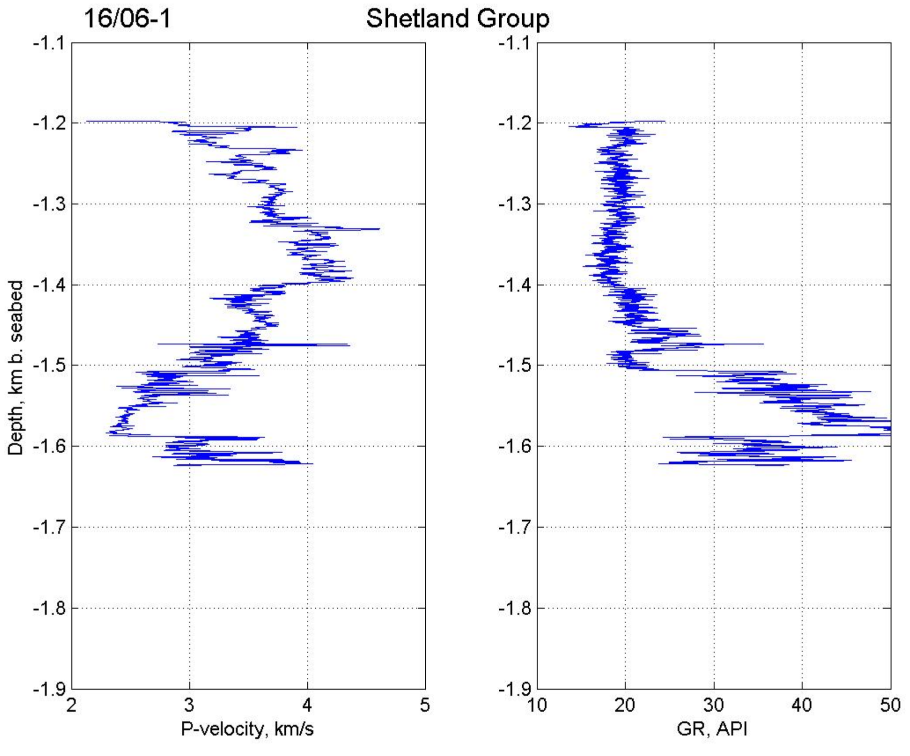
16/06-1
Shetland Group
Depth, km b. seabed
P-velocity, km/s
GR, API

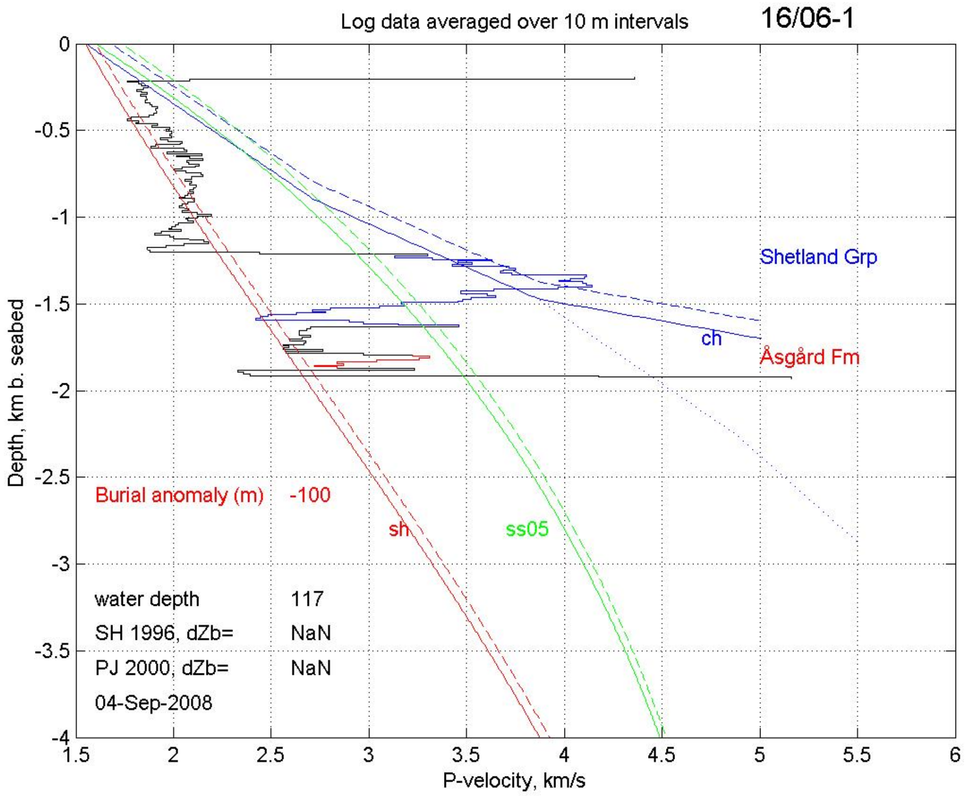

16/06-1

Post-chalk: Moderate sonic variations with no clear depth trend, 0.2-1.0 km, above low-velocity unit, 1.0-1.2 km.

Chalk: Increase of velocity with depth in upper part of the chalk, 1.2-1.4 km. Lower part characterised by velocity inversion corresponding to high gamma. Base Shetland too deep; should be at 1.51 km above very high gamma peak.

Pre-chalk: Rapid sonic variations with pronounced peaks.

cf. NPD paper no. 9.

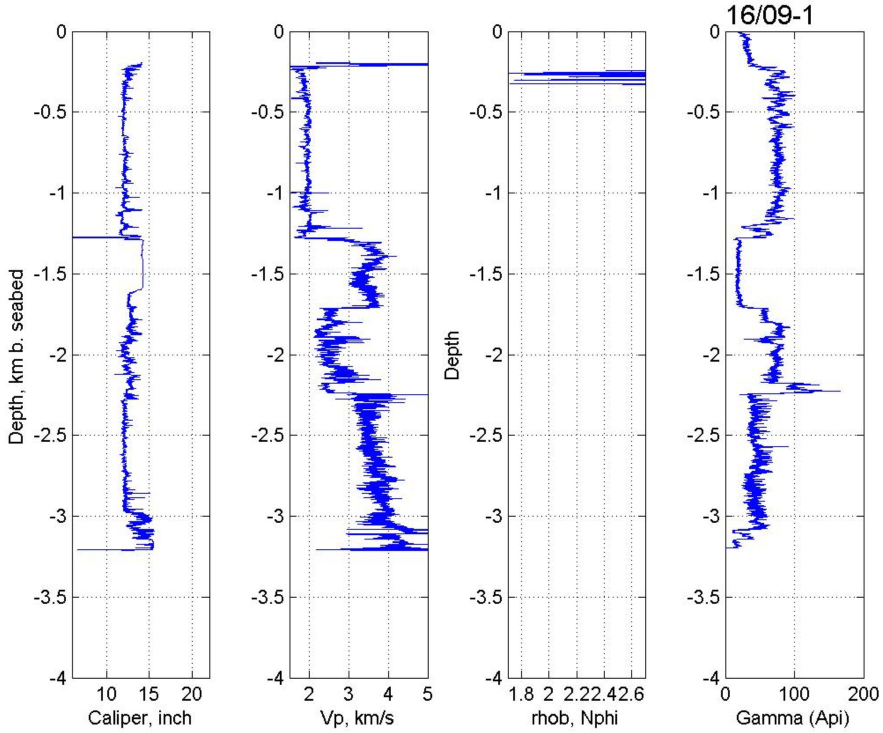
16/09-1
Depth, km b. seabed
Caliper, inch
Vp, km/s
Depth
rhob, Nphi
Gamma (Api)

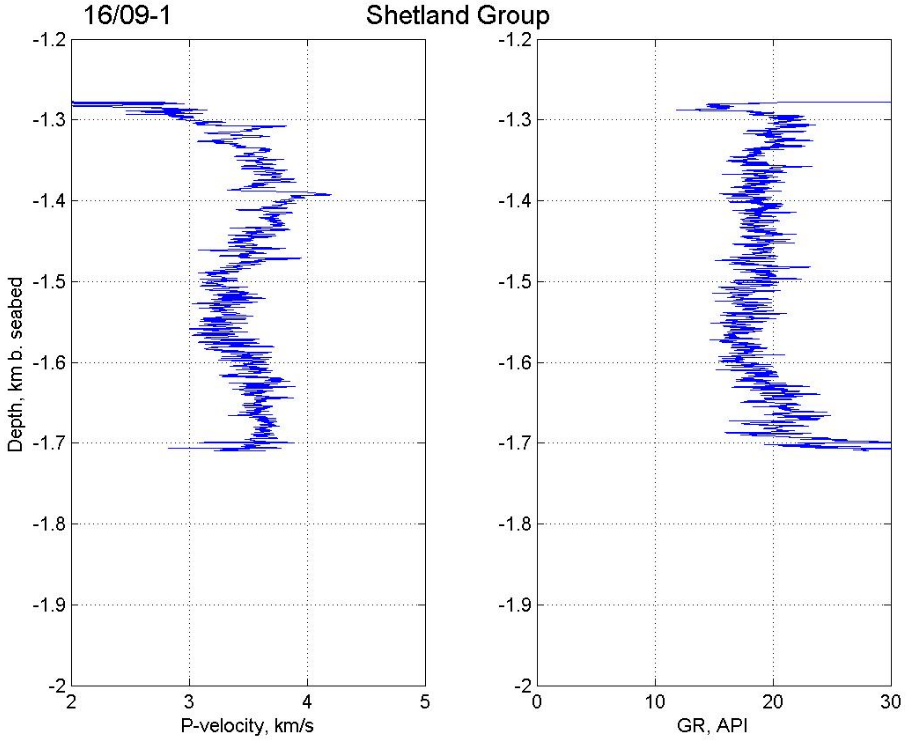
16/09-1
Shetland Group
Depth, km b. seabed
P-velocity, km/s
GR, API

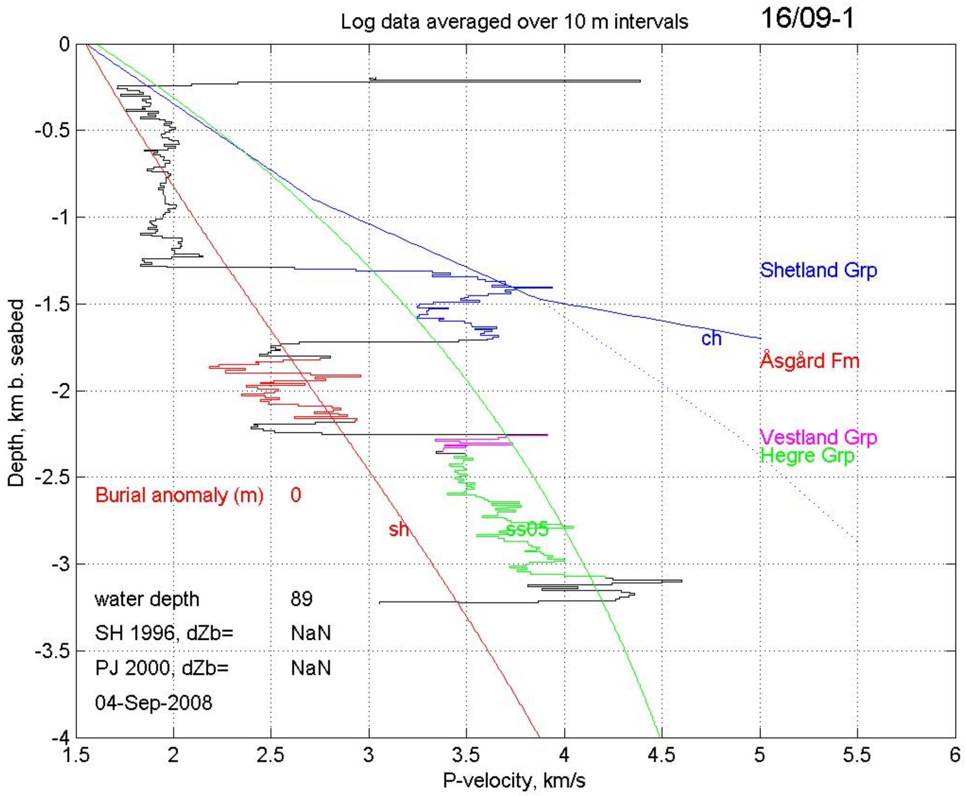

16/09-1

Post-chalk: Minor velocity variations, 0.3-1.3 km – increasing velocity with depth above 0.5 km followed by constant velocity interrupted by low-velocity units, 0.5-1.3 km. This could be indicative of moderate buildup of overpressure towards the top of the Shetland Group.

Chalk: Increasing velocity with depth in the uppermost part, 1.28-1.40 km followed by a broad low-velocity zone (typically indicative of impure chalk) followed by basal high-velocity chalk. This pattern is not reflected on the gamma log that could be erroneous.

Pre-chalk: Pronounced and rapid sonic variations above the Tau Fm, 1.7-2.2 km (mainly over the Åsgård Fm). High velocities in the thick series of interbedded sandstone, silt-stones and clays of the Hegre Group (Skagerrak Fm), 2.4-3.1 km.

Cf. NPD paper no. 11.

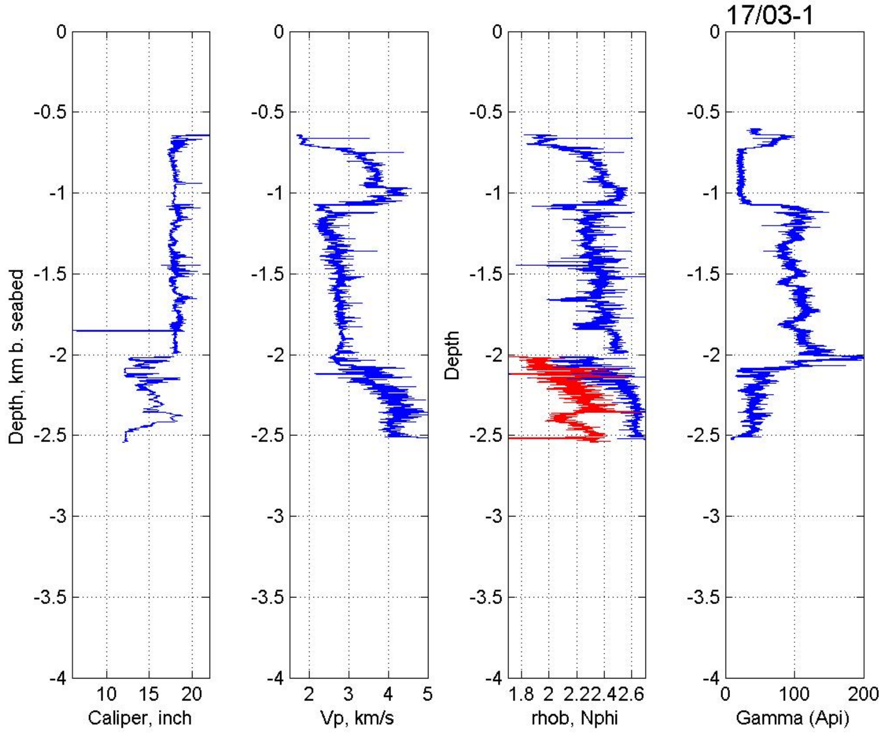
17/03-1
Depth, km b. seabed
Caliper, inch
Vp, km/s
Depth
rhob, Nphi
Gamma (Api)

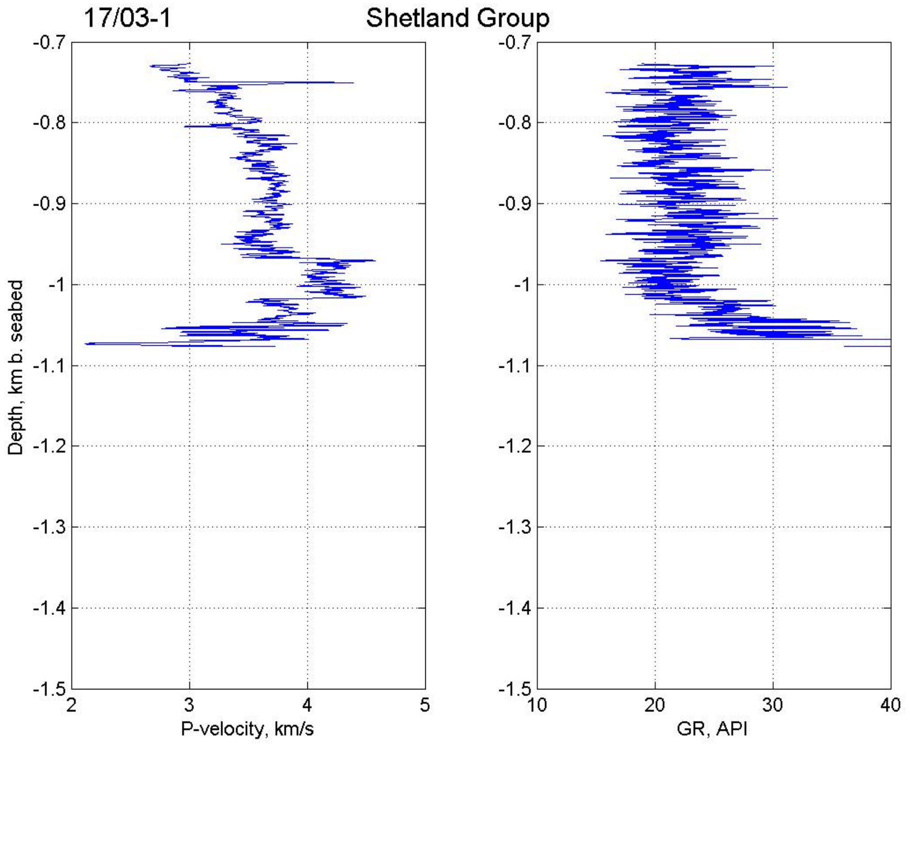
17/03-1
Shetland Group
Depth, km b. seabed
P-velocity, km/s
GR, API

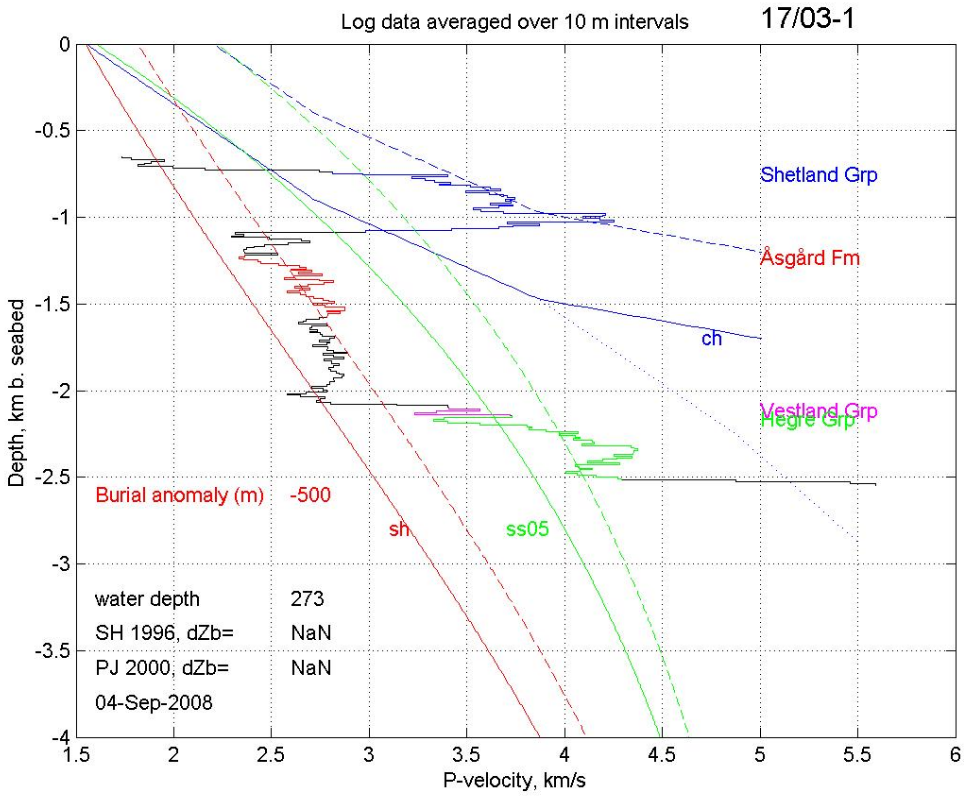

17/03-1
Post-chalk: Almost no data

Chalk: General increase of velocity over the uppermost part of the chalk, 0.73-1.2 km, with a very high velocity unit at c. 1 km. Fluctuating gamma log with very high values above the base of the chalk.

Pre-chalk: General increase of velocity with depth and only minor fluctuations above the Tau Fm (excluding very low values between the chalk and Åsgård Fm), 1.2-1.8 km. High velocities that probably reflect thick sandstone units of the Hegre Group (Smith Bank Fm) at c. 2.3 km (no details available).

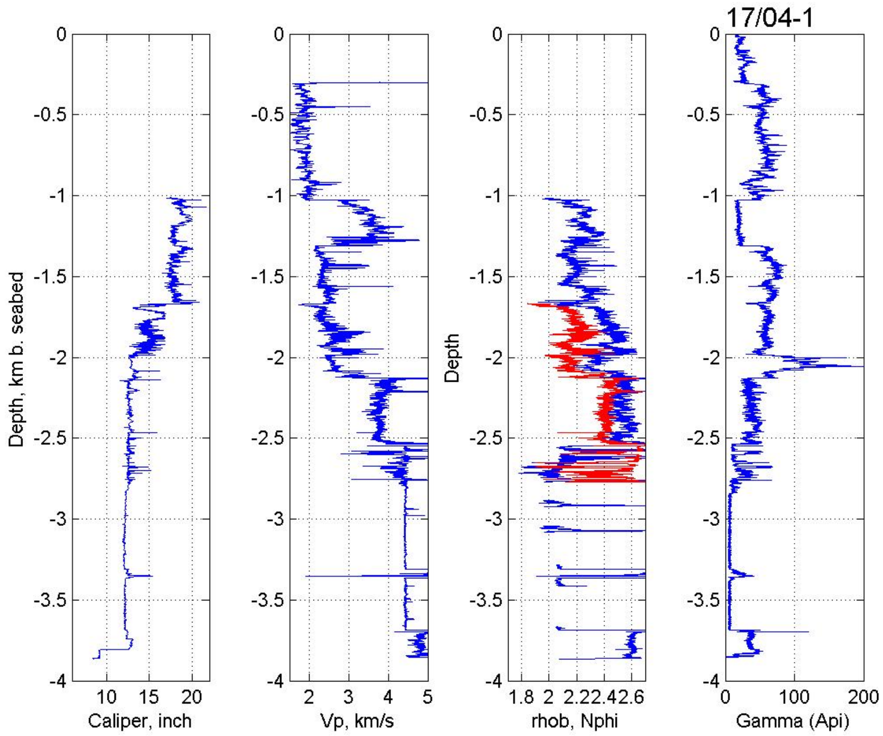
17/04-1
Depth, km b. seabed
Caliper, inch
Vp, km/s
Depth
rhob, Nphi
Gamma (Api)

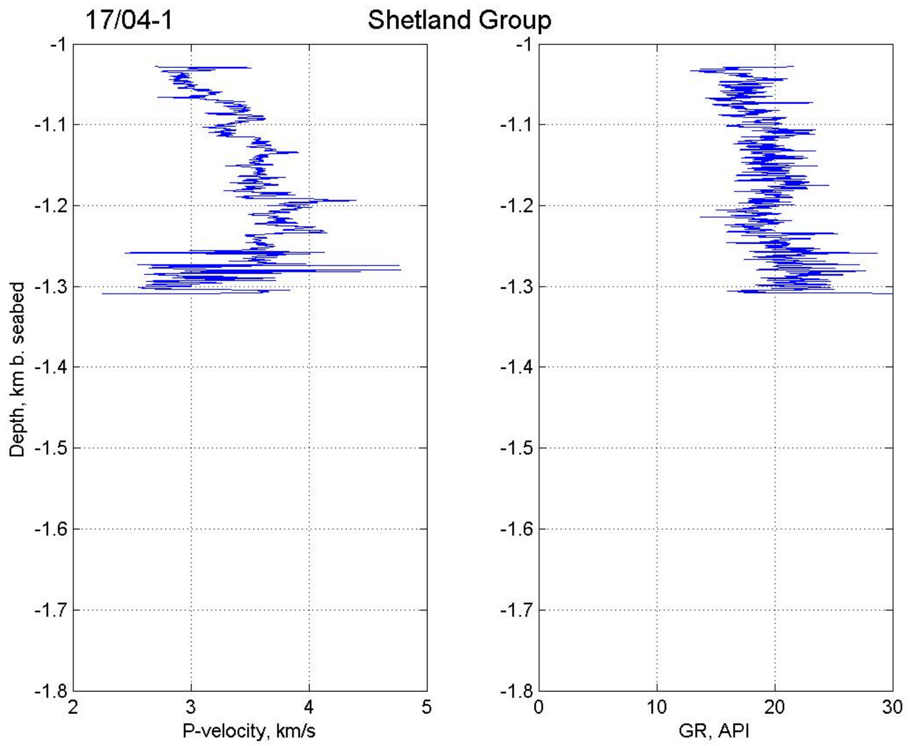
17/04-1
Shetland Group
Depth, km b. seabed
P-velocity, km/s
GR, API

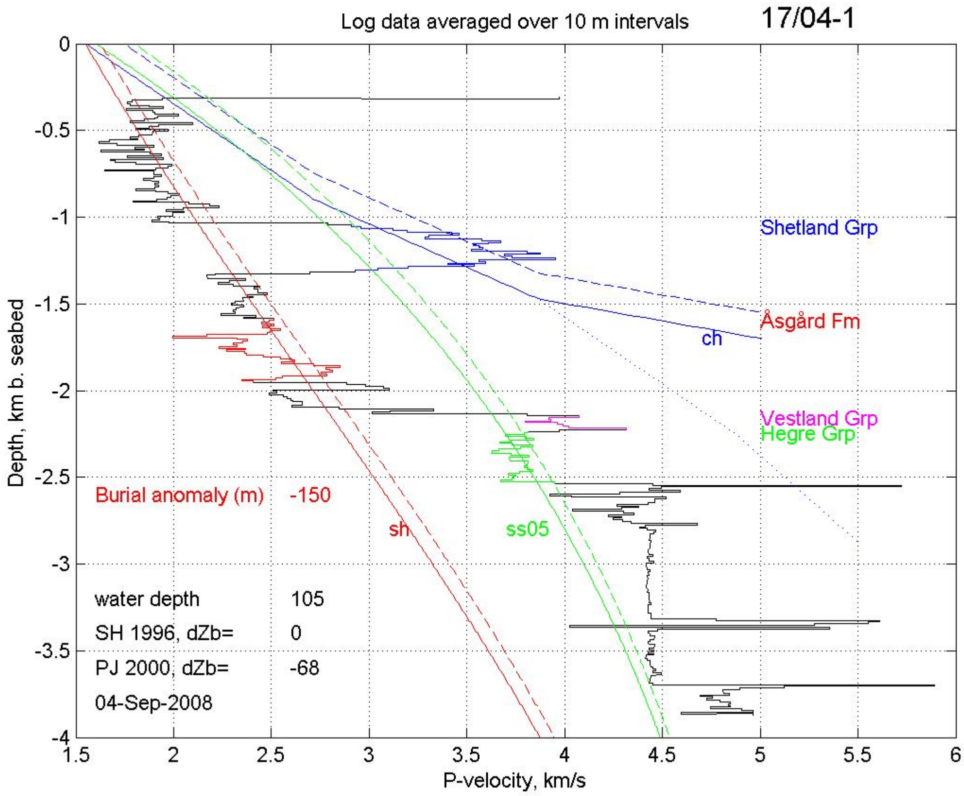

17/04-1

Post-chalk: Scattered sonic data with steady increase of maximum values in the deeper part, 0.5-1.1 km.

Chalk: General increase of velocity with depth, 1.03-1.24 km, above basal impure chalk unit (high gamma). Small gamma variations relative to low basal level.

Pre-chalk: Rapidly changing velocities above the Vestland Group, 1.3-2.2 km. High velocities (c. 4 km/s) in the Middle Jurassic sandstones of the Vestland Group, 2.2-2.3 km. overlying less high-velocity sandstones interbedded with claystone of the Hegre Group.

Cf. NPD paper no. 14.

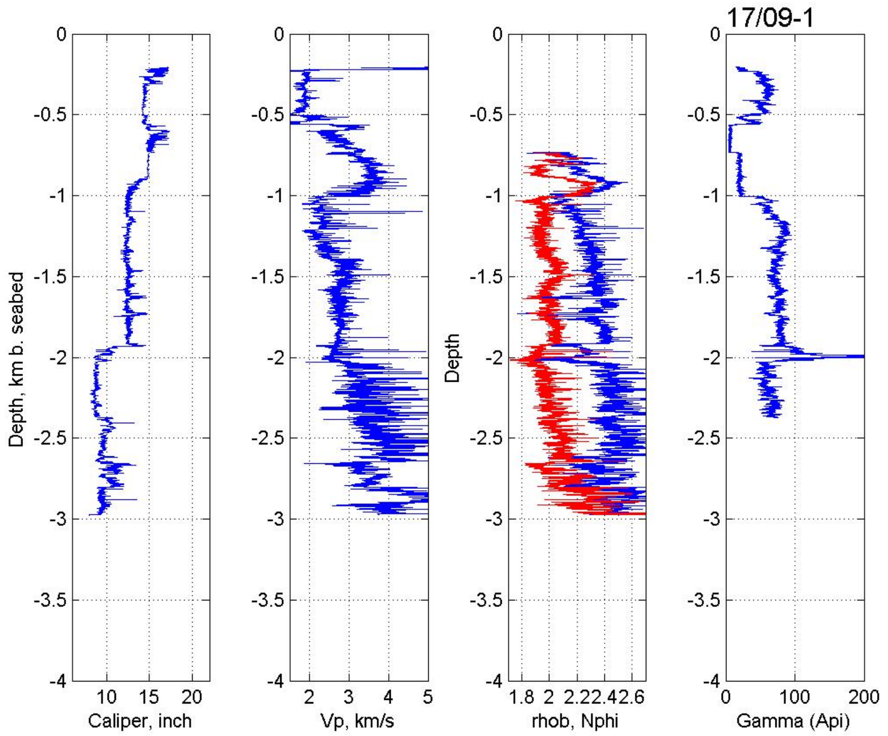
17/09-1
Depth, km b. seabed
Caliper, inch
Vp, km/s
Depth
rhob, Nphi
Gamma (Api)

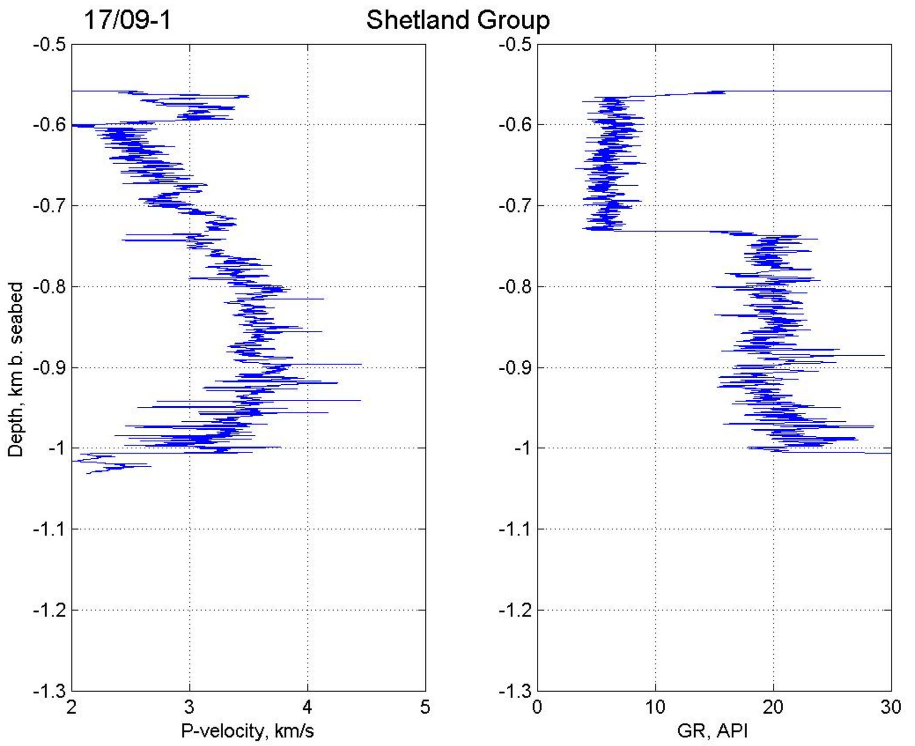
17/09-1
Shetland Group
Depth, km b. seabed
P-velocity, km/s
GR, API

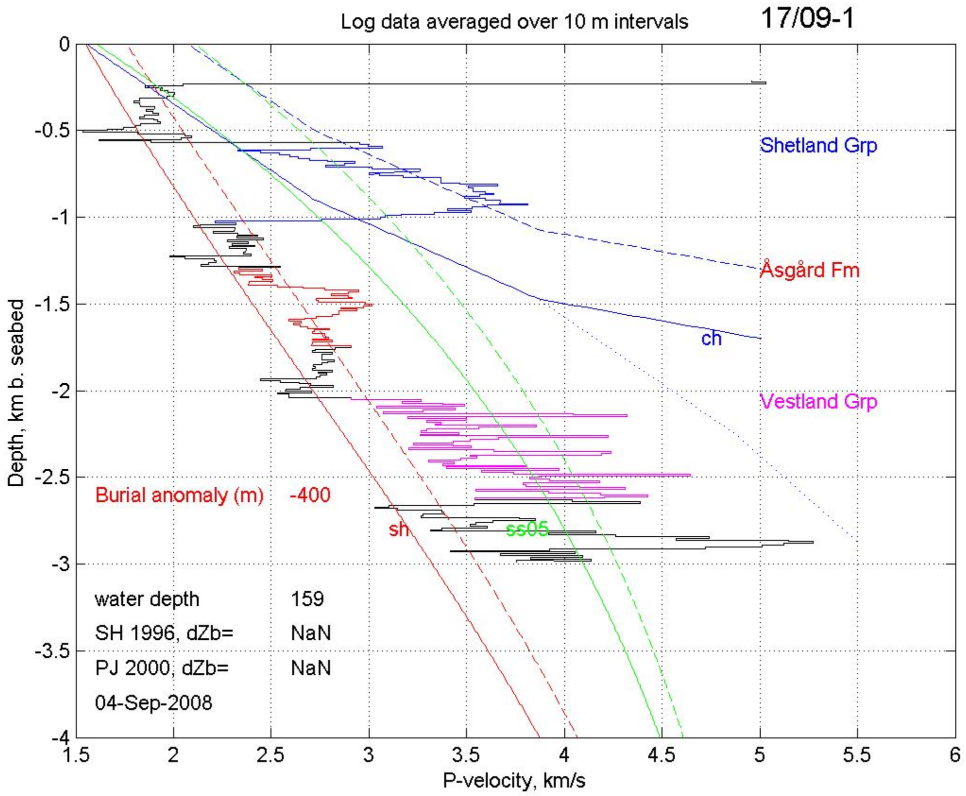

17/09-1

Post-chalk: Moderate sonic variations (disregarding erroneous low-velocity intervals), 0.2-0.5 km.

Chalk: Increase of velocity with depth, 0.6-0.9 km, between high-velocity Ekofisk Fm (low gamma) and basal impure chalk unit. Gamma log jumps to high values across casing at 0.73 km, but probably small gamma variations relative to low basal level. Anomalously low velocities, <3 km/s, in upper part of Tor Fm compared to its lower part. Porosity preservation due to former presence of hydrocarbons?

Pre-chalk: Varying sonic data above Tau Fm, 1.0-2.1 km. Velocity troughs correspond to the Sola and Tau Fms. Sonic increase with depth disregarding these troughs and the high-velocity upper part of the Åsgård Fm. Rapid sonic variations over the Vestland Group.

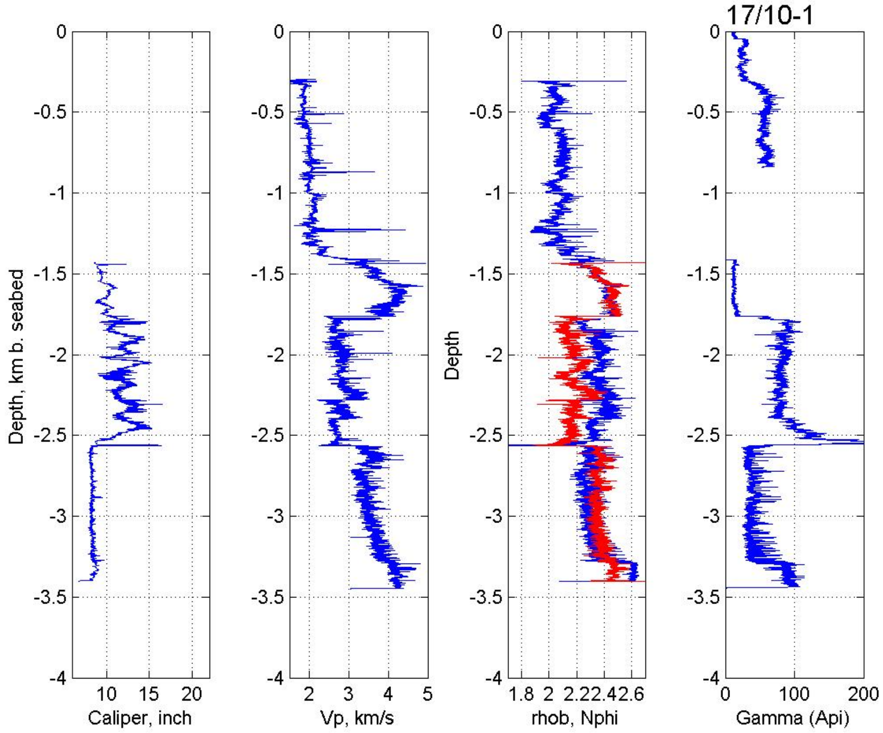
17/10-1
Depth, km b. seabed
Caliper, inch
Vp, km/s
Depth
rhob, Nphi
Gamma (Api)

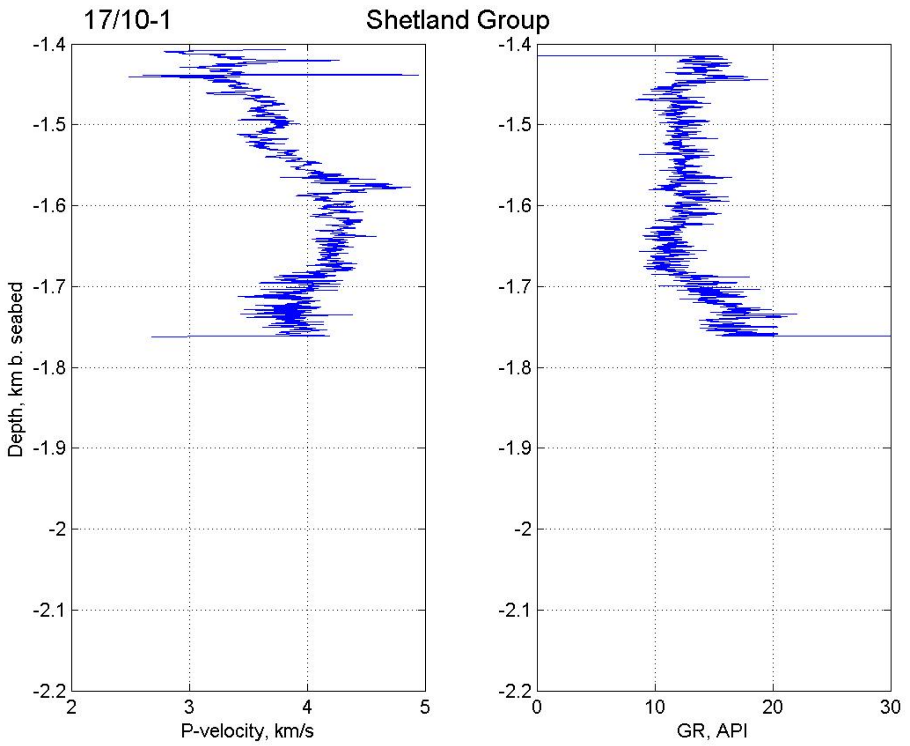
17/10-1
Shetland Group
Depth, km b. seabed
P-velocity, km/s
GR, API

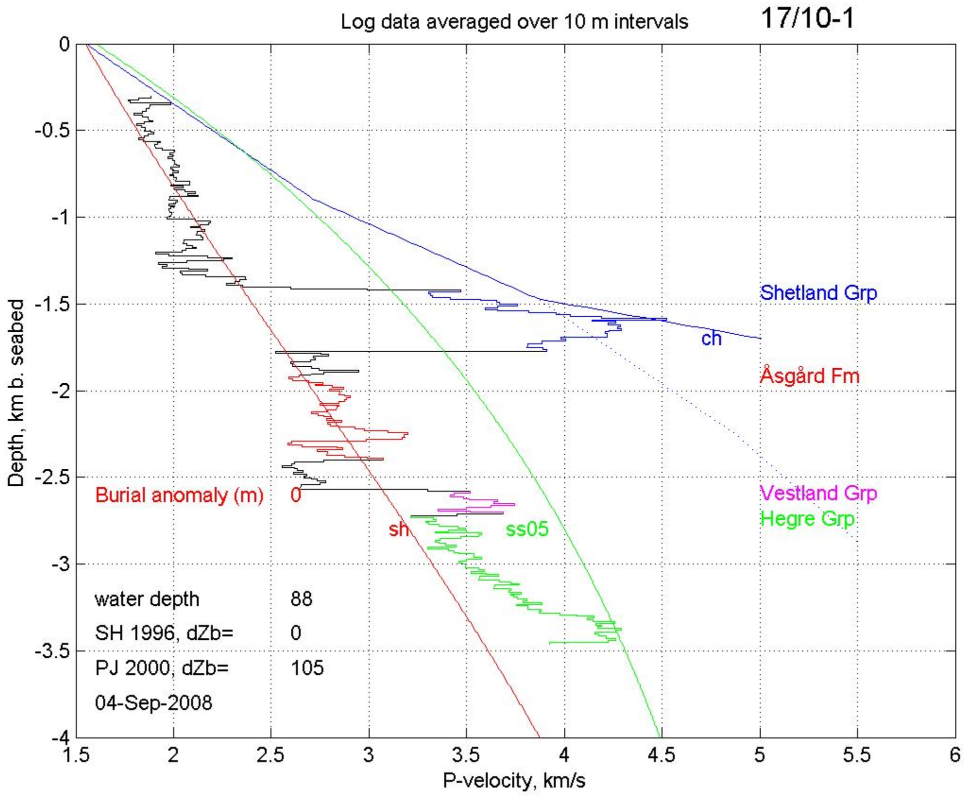

17/10-1

Post-chalk: Moderate velocity variations with more low-velocity intervals towards the base (indicating overpressure?), 0.3-1.3 km. Almost constant velocity, 0.6-1.0 km.

Chalk: General increase of velocity with depth, 1.4-1.58 km (pronounced peak at c. 1.58 km). Low gamma base level apart from gamma peaks in the upper- and lowermost chalk where both intervals have relatively low velocities.

Pre-chalk: Moderate sonic variations above Vestland Group (disregarding low-velocity trough corresponding to Tau Fm and the overlying remaining part of the Boknfjord Group; high gamma), 1.75-2.4 km. High velocities of the Vestland Group (Gassum Fm) reflect an interval of mainly arenaceous sandstone with only thin layers of shale. Velocity is increasing with depth throughout the Hegre Group; the basal high-velocity unit, c. 3.3-3.4 km, is interpreted as silty claystone of the Smith Bank Fm with increasing amounts of anhydrite towards the base and this may be responsible for the high sonic velocity of this interval. The overlying interval, 2.7-3.3 km with lower velocities is the Skagerrak Fm where the interval below c. 3 km is dominantly sandstone.

Cf. NPD paper no. 21.

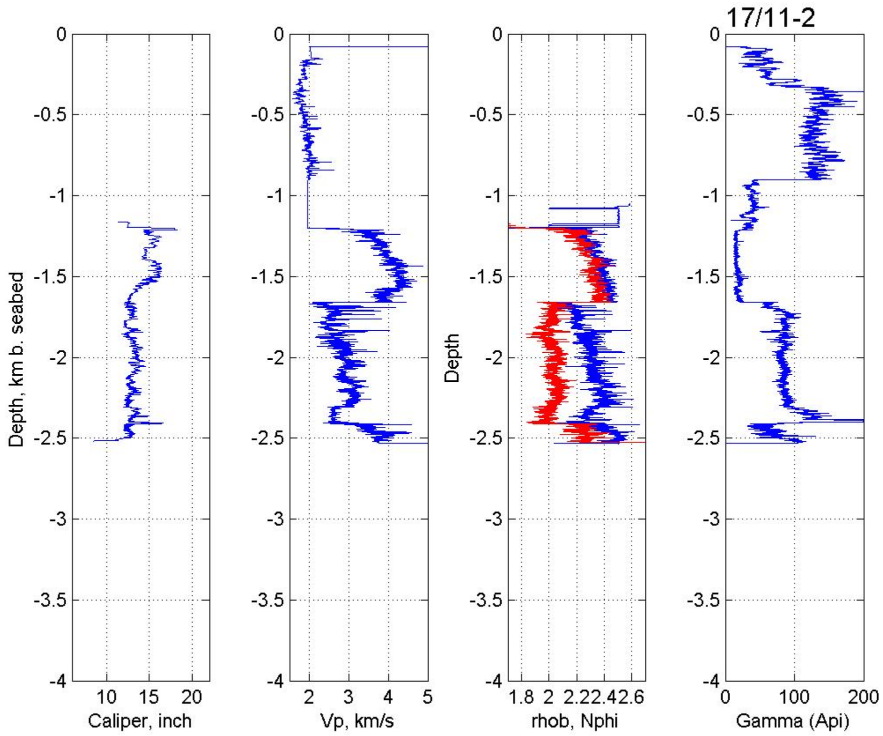
17/11-2
Depth, km b. seabed
Caliper, inch
Vp, km/s
Depth
rhob, Nphi
Gamma (Api)

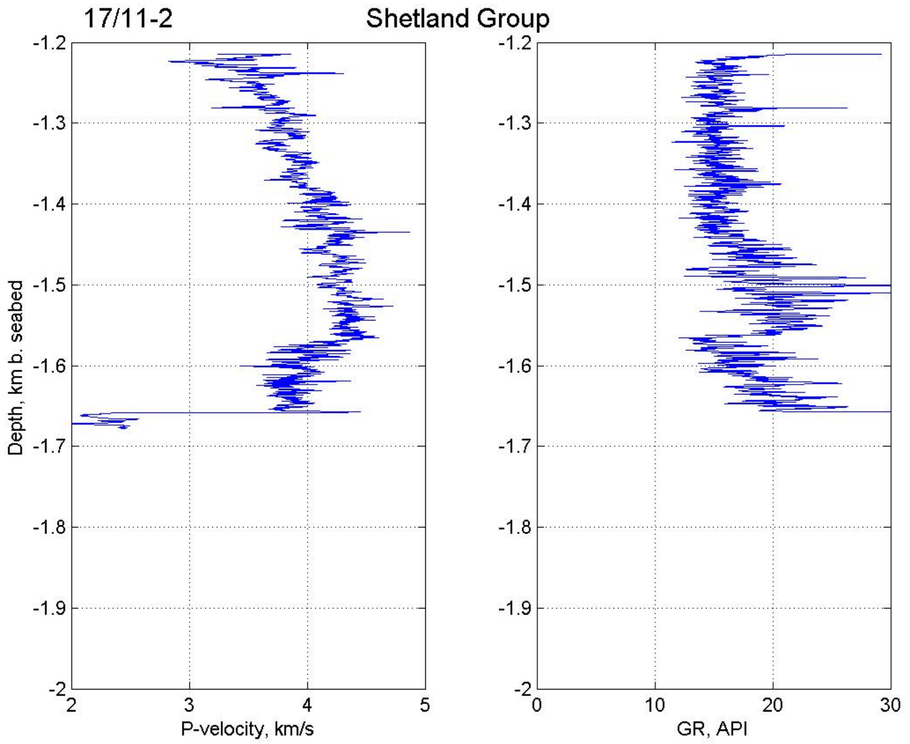
17/11-2
Shetland Group
Depth, km b. seabed
P-velocity, km/s
GR, API

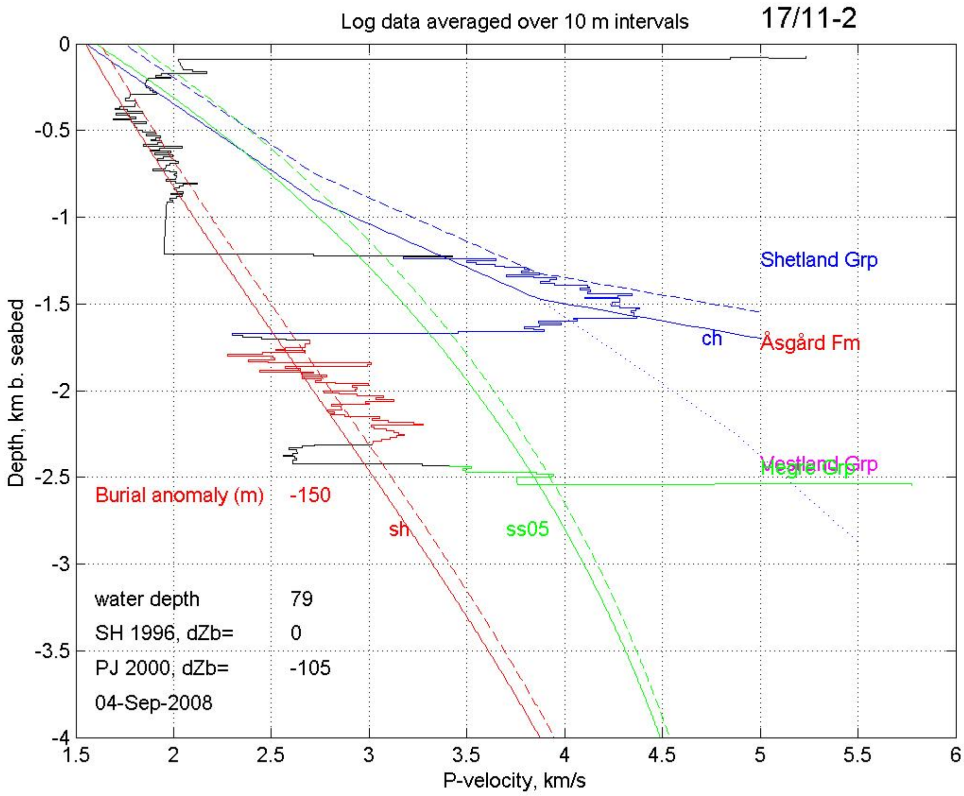

17/11-2

Post-chalk: Increase of sonic with depth, 0.3-0.8 km (data gap, 0.8-1.2 km).

Chalk: Increase of sonic with depth above basal low-velocity chalk, 1.2-1.5 km. Small gamma variations relative to low basal level, however, atypical pattern in the lower part of the chalk where high gamma at c. 1.5 km does not correspond to increase in sonic velocities whereas a drop in gamma below that depth results in a reduction in velocity.

Pre-chalk: Rapid sonic variations above Tau Fm, 1.7-2.3 km.

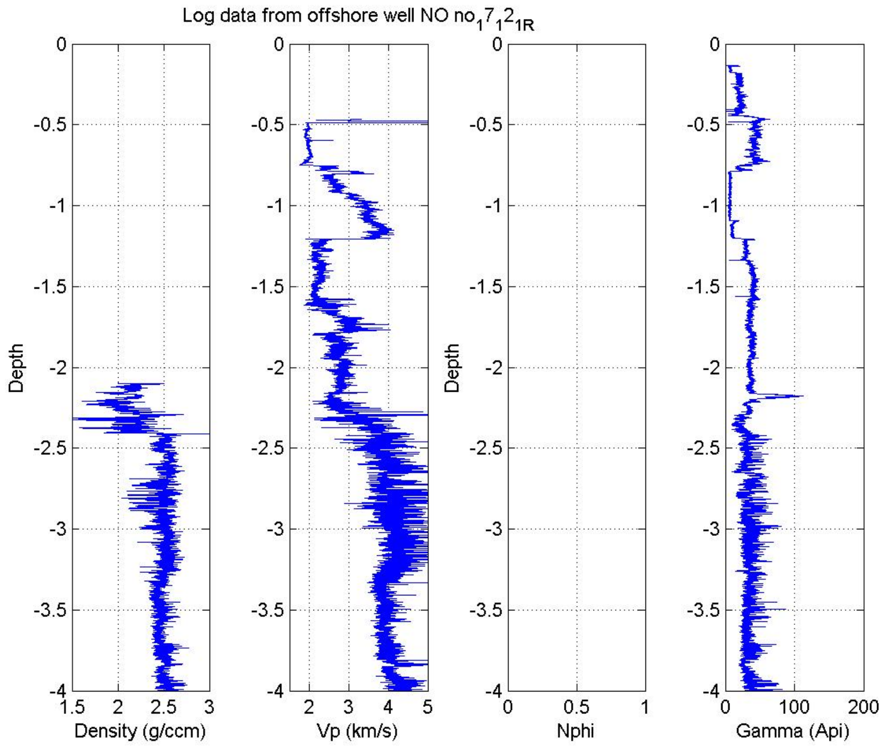
Log data from offshore well NO no_7_2_1R
Depth
Density (g/ccm)
Vp (km/s)
Nphi
Gamma (Api)

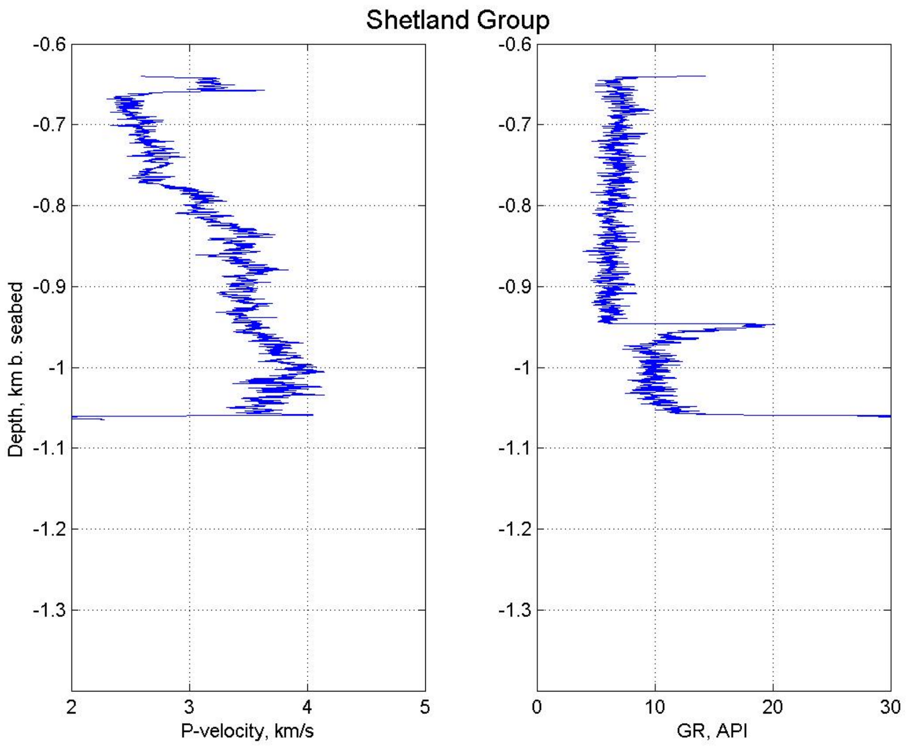
Shetland Group
Depth, km b. seabed
P-velocity, km/s
GR, API

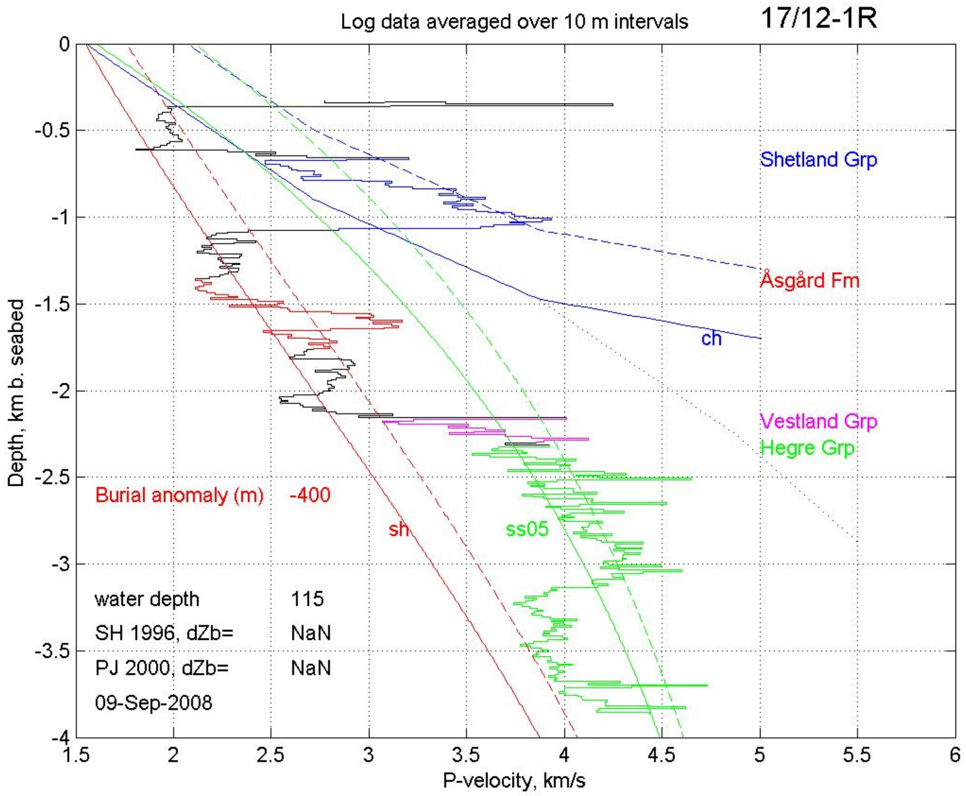

17/12-1R

Post-chalk: Only data over a limited interval, 0.4-0.6 km, but a well-defined upper level for the sonic data is identified.

Chalk: General increase of velocity with depth (below high-velocity Ekofisk Fm; bryozoans?), 0.68-1.0 km. Low gamma readings with few fluctuations above casing at 0.96 km. Relatively low velocities in uppermost chalk below Ekofisk Fm; 0.68-0.78 km. Porosity preservation caused by hydrocarbons?

Pre-chalk: Ample sonic variations across fairly thick units above Tau Fm, 1.1-2.0 km. General sonic increase with depth over the upper part of the Hegre Group (Skagerrak Fm) interrupted with thin velocity peaks (anhydrate?), 2.3-3.1 km. Lower part of Skagerrak Fm also reveals a general increase of velocity with depth, but with much lower values; 3.2-3.7 km. No lithological interpretation available for comparison; only “sand development within the Triassic was limited to thin, fine to course grained, continental-type clastic beds” (npd.no).

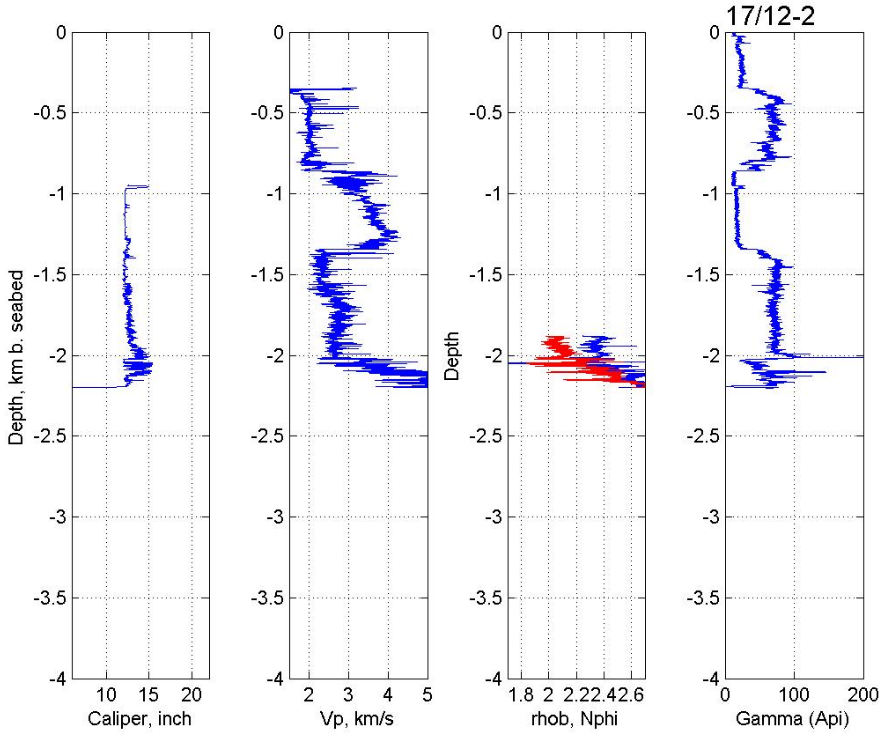
17/12-2
Depth, km b. seabed
Caliper, inch
Vp, km/s
Depth
rhob, Nphi
Gamma (Api)

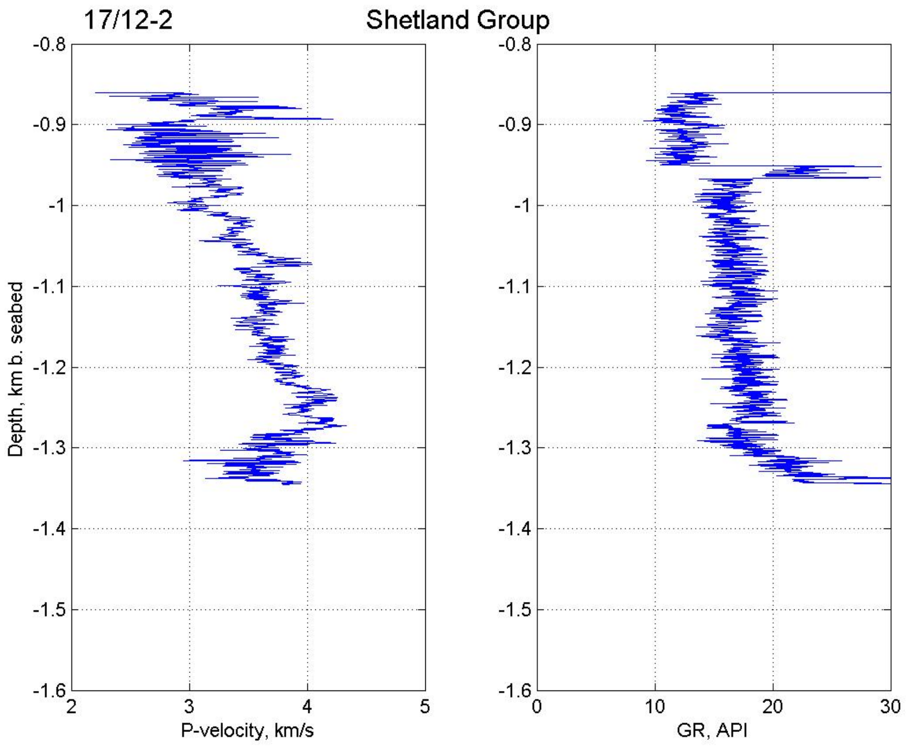
17/12-2
Shetland Group
Depth, km b. seabed
P-velocity, km/s
GR, API

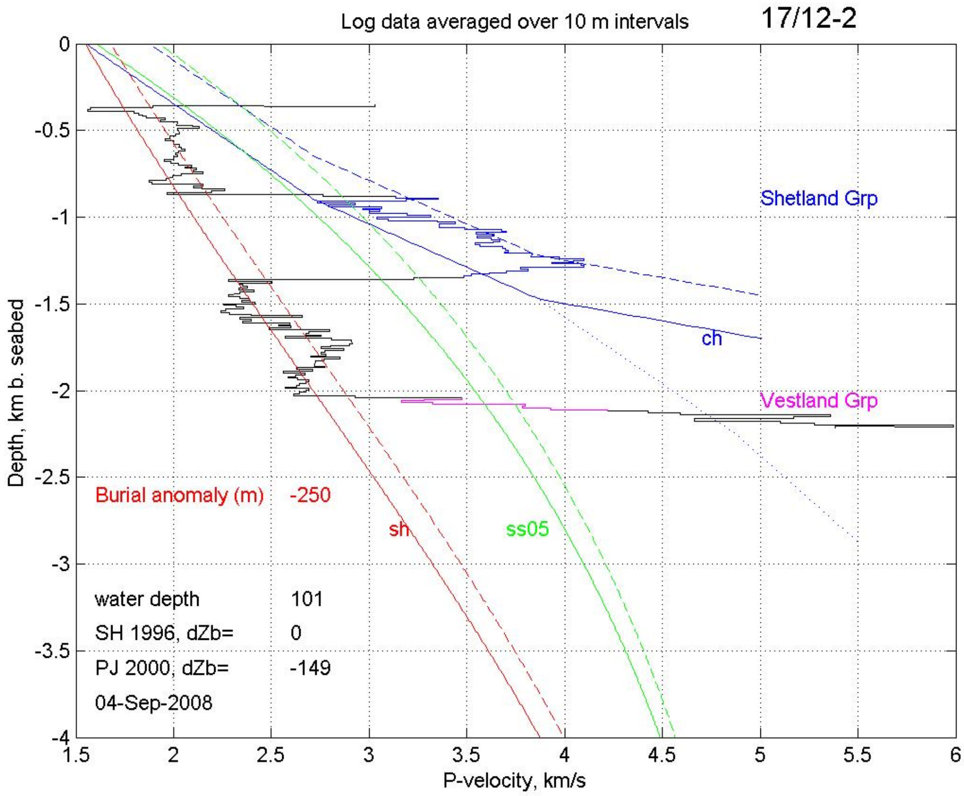

17/12-2

Post-chalk: Data over a limited interval, 0.4-0.8 km, but a well-defined upper level for the sonic data is identified.

Chalk: General increase of velocity with depth over a thick interval (below high-velocity Ekofisk Fm; bryozoans?), 0.85-1.25 km. Low gamma readings with few fluctuations above casing at 0.95 km. Relatively low velocities in uppermost chalk below Ekofisk Fm; 0.9-1.0 l km. Porosity preservation caused by hydrocarbons?

Pre-chalk: Pronounced variations across undifferentiated Cromer Knoll Group, 1.4-2.0 km.

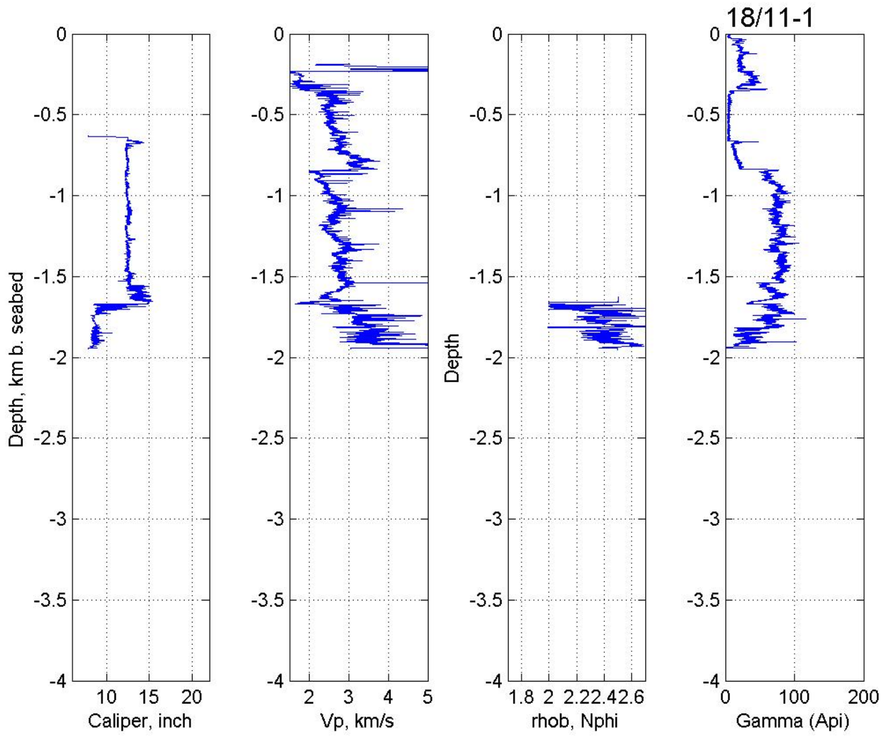
18/11-1
Depth, km b. seabed
Caliper, inch
Vp, km/s
Depth
rhob, Nphi
Gamma (Api)

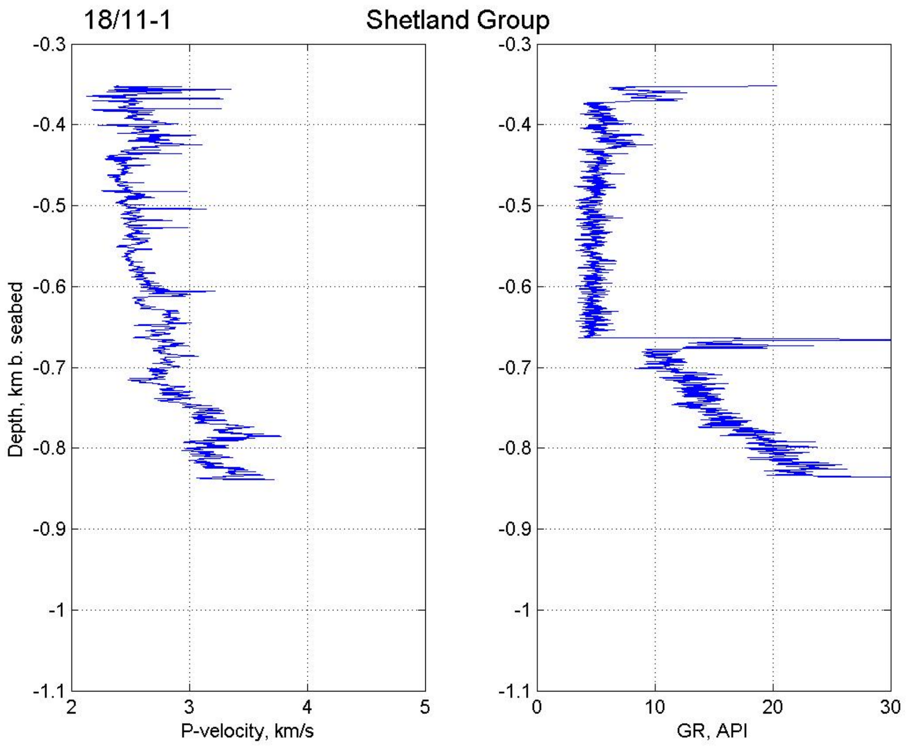
18/11-1
Shetland Group
Depth, km b. seabed
P-velocity, km/s
GR, API

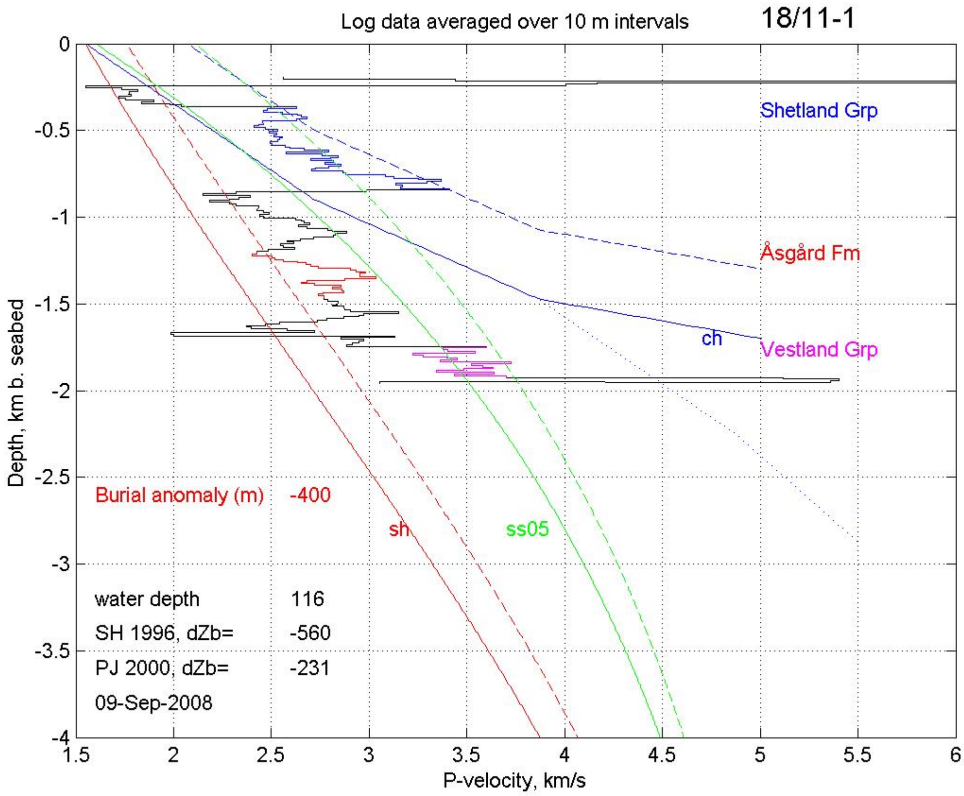

18/11-1
Post-chalk: Almost no data.

Chalk: Irregular variations of the sonic log. Low gamma level with few variations indicate pure chalk between the Ekofisk Fm and the casing at 0.65 km, below which level the gamma log shows an atypical pattern of increase with depth. High-velocity Ekofisk Fm with low gamma level may reflect bryozoan limestone. Section below Ekofisk Fm has relatively low velocities ("excellent reservoir properties", npd.no), porosity-preservation due to hydro-carbons?. Pattern similar to wells on Yme field.

Pre-chalk: Cyclic variations of the sonic log (peaks 500 m/s wide) above Tau Fm, 0.8-1.6 km. The Vestland Group, 1.7-1.9 km, is dominated by sandstone.

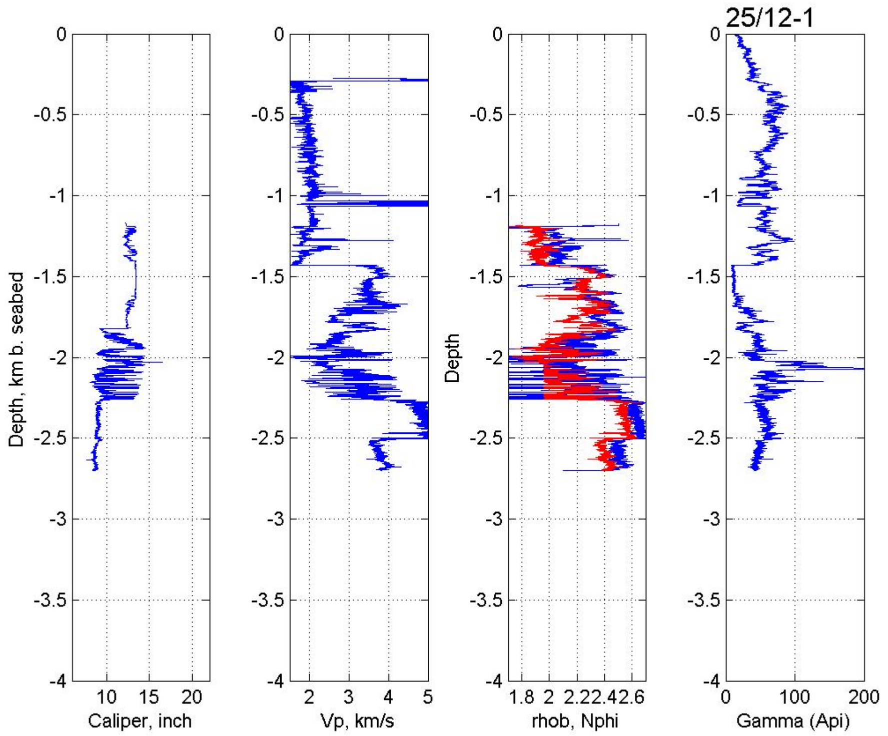
25/12-1
Depth, km b. seabed
Depth
Caliper, inch
Vp, km/s
rhob, Nphi
Gamma (Api)

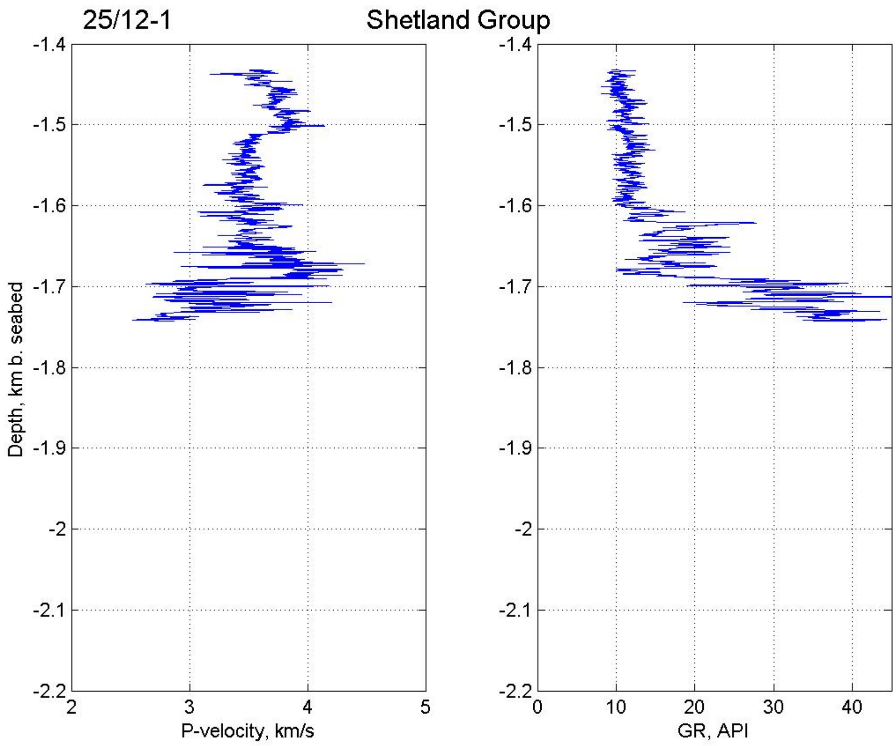
25/12-1
Shetland Group
Depth, km b. seabed
P-velocity, km/s
GR, API

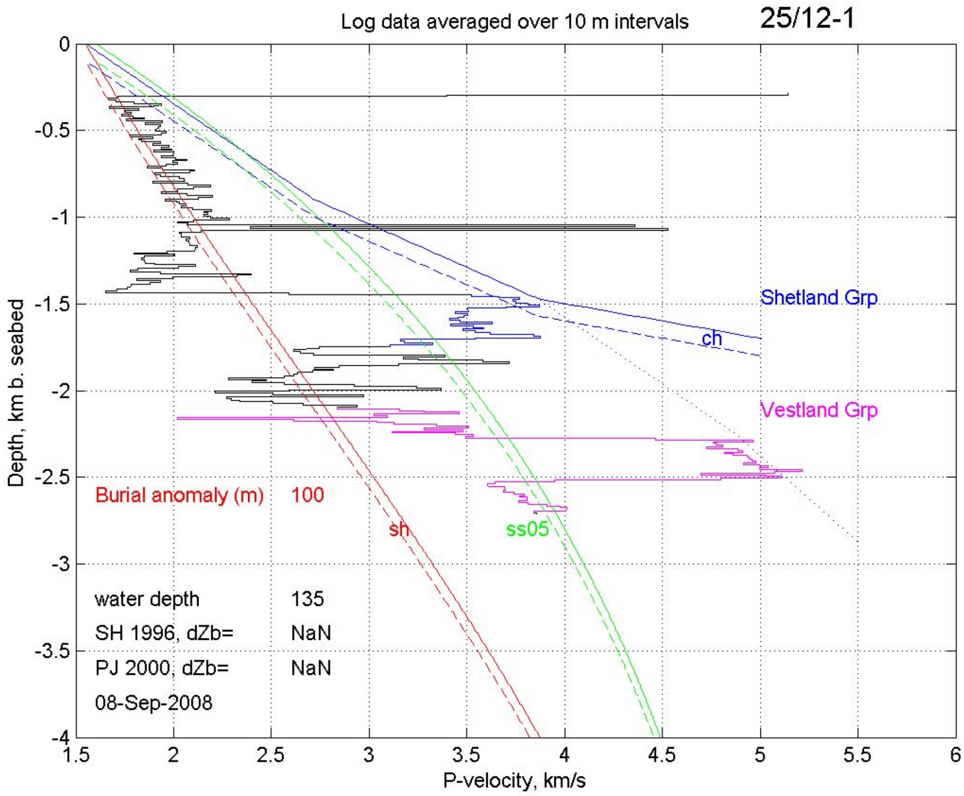

25/12-1

Post-chalk: Well-defined velocity-depth trend, 0.3-1.2 km. Velocity inversion in the underlying strata, 1.2-1.4 km, probably due to build-up of overpressure.

Chalk: Atypical variations of the sonic log. Constant and low gamma readings from the top of the chalk to 1.6 km indicate pure chalk. High velocities in the uppermost chalk at c. 1.5 km, but no bryozoans reported. Common mineral fluorescence reported in uppermost Tor Fm, c. 1.55 km; indicative of remnants of hydrocarbons that could have preserved the high porosities (low velocities) at this level. Low velocities, 1.5-1.65 km, could be caused by presence of hydrocarbons at an early stage of the compaction process.

Pre-chalk: Ample velocity variations above Vestland Group probably due to bad data. An undefined high-velocity (<5 km/s) unit (here erroneously indicated as part of the Vestland Group) is reported to be sandstone of possible Devonian age, 2.3-2.5 km.

Appendix B – Constraints on velocity-depth trends from rock physics models (Japsen et al. 2007b)

Geophysical Prospecting, 2006, **55**, 135–154

Constraints on velocity-depth trends from rock physics models

Peter Japsen,[1]* Tapan Mukerji[2] and Gary Mavko[2]

[1]*Geological Survey of Denmark and Greenland (GEUS), Øster Voldgade 10, DK-1350 Copenhagen n K, Denmark, and* [2]*Stanford Rock Physics Laboratory, Stanford University, California 94305, USA*

Received June 2005, revision accepted July 2006

ABSTRACT

Estimates of depth, overpressure and amount of exhumation based on sonic data for a sedimentary formation rely on identification of a normal velocity–depth trend for the formation. Such trends describe how sonic velocity increases with depth in relatively homogeneous, brine-saturated sedimentary formations as porosity is reduced during normal compaction (mechanical and chemical). Compaction is 'normal' when the fluid pressure is hydrostatic and the thickness of the overburden has not been reduced by exhumation. We suggest that normal porosity at the surface for a given lithology should be constrained by its critical porosity, i.e. the porosity limit above which a particular sediment exists only as a suspension. Consequently, normal velocity at the surface of unconsolidated sediments saturated with brine approaches the velocity of the sediment in suspension. Furthermore, porosity must approach zero at infinite depth, so the velocity approaches the matrix velocity of the rock and the velocity–depth gradient approaches zero. For sediments with initially good grain contact (when porosity is just below the critical porosity), the velocity gradient decreases with depth. By contrast, initially compliant sediments may have a maximum velocity gradient at some depth if we assume that porosity decreases exponentially with depth. We have used published velocity–porosity–depth relationships to formulate normal velocity–depth trends for consolidated sandstone with varying clay content and for marine shale dominated by smectite/illite. The first relationship is based on a modified Voigt trend (porosity scaled by critical porosity) and the second is based on a modified time-average equation. Baselines for sandstone and shale in the North Sea agree with the established constraints and the shale trend can be applied to predict overpressure. A normal velocity–depth trend for a formation cannot be expressed from an arbitrary choice of mathematical functions and regression parameters, but should be considered as a physical model linked to the velocity–porosity transforms developed in rock physics.

INTRODUCTION

A normal velocity–depth trend is a function describing how sonic velocity increases with depth in a relatively homogeneous, brine-saturated sedimentary formation when porosity is reduced during normal compaction (mechanical or chemical). Compaction is 'normal' when the fluid pres-sure of the formation is hydrostatic and the formation is at maximum burial depth, i.e. the thickness of the overburden has not been reduced by exhumation. The term baseline is frequently used as a synonym for a normal velocity–depth trend, typically to refer to reference trends established from a given database. The sonic velocity may be represented by the velocity V [m/s] or by transformations like transit time, $tt = 1/V \cdot 10^6$ [μs/m].

Velocity–depth studies are useful because they are based on easily accessible data with a wide lateral and vertical coverage, and can thus prescribe simple constraints on both physical and

*E-mail: pj@geus.dk

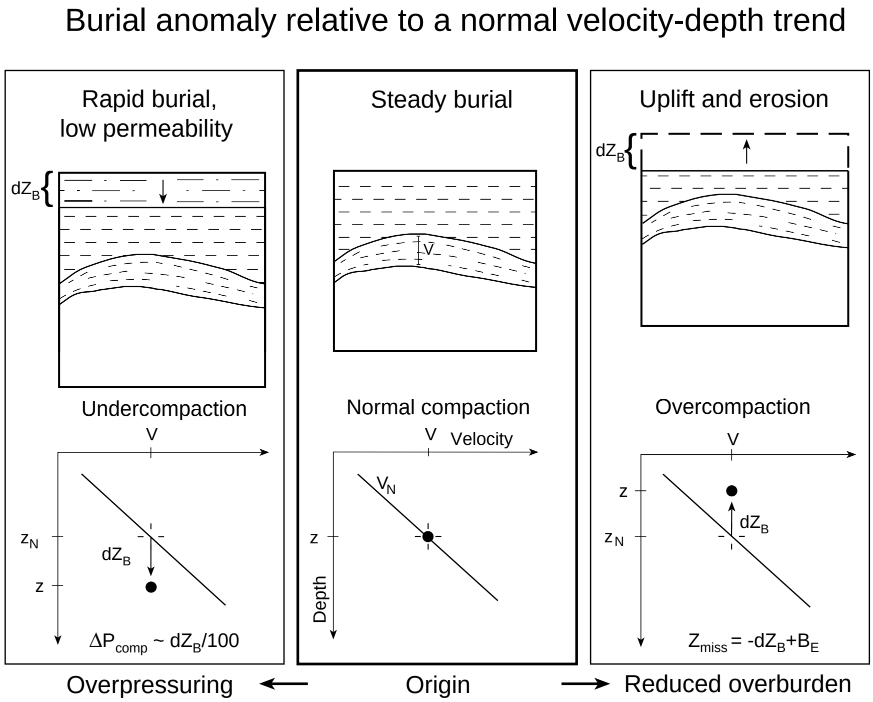

Figure 1 Burial anomaly dZ_B [m], relative to a normal velocity–depth trend V_N, for a sedimentary formation. In the North Sea Basin, burial anomalies of ±1 km for pre-Miocene formations result from late Cenozoic exhumation along basin margins and overpressuring due to rapid, late Cenozoic burial in the basin centre (cf. Figure 11). Rapid burial and low permeability cause undercompaction and overpressure ΔP_{comp} [MPa], and velocities that are low relative to depth (positive dZ_B) (cf. Equation 9). Exhumation due to uplift reduces the overburden thickness and causes overcompaction expressed as velocities high relative to depth (negative dZ_B); however, post-exhumational burial, B_E, will mask the magnitude of the missing section Δz_{miss}. The normalized depth z_N is the depth corresponding to normal compaction for the measured velocity (cf. Terzaghi's principle; Terzaghi and Peck 1968). Modified after Japsen (1998).

geological parameters because acoustic waves are affected by bulk properties as they propagate through the sediment. Disagreement between predicted and measured velocity at a given depth may indicate that a formation has become overpressured due to rapid burial (resulting in a lower velocity than expected) or that the overburden has been partially removed subsequent to maximum burial (resulting in a higher velocity than expected) (Fig. 1). A velocity–depth anomaly can also be measured along the depth axis as the burial anomaly dZ_B [m] (Japsen 1998). Velocity–depth trends are used for:

- estimating the amount of removed overburden ('uplift') relative to an overcompacted formation (e.g. Acheson 1963; Magara 1978; Bulat and Stoker 1987; Japsen 1993, 1998, 2000; Hillis 1995; Hansen 1996b; Heasler and Kharitonova 1996; Ware and Turner 2002; Corcoran and Doré 2005; Corcoran and Mecklenburgh 2005; Walford and White 2005; Mackay and White 2006);
- estimating overpressure due to undercompaction (e.g. Hottmann and Johnson 1965; Magara 1978; Chapman 1983; Japsen 1998, 1999; Winthaegen and Verweij 2003);
- converting traveltime to depth (e.g. Slotnick 1936; Japsen 1993; Al-Chalabi 1997b);
- determining background velocity – or the low-frequency model – for inversion of seismic data (e.g. Snieder *et al.* 1989);
- modelling the manner in which amplitude variation with offset (AVO) intercept and gradient change with increasing burial (e.g. Smith and Sondergeld 2001).

Rock-physics relationships, such as the empirical time-average of Wyllie *et al.* (1956), the relationships of Raymer *et al.* (1980) or the modified Voigt model (Nur *et al.* 1998), relate velocity to porosity for different rock types (cf. Dvorkin *et al.* 2002), but even though the concept of velocity–depth trends is as old as exploration geophysics (e.g. Slotnick 1936; Haskell 1941), few attempts have been made to constrain them for different lithologies, rather than just considering velocity–depth trends as fits of arbitrary functions to local data sets.

Chapman (1983) combined the time-average equation with the exponential decay of porosity with depth and thus derived an expression for the increase in shale velocity with depth that is constrained by the velocity of the sediment at the surface and does not approach infinite velocity at depth. Bulat and Stoker (1987) and Hillis (1995) estimated baselines for different lithologies but did not consider that the physical properties of the rock influence the curvature of velocity–depth trends and that velocity is finite even at great depth. Japsen (1998, 1999, 2000) defined normal velocity–depth trends for chalk and shale in such a way that the predicted velocities agreed with those of recent deposits at the surface and that they did not approach infinity at depth. Velocity–depth anomalies relative to these trends were found to be in agreement with estimates of the amount of exhumation along the margins of the North Sea Basin, as well as with measurements of overpressure in the centre of this basin.

Much empirical and theoretical insight into the physics of rocks has been gained since the formulation of the time-average equation, and consequently the analysis of Bulat and Stoker (1987) and others can be refined. In this paper, we investigate how joining rock-physics V–ϕ models with the ϕ–z relationship during normal compaction for the rock in question can introduce sensible simple constraints on V–z trends (z is depth below the sea-bed or ground level [m], ϕ is porosity [fraction]). We find that the normal velocity at the surface for a given rock is constrained by its critical porosity, and demonstrate that differences in the initial grain contact in sandstone and shale influence the curvature of the velocity–depth trends for these sediments. We conclude that normal velocity–depth trends should be considered as physical models for specific lithologies.

ROCK-PHYSICS MODELS

Critical porosity

For most porous materials there appears to be a critical porosity ϕ_c, that separates mechanical and acoustic behaviour into two distinct domains (Nur *et al.* 1991; Chen and Nur 1994; Nur *et al.* 1998). By definition, ϕ_c is the porosity below which the mineral grains in a sediment become load-bearing. At porosities above ϕ_c, the sediment loses all rigidity and falls apart: the sediment is in suspension and the fluid phase is load-bearing. Critical porosity has also been called elastic percolation porosity (Feng and Sen 1985; Guéguen *et al.* 1997) or the precompaction porosity (Nolen-Hoeksema 1993).

The transition from suspension to solid is implicit in the empirical velocity–porosity relationship of Raymer *et al.* (1980). If critical porosity is exceeded at the time of initial deposition of grains, they are barely in contact and consequently have no rigidity (Guéguen and Palciauskas 1994). The value of ϕ_c is determined by sediment type, grain sorting and angularity at deposition, and can thus vary within the same rock type (Table 1a). The concept of critical porosity is developed for sediments saturated with brine, and the arguments presented here do not necessarily apply to aeolian sediments, for example. Critical porosity behaviour is a general geometric property and is a powerful constraint on theoretical models.

V–ϕ trajectories

The velocity (or effective modulus) of a rock with a given porosity and fluid composition always falls between the Voigt upper and the Reuss lower bounds, but its precise value depends on the geometric details of the grain-pore microstructure (see Appendix A). Stiffer pore shapes cause the velocity to be closer to the upper bound; softer or more compliant shapes cause the velocity to be lower (e.g. Mavko *et al.* 1998). When compaction and diagenesis reduce porosity and thus increase the elastic stiffness, data points for a given rock type and diagenetic history will fall along a specific path or trajectory (V–ϕ path) in a plot of velocity versus porosity.

Initially stiff rocks

The V–ϕ path is concave for rocks that show a strong increase in velocity for porosity reduction just below the critical porosity (curve V_N^{ss10} in Fig 2; e.g. consolidated sandstone), i.e.

$$\left(\frac{dV}{d\phi}\right)_{\phi\approx\phi_c} << 0, \quad \frac{d^2V}{d\phi^2} < 0.$$

A concave V–ϕ curve has a negative second derivative. The initial sensitivity to porosity reduction may be due to the growth and cementation of grain contacts (e.g. Dvorkin and Nur 1996), while mechanical compaction is limited. Here, we refer to such rocks as 'initially stiff rocks'.

Initially compliant rocks

The V–ϕ path is convex for rocks that show a weak increase in velocity for porosity reduction just below the critical porosity close to ϕ_c (curve V_N^{sh} in Fig 2; e.g. shale, chalk), i.e.

$$\left(\frac{dV}{d\phi}\right)_{\phi\approx\phi_c} \approx 0, \quad \frac{d^2V}{d\phi^2} < 0.$$

A convex V–ϕ curve has a positive second derivative. This initial insensitivity to porosity reduction may be attributed to dominance of compaction, poor sorting and growth of pore-filling cement. Here, we refer to such rocks as 'initially compliant rocks'.

Table 1 Parameters and velocity-depth models
a. Critical porosity and exponential porosity decay with depth

Lithology	Critical porosity[a] ϕ_c [%]	Compaction models, literature				Compaction model, applied	
		Area, depth data	ϕ_0 [%]	β [m]	Reference	ϕ_0 [%]	β [m]
Sandstone	40	North Sea, 2–3 km	49	3704	Sclater and Christie (1980)	40	4872
		Nigeria, 0.6–4.3 km	44	4631	Serra (1986)		
Shale	60–90	North Sea, 0.3–2.6 km	71	1961	Hansen (1996a)	71	1961
		North Sea, -	63	1961	Sclater and Christie (1980)		

b. Rock physical properties.

Material	ϕ [%]	V_p [km/s]	V_s [km/s]	K [GPa]	μ [GPa]	ρ [g/cm^3]	Source
Quartz	-	6.04	4.12	36.6	45.0	2.65	Mavko *et al.* (1998)
Water	-	1.50	0	2.25	0	1	
At 4 km depth [b]							
Sandst. 0% clay	17.6	4.66	2.95	25.1	21.6	2.48	Han *et al.* (1986)
Sandst. 10% clay	17.6	4.15	2.47	21.7	14.5	2.38	Han *et al.* (1986)
Sandst. 20% clay	17.6	3.93	2.28	20.0	12.1	2.34	Han *et al.* (1986)
Sandst. 30% clay	17.6	3.72	2.09	18.3	10.0	2.29	Han *et al.* (1986)
At ϕ_c [c]		$\boldsymbol{V_c}$		$\boldsymbol{K_c}$		$\boldsymbol{\rho_c}$	
Quartz	40	1.60	0	5.15	0	2.00	Equation (A-1)

c. Velocity-depth models.

$V-z$ trend z [km]	V_N^{ss00} [d]	V_N^{ss10} [d]	V_N^{ss20} [d] V [km/s]	V_N^{ss30} [d]	V_N^{sh} [e]
0	1.55	1.58	1.59	1.60	1.55
1	3.07	2.80	2.68	2.58	2.10
2	3.83	3.44	3.27	3.11	2.71
3	4.32	3.86	3.66	3.47	3.32
4	4.66	4.15	3.93	3.72	3.87
$z_i - z_{i+1}$ [km]			$\boldsymbol{k}$ [s^{-1}]		
0-1	1.52	1.22	1.10	0.97	0.55
1-2	0.76	0.64	0.59	0.54	0.61
2-3	0.49	0.42	0.39	0.35	0.61
3-4	0.34	0.29	0.27	0.25	0.55
0-4	0.78	0.64	0.59	0.53	0.58

[a]Critical porosities found by evaluation of velocity-porosity data (Nur *et al.* 1998; Mavko *et al.* 1998).
[b]Based on laboratory data and linear dependency of rock physical parameters on porosity. Porosity based on compaction models in Table 1a.
[c]Reuss bound (equation A-1).
[d]Sandstone model computed from the $V-\phi$ trend given by equation, the appropriate rock physical properties for 0, 10, 20 and 30% clay content (Table 1b) (A2) and the $\phi-z$ model for sandstone (Table 1a).
[e]Marine shale (equation 5).

COMPACTION TRENDS

Burial of sediment leads to initial compaction and reduction of porosity to less than ϕ_c. We therefore assume that critical porosity of the sediment is reached only at the surface when pressure remains hydrostatic. We make the important assumption that ϕ_0, the porosity at the surface of the sedimentary succession, is constrained by the critical porosity of the freshly deposited sediment, i.e.

$$\phi_0 \leq \phi_c. \tag{1}$$

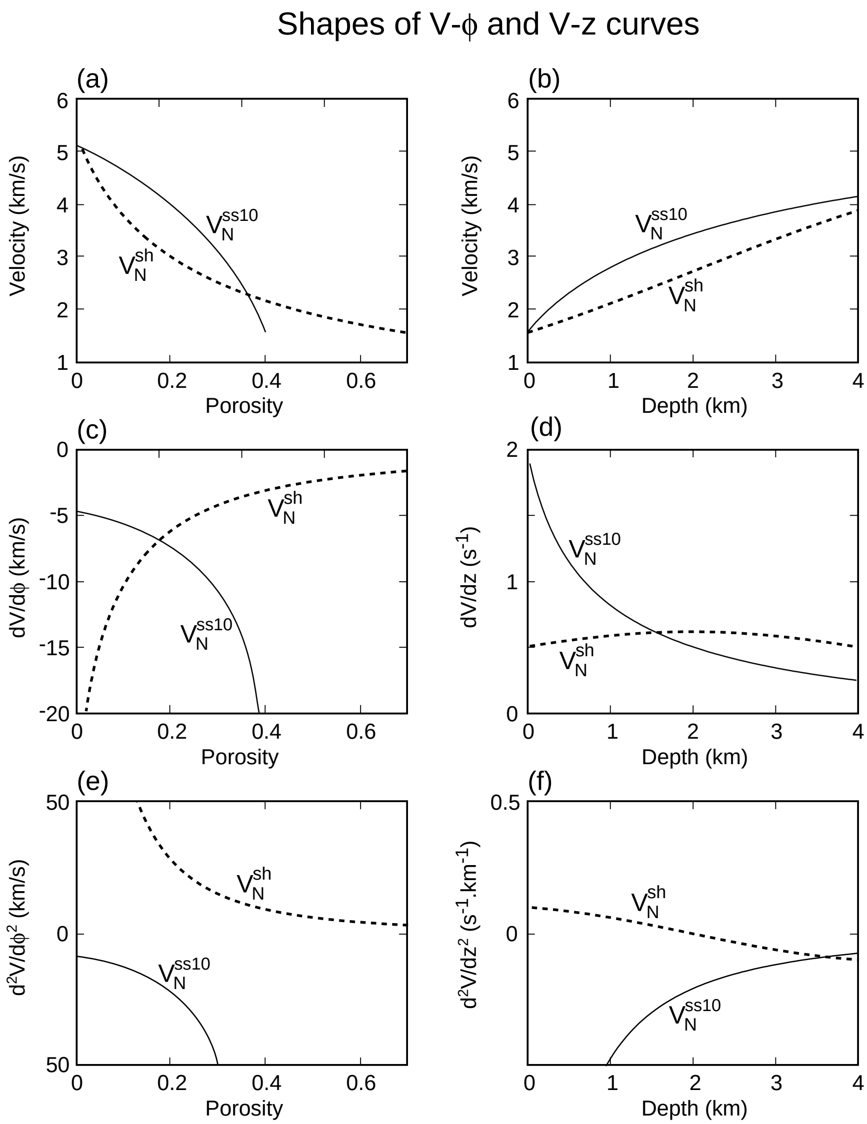

Figure 2 Shapes of V–ϕ and V–z curves for sediments characterized by initially stiff or initially compliant pore space (e.g. consolidated sandstone and marine shale, Figs 3 and 4). The two sediments have concave and convex V–ϕ trajectories, and thus $\mathrm{d}^2V/\mathrm{d}\phi^2$ for each type becomes negative and positive, respectively. The velocity gradient $k = dV/dz$ decreases with depth for the first type, while it has a maximum for the other type. (a) (c) and (e): V–ϕ trend and first and second derivatives with respect to ϕ. (b) (d) and (f): V–z trend and first and second derivatives with respect to z. The exponential ϕ–z relationships for both sediments are given in Table 1(a). V_N^{ss10}: modified Voigt model for sandstone, 10% clay content (equation (A2)). V_N^{sh}: marine shale trend (equations 5 and 6, V–ϕ and V–z relationships, respectively).

The geological interpretation of this statement is that, at least for clastics, the weak suspension state at critical porosity describes the sediment when it is first deposited, before compaction and diagenesis. The overall agreement between independent estimates of ϕ_c and ϕ_0 for different rock types supports the assumption that the limiting porosity at the surface is close to the critical porosity, e.g. for chalk $\phi_0 = 70\%$ (Scholle 1977) and $\phi_c = 65\%$ (Nur *et al*. 1998; cf. Fabricius 2003) (see Table 1a).

The porosity-reduction in sedimentary rocks during normal compaction has frequently been approximated by exponential functions (e.g. Athy 1930; Rubey and Hubbert 1959; Magara 1978; Sclater and Christie 1980; Hansen 1996a). Exponential functions have convenient mathematical properties and predict a physically constrained variation of porosity. Exponential porosity decay is a first-order approximation and thus does not include, for example, the onset of cementation below a certain depth. If we apply this approximation and set porosity at the surface to ϕ_c, we obtain

$$\phi = \phi_0 e^{-z/\beta} = \phi_c e^{-z/\beta}, \tag{2}$$

where the constant β [m] is a measure of the rate of porosity decay. The assumption $\phi_0 = \phi_c$ allows us to link knowledge from rock physics with compaction trends.

NORMAL VELOCITY–DEPTH TRENDS

General conditions

We will consider velocity as a function of porosity and porosity as a function of depth, i.e.

$$V(z) = V\left[\phi(z)\right],$$

where z may range from the surface to infinite depth. The velocity–depth gradient, k [m/s/m = s^{-1}], can be calculated by differentiation of the above expression, i.e.

$$k = \frac{dV}{dz} = \frac{d}{dz} V\left[\phi(z)\right] = \frac{d}{d\phi} V(\phi) \frac{d}{dz}\phi(z), \tag{3}$$

showing that the shape of the V–z trend depends on the shape of the V–ϕ and ϕ–z curves. As both terms on the right are negative or zero, we get $k \geq 0$ (cf. Figure 2c).

We can set up three simple boundary conditions for $V(z)$ for $z = 0$ and $z \to \infty$:

- $V_0 \geq V_c$. The velocity of unconsolidated sediments at the surface, V_0, is constrained by the velocity at critical porosity, V_c, given by the Reuss average at ϕ_c (equation (A1)). This follows from equation (1). Thus V_0 will, in general, differ from the velocity of water (Tables 1b,c).
- $V_\infty \to V_m$. Since porosity at infinite depth approaches zero, the velocity V_∞ of the sedimentary rock at infinite depth approaches the velocity at zero porosity, the velocity V_m, of the matrix mineral at high pressure and temperature.
- $k \to 0$ for $z \to \infty$. The velocity–depth gradient must approach zero at infinite depth as velocity cannot increase beyond the finite value of V_m.

Assuming exponential form for ϕ–z trends

We can simplify the relationship between velocity and depth by introducing exponential porosity decay with depth (equation 2):

$$V(z) = V\left[\phi(z)\right] = V(\phi_0 e^{-z/\beta}).$$

The velocity–depth gradient is found by making the same substitution in equation (3):

$$k = \frac{dV}{d\phi} \cdot \frac{d\phi_0 e^{-z/\beta}}{dz} = \frac{dV}{d\phi}\left(-\frac{1}{\beta}\phi_0 e^{-z/\beta}\right) = -\frac{dV}{d\phi}\phi/\beta.$$

The proportionality between k and $dV/d\phi$ means that the shape of the V–z path reflects the shape of the V–ϕ path. We can compare V–z trends for rocks with different curvature in the V–ϕ plane by differentiating the above expression for k assuming exponential porosity-decay with depth (equation 2):

$$\begin{aligned}\frac{dk}{dz} &= \frac{d}{dz}\left[-\frac{dV}{d\phi}\frac{\phi}{\beta}\right] = \frac{dV}{d\phi}\frac{d}{dz}\left[-\frac{\phi}{\beta}\right] - \frac{\phi}{\beta}\frac{d}{dz}\left[\frac{dV}{d\phi}\right] \\ &= \frac{1}{\beta^2}\left(\frac{dV}{d\phi} + \phi\frac{d^2V}{d\phi^2}\right)\phi.\end{aligned}$$

The first term on the right is negative for any rock, while the sign of the second term depends on the curvature of the V–ϕ path, i.e. positive or negative for rocks that are initially compliant or stiff, respectively (curves V_N^{sh} and V_N^{ss10} in Fig. 2e).

- For initially stiff rocks ($d^2V/d\phi^2 < 0$), we get $dk/dz < 0$, indicating that $k(z)$ decreases monotonously with increasing depth from the surface, i.e. with no local maxima for the velocity–depth gradient (curve V_N^{ss10} in Figs 2d,f). This decreasing velocity–depth gradient at shallow depths reflects the slowdown in the velocity increase, perhaps after the initial growth and cementation of grain contacts (see the sandstone case below; Fig. 3).
- For initially compliant rocks ($d^2V/d\phi^2 > 0$), dk/dz may become zero (curve V_N^{sh} in Figs 2d,f). Therefore, an increasing velocity–depth gradient at shallow depths may reflect the accelerated increase in velocity as mechanical compaction takes place, whereas the slow-down in porosity-reduction at depth leads to a decreasing velocity–depth gradient. Initially compliant rocks may thus have a maximum velocity gradient at an intermediate depth due to the combined effect of these two processes (see the shale case below; Fig. 4).

We investigate velocity–depth relationships for specific velocity–porosity trends in Appendix B and we discuss analytical functions that have been applied to represent the increase in ve-locity with depth in Appendix C (see also Table 2).

BASELINES FOR SANDSTONE AND SHALE ESTIMATED FROM NORTH SEA DATA

It can be difficult to estimate the normal velocity–depth trend for a formation because the formation may not easily be found under normally compacted conditions, e.g. the formation may either be undercompacted due to overpressuring or it may be

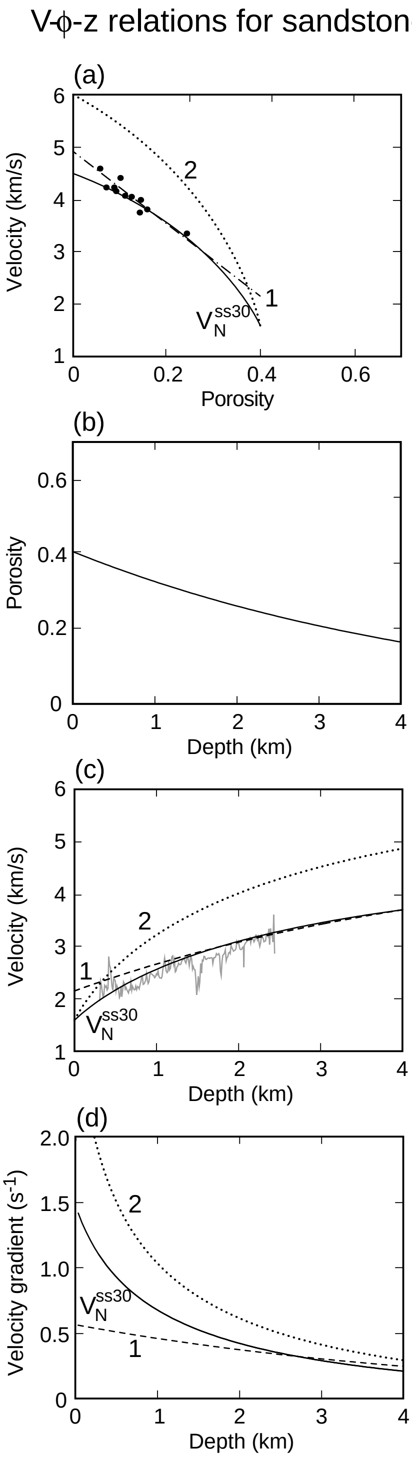

Figure 3 Sandstone; relationships between velocity, porosity, depth and velocity–depth gradient. A modified Voigt upper bound (V_N^{ss30}) represents the transition from sand to sandstone during normal compaction by constraining the porosity to vary between critical porosity and estimated porosity at a depth of 4 km (equation (A2)) (Nur *et al.* 1991). (a) V–ϕ trends and data points for clay content between 20 and 40% at 40 MPa confining pressure (cf. Table 1b) (Han *et al.* 1986); (b) ϕ–z trend based on models for the North Sea and Nigeria (Table 1a); (c) V–z trends resulting from elimination of ϕ in (a) and (b) and sonic log covering normally compacted, Cenozoic sandstones in the Kangâmiut-1 well, offshore SW Greenland (Rolle 1985); (d) k–z trends from (c). 1: linear trend from laboratory data; 2: modified Voigt trends from mineral properties at $\phi = 0$; V_N^{ss30}: modified Voigt trend from laboratory data, 30% clay content, anchor point at $\phi_{4\,\mathrm{km}}$.

overcompacted due to exhumation of its overburden (Fig. 1). It may, however, be possible to estimate the maximum burial of the formation independently: along the margins of the North Sea Basin, the amount of Cenozoic exhumation can be calculated from the burial anomaly of the thick and uniform Upper Cretaceous–Danian chalk relative to the normal velocity–depth trend for the chalk (Japsen 1998, 2000). Baselines can be more easily traced in plots of velocity versus pre-exhumation depths because the formations underlying the chalk were at maximum burial at more locations prior to the exhumation (Fig. 5). Data points at shallow depth relative to the baseline may thus represent locations where the formation experienced maximum burial during the Mesozoic (cf. Japsen 2000).

Normal velocity–depth trends for sandstone and shale were established by Japsen (2000) from a regional database of interval velocities estimated in UK and Danish wells in the North Sea Basin (cf. Hillis 1995). The wells have interval velocities from a marine Jurassic shale (the F-1 Member of the Lower Jurassic Fjerritslev Formation), from the Triassic redbeds of the Bunter Sandstone or the Bunter Shale, as well as from the North Sea Chalk. The Triassic redbeds were deposited in a supratidal or continental environment during a hot, semiarid climate (Bertelsen 1980; Johnson *et al.* 1994). The Fjerritslev Formation was deposited in a marine environment (Michelsen 1989) and its clay mineralogy is dominated by smectite/illite in distal parts of the basin (H. Lindgreen, pers. comm. 2000).

A baseline for sandstone based on data for Triassic formations

Bunter Shale

The plot of velocity versus pre-exhumation depths for the Bunter Shale in Fig. 6(b) shows a reasonably well-defined trend of data points at maximum burial ($2.6 < V < 4.8$ km/s). By

Table 2 Functional forms of velocity-depths trends

Linearity	$V(z)$ or $tt(z)$ (equation no.)	Degrees of freedom	$V(0)$	$k = \mathrm{d}V/\mathrm{d}z$	$z \to \infty$ $k \to$	$V \to$	Selected references
$V - z$	$V = V_0 + k \cdot z$ (C-1)	2	V_0	k	k	∞	Slotnick (1936), Bulat and Stoker (1987)
$tt - z$	$tt = tt_0 + q \cdot z$ (C-2)	2	$1/tt_0$	$-q \cdot V^2$	∞^b	∞^b	Hillis (1995), Al-Chalabi (1997a)
$\ln(tt) - z$	$tt = tt_0 \cdot e^{-z/b_1}$ (C-3)	2	$1/tt_0$	V/b_1	∞	∞	Magara (1978), Hansen (1996b)
$\ln(V) - \ln(z)$	$V = c \cdot z^{1-n}$, $0.83 < n < 1$ (C-4)	2	0	$(1-n) \cdot V/z$	0	∞	Faust (1951), Acheson (1963)
$\ln(tt - tt_\infty) - z$, $\ln(tt - tt_\infty) - \phi^e$	$tt = (tt_0 - tt_\infty)e^{-z/b_2} + tt_\infty$ (C-5)	3	$1/tt_0$	$(V - tt_\infty \cdot V^2)/b_2{}^c$	0	$1/tt_\infty$	Chapman (1983), Al-Chalabi (1997a), Japsen (1999)
$V - z$, N segments	$V = V_{0i} + k_i \cdot z$, $z_{ai} < z < z_{bi}$ (C-6)	$2N$	V_{01}	k_i	-[a]	-[a]	Japsen (1998, 2000)
$\ln(V_\infty - V) - z$, $\ln(V_\infty - V) - \ln(\phi)^e$	$V = V_\infty - (V_\infty - V_0)e^{-z/b_3}$ (B-2)[d]	3	V_0	$(V_\infty - V)/b_3$	0	V_∞	This paper

Units of model parameters: b_1, b_2, b_3, z [m], c, V, V_0, V_∞ [m/s], k [s^{-1}], q [s/m^2], tt, tt_0, tt_∞ [s/m], n [−].
[a] Arbitrary, depending on actual parameters.
[b] For $z \to -tt_0/q$.
[c] Maximum velocity gradient for $z = b_2 \cdot \ln[(tt_0 - tt_\infty)/tt_\infty]$.
[d] Constrained approximation to the modified Voigt trend based on exponential porosity-decay (equation A2).
[e] Combined with exponential porosity decay with depth.

contrast, the plot of velocity versus present depth in Fig. 6(a) reveals no clear trend. Some data points are plotted above the trend in Fig. 6(b) and thus represent areas where the Bunter Shale was at maximum burial prior to Cenozoic exhumation or areas of anomalous lithology.

The trend of data points at maximum burial reveals a slight curvature that reflects the decrease in the velocity gradient with depth, and this trend is approximated by three linear segments plus a fourth segment that connects the observed trend with a physically reasonable velocity at the surface. The normal velocity–depth trend for the Bunter Shale, V_N^B, can be approximated by the following expression (Japsen 2000):

$$
\begin{aligned}
V_N^B &= 1550 + 0.6z, && 0 < z < 1393\,\text{m}, \\
V_N^B &= -400 + 2z, && 1393 < z < 2000\,\text{m}, \\
V_N^B &= 2600 + 0.5z, && 2000 < z < 3500\,\text{m}, \\
V_N^B &= 3475 + 0.25z, && 3500 < z < 5300\,\text{m}.
\end{aligned}
\tag{4}
$$

The gradient is 2 s^{-1} for depths around 2 km, from where it decreases gradually with depth to 0.5 and then to 0.25 s^{-1} 0. The gradient is taken to be 0.6 s^{-1} in the upper part in order to arrive at a physically reasonable velocity at the surface.

Bunter Sandstone

The plot of velocity versus pre-exhumation depths for the Bunter Sandstone in Fig. 7(b) has a scattered trend of data at maximum burial that coincides with the trend for the Bunter Shale (3.0 < V < 4.3 km/s), and equation (4) is thus considered as an approximation for the observed Bunter Sandstone trend. See the section 'V–ϕ–z relationships for consolidated sandstone' for further discussion.

A shale trend based on data for a Jurassic formation

The plot of velocity versus pre-exhumation depths for the marine Lower Jurassic shale in Fig. 8(b) shows a well-defined trend of data points at maximum burial (2.6 < V < 3.6 km/s). A number of data points are plotted above the trend and presumably represent either areas where the shale was at maximum burial prior to Cenozoic exhumation or areas of anomalous lithology. The normal velocity–depth trend for the marine shale, V_N^{sh}, can be approximated by a constrained exponential

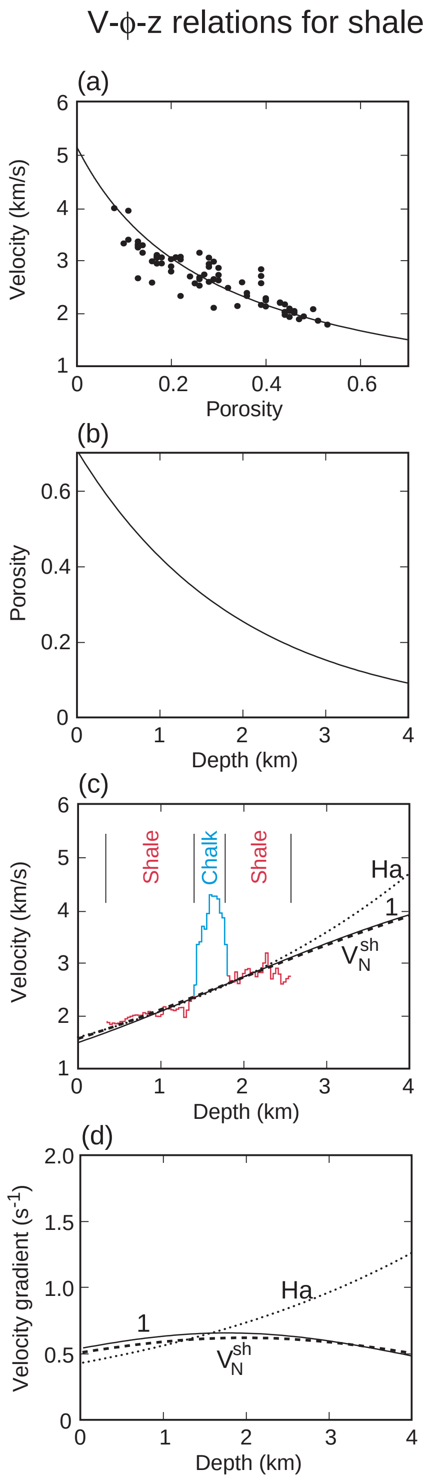

Figure 4 Shale; relationships between velocity, porosity, depth and velocity–depth gradient based on North Sea data. The constrained transit-time–depth model derived from log and core data (line 1) corresponds to a normal velocity–depth trend derived from interval velocity data (V_N^{sh}). (a) V–ϕ trend based on log and core data (equation 6; Hansen 1996a); (b) ϕ–z trend based on transit times converted by equation (6) (Table 1a; Hansen 1996a); (c) V–z trends and sonic log from normally compacted sediments (1.1 km Cenozoic shale, 0.3 km mainly Mesozoic chalk and 0.8 km Mesozoic shale; Norwegian well 17/10−1; cf. Olsen 1979; Hansen 1996b); (d) k–z trends from (c). 1: trend resulting from elimination of ϕ in (a) and (b) (equation 7); Ha: Hansen (1996b) (exponential tt–z trend, equation 8); V_N^{sh}: trend for marine shale dominated by smectite/illite (equation 5; Japsen 1999, 2000).

transit-time–depth model of the form given by equation (C5) (Japsen 2000):

$$V_N^{sh} = 10^6/(460e^{-z/2175} + 185). \qquad (5)$$

The trend fulfils reasonable boundary conditions at the surface and at infinite depth, $V_0 = 1550$ m/s and $V_\infty = 5405$ m/s, and it is well-defined at depths where velocity–depth data for normally compacted shale can be difficult to identify ($2 < z < 4$ km). The trend has a maximum velocity–depth gradient of 0.6 s^{-1} at $z = 2.0$ km. See the section 'V–ϕ–z relationships for shale' for further discussion.

The depth shift between the observed trends for the Bunter and for the marine shale exceeds 1 km for $V > 3$ km/s. This shift must be related to physical differences between the two lithologies that have the word 'shale' in common because an explanation related to a previous greater burial for the data points defining the Bunter trend than for the marine shale trend is not compatible with the geology of the area (see Japsen 2000).

CONSTRAINTS ON VELOCITY–DEPTH RELATIONSHIPS FOR SANDSTONE AND SHALE

Here we study the effect of porosity reduction on velocity in both the V–ϕ plane and the V–z plane for rock types with depth-dependent compaction such as consolidated sandstone and shale. By estimating V–ϕ and ϕ–z relationships for these lithologies, we can eliminate the dependence on ϕ in order to find likely V–z trends that we can compare with the North Sea baselines described in the preceding section. S-wave velocity may be predicted from V (P-wave velocity) based on empirical relationships for sandstone or shale (e.g. Han *et al.* 1986; Greenberg and Castagna 1992).

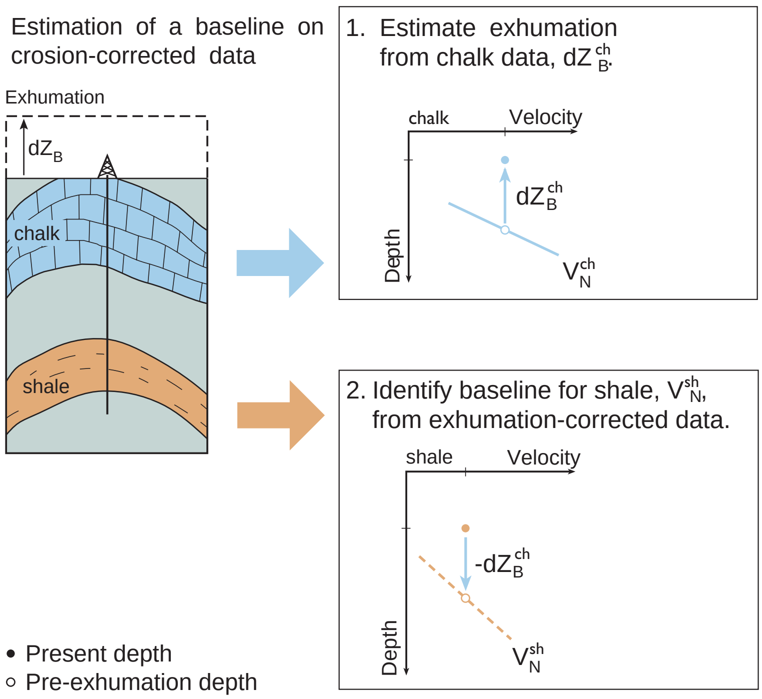

Figure 5 Identification of a normal velocity–depth trend for shale based on data from wells where Cenozoic exhumation can be estimated from velocity–depth data for the overlying North Sea chalk. Maximum burial is assumed to have occurred during the Cenozoic for both layers. 1 Estimate the Cenozoic exhumation in each well as the burial anomaly of the chalk, dZ_B^{ch}, relative to the chalk baseline, V_N^{ch}. 2 Identify the baseline, V_N^{sh}, for the shale unit by plotting velocity data versus depths corrected for exhumation as estimated by the chalk data. The shale baseline can be traced more easily because the shale was at maximum burial at more locations prior to Cenozoic exhumation.

V–ϕ–z relationships for consolidated sandstone

V–ϕ model

We construct modified Voigt upper bounds to describe the V–ϕ trend for consolidated sandstone with varying clay content during normal compaction (Han *et al.* 1986; Nur *et al.* 1991). The velocity varies between two end-members (equation (A2)): the maximum-porosity end-member for the mineral suspension at critical porosity (ϕ_c, V_c) (equation (A1)) and the minimum-porosity end-member (anchor point) representing maximum compaction for practical purposes, i.e. the porosity estimated at a depth of 4 km (ϕ_{4km}, V_{4km}) (Table 1a; curve V_N^{ss10} in Fig. 3a). We calculate rock properties for consolidated sandstones with clay contents of 0, 10, 20 and 30%, using $\phi_{4km} = 17.6\%$, from Han's empirical relationships based on a data set with mean porosity 16% (Table 1b) (Han *et al.* 1986).

This modified Voigt model is appropriate where data extend over depths ranging from partially consolidated shallow rocks to deeper well-consolidated rocks. In such situations, diagenesis is the dominant control over the V–ϕ trend, and the modified Voigt model seems to capture this behaviour. However, in cases where data all come from similar diagenetic ages, such as from a selected reservoir zone within a relatively narrow depth range, variations in texture, sorting and clay content dominate the V–ϕ trend, and models other than the modified Voigt are more appropriate (e.g. Dvorkin and Nur 1996).

ϕ–z model

Sclater and Christie (1980) suggested an exponential porosity–depth trend for sandstones in the North Sea, constrained by a surface porosity of 49% estimated for sand in Holocene beach and dune deposits by Pryor (1973). This value is above the surface value of 41% for river-bar sediments given by Pryor (1973), and above the critical porosity for clean and well-sorted sand, $\phi_c = 40\%$ (Nur *et al.* 1998). Furthermore, a surface porosity of 44% for sandstones was found by fitting an exponential decay function with porosities based on density log data (Serra 1986). Both trends, however, indicate similar porosities at depth, i.e. a mean value of $\phi_{4km} = 17.6\%$. We calculate the exponential decay constant (β in equation 2) for that value and $\phi_0 = 40\%$, and do not include the influence of clay content (Fig. 3b; Table 1a).

Resulting V–z model

V–z trends for sandstone are found by eliminating ϕ from the above two models (curve V_N^{ss30} in Fig. 3c; equations (A2) and (2)). The modified Voigt model defined by the minimum-porosity anchor point has a V–z gradient that decreases monotonously from values greater than 1 s^{-1} for $z < 0.4$ km and 30% clay content (Fig. 3d; Table 1c). Reduction of the clay content leads to higher velocity and velocity gradient (Fig. 9).

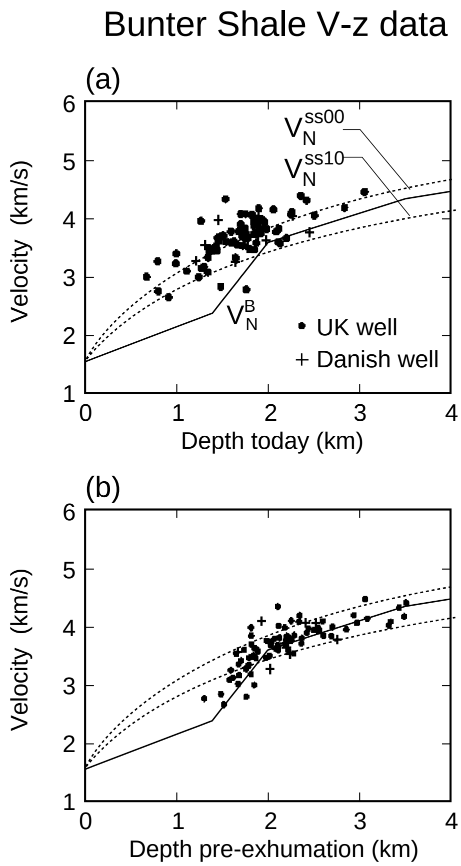

Figure 6 Plot of interval velocity versus midpoint depth for the Lower Triassic Bunter Shale. The Bunter model, V_N^B (equation 4) can be traced more easily if present depths are corrected for the Cenozoic exhumation in each well (Figure 5). Note the agreement between the Bunter trend and the modified Voigt model for sandstone below a depth of approximately 2 km. (a) Present-day depth below top of sediments; (b) depth prior to exhumation estimated by correcting present depths by the chalk burial anomaly in each well. One data point constrains V_N^B for a pre-exhumation depth of 5.5 km. V_N^{ss00}, V_N^{ss10}: modified Voigt models for sandstone, 0–10% clay content (equation (A2)). Modified after Japsen (2000).

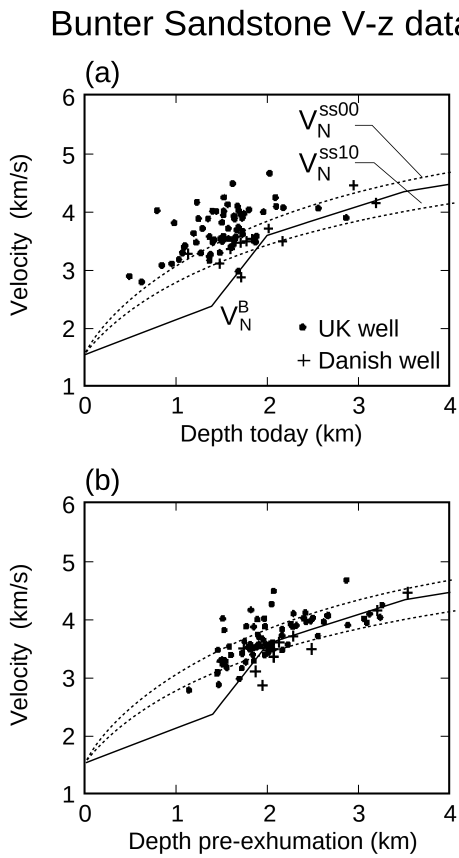

Figure 7 Plot of interval velocity versus midpoint depth for Bunter Sandstone. The Bunter model, V_N^B (equation 4), follows the scattered trend of the Bunter Sandstone data in the plot of depths corrected for exhumation in each well. (a) Present-day depth below top of sediments; (b) depth prior to exhumation estimated by correcting present depths by the chalk burial anomaly in each well. Three data points are plotted close to for a pre-exhumation depths of approximately 5 km. V_N^{ss00}, V_N^{ss10}: modified Voigt models for sandstone, 0–10% clay content (equation (A2)). Modified after Japsen (2000).

We can approximate the modified Voigt model by a modified velocity-average equation (equation (B2)).

If we compare the modified Voigt model with the normal trend for the Bunter Shale and Sandstone (Figs 6 and 7), we see that the Bunter trend – and most data points corrected for exhumation – are plotted between the sandstone models for 0% and 10% clay content for depths below approximately 2 km. The match between the modified Voigt model and the data points for the Bunter Sandstone supports the application of the modified Voigt model for sandstone (Fig. 3) as well as the estimation of the amount of exhumation by means of chalk velocities (Fig. 5).

The match between the modified Voigt model and the data points for the Bunter Shale suggests that the lithology of the Bunter Shale is dominated by quartz in the wide area covered by the data set (southern and eastern North Sea Basin). Consequently, the term 'Shale' seems to be an indication of grain size rather than of mineralogy.

The low velocities of the Bunter trend relative to the modified Voigt model at shallow depths may be explained by slow porosity-reduction in the Bunter Shale and Sandstone due to mechanical compaction above approximately 2 km, followed by a more rapid reduction due to the onset of quartz cementation below that depth (cf. Bjørlykke and Egebjerg 1993; Lander and Walderhaug 1999).

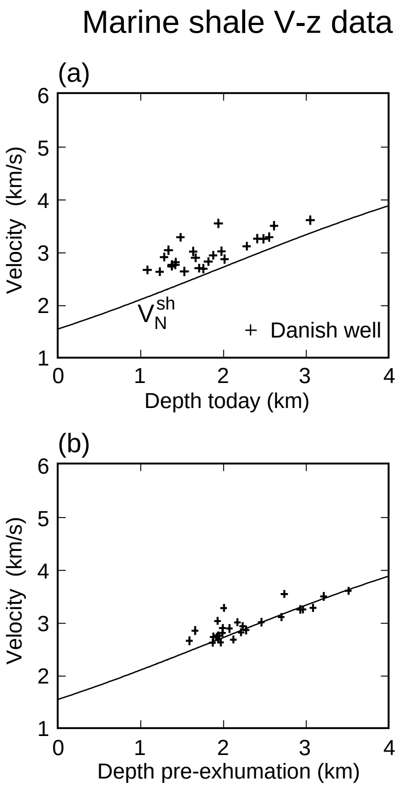

Figure 8 Plot of interval velocity versus midpoint depth for a marine Lower Jurassic shale (F-1 Member of the Fjerritslev Formation). The shale trend, V_N^{sh} (equation 5), can be traced more easily if present depths are corrected for Cenozoic exhumation in each well. (a) Present-day depth below top of sediments; (b) depth prior to exhumation estimated by correcting present depths by the chalk burial anomaly in each well. Modified after Japsen (2000).

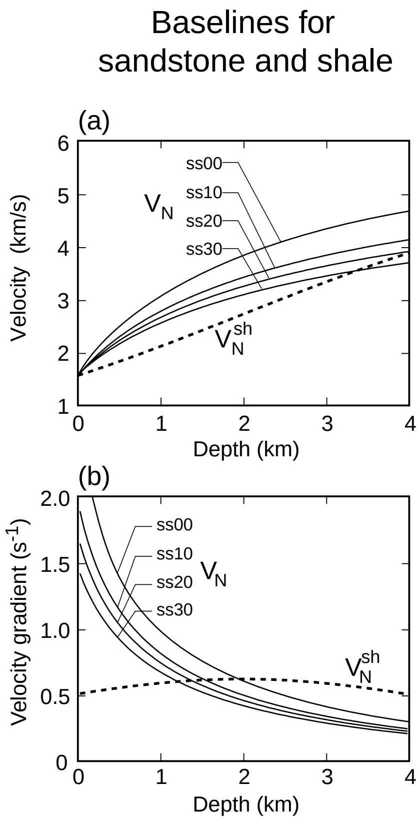

Figure 9 Composite plot of normal velocity–depth trends for sandstone and shale. The velocity of shale is predicted to be lower than that predicted for sandstone with a 30% clay content for $z < 4$ km. The velocity gradient for sandstone is predicted to decrease with depth whereas that of shale has a maximum at an intermediate depth. (a) V–z trends; (b) k–z trends. V_N^{sh}: marine shale trend (equation 5). $V_N^{ss00} - V_N^{ss30}$: modified Voigt models for sandstone, 0–30% clay content (equation (A2)).

The velocity–depth relationships for the Triassic Bunter Sandstone established by Bulat and Stoker (1987) and Hillis (1995) predict velocities at intermediate depths that are in agreement with the modified Voigt model for sandstone with 10% clay (e.g. $z \approx 2$ km; curves B&S, H and V_N^{ss10} in Fig. 10a). However, only the modified Voigt model complies with reasonable boundary conditions at the surface and at infinite depth (Fig. 10b). By contrast, the Bunter Sandstone model of Hillis (1995) predicts that the velocity–depth gradient increases towards infinity (cf. Equation (C2)). Consequently, exhumation may be underestimated by more than 500 m when this unconstrained sandstone trend is applied for velocities greater than 3.7 km/s compared to the modified Voigt model presented here. Underestimation by such amounts, which is only due to an unconstrained formulation of the baseline, is considerable compared to, for example, the amount of Cenozoic exhumation of the North Sea Basin that reaches approximately 1 km where the Upper Cretaceous Chalk is truncated (Japsen 1998, 2000).

V–ϕ–z relationships for shale

V–ϕ model

Hansen (1996a) calculated porosities from grain densities measured on cuttings and sidewall cores and from bulk densities estimated from density logs for Cretaceous-Cenozoic shales in three wells on the Norwegian Shelf. Corresponding transit times were determined by averaging sonic log values near the sampling depth. A modification of the Wyllie *et al.* (1956) time-average equation yielded a good fit for this data set (Fig. 4a) (Hansen 1996a). The modified time-average equation is in the form of equation (B1) where $1/\phi_c$ is substituted by a correction factor C_P. Hansen (1996a) found

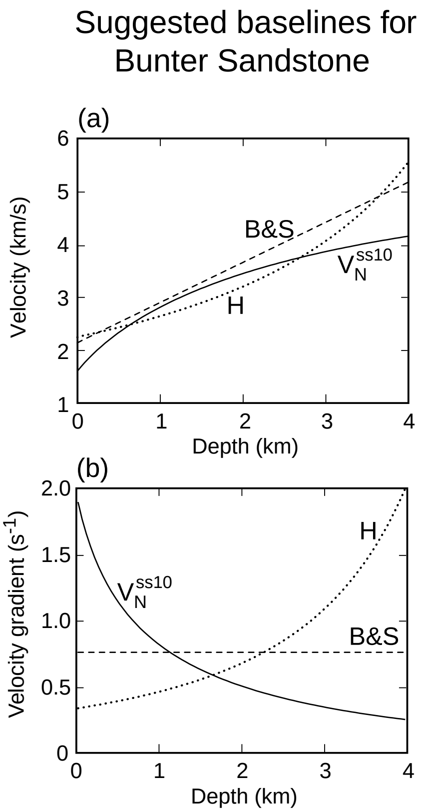

Figure 10 Comparison of suggested velocity-depth trends for the Triassic Bunter Sandstone, North Sea, with the modified Voigt model for sandstone with 10% clay (V_N^{ss10}). The two trends (B&S and H) show behaviour similar to the Voigt model at intermediate depths for which the trends were derived. Only the velocity gradient of the Voigt model converges towards zero at great depth. Data for the Bunter Sandstone are shown in Figure 7 (cf. Japsen 2000). (a) *V–z* trends; (b) *k–z* trends. B&S: Bulat and Stoker (1987) (linear *V–z* trend, cf. equation (C1)). H: Hillis (1995) (linear *tt–z* trend, cf. Equation (C2)). V_N^{ss10}: modified Voigt model for sandstone, 10% clay content (equation (A2)).

$C_P = 1.57$ ($\phi_c = 64\%$; $V_c = 1610$ m/s; $V_m = 5155$ m/s), and

$$tt = 670\phi + 194. \tag{6}$$

According to Hansen (1996a), differences in the determination of shale porosity are the main causes of differences between this result and the V–ϕ relationships for shale of Magara (1976), Issler (1992) and Liu and Roaldset (1994).

ϕ–z model

Hansen (1996a) calculated shale porosities from transit times based on the above tt–ϕ relationship for normally compacted Cretaceous-Cenozoic shale intervals in 29 wells on the Norwegian Shelf. Exponential and linear ϕ–z trends were fitted to the data, giving $\phi_0 = 71\%$ and 62%, respectively, which are in reasonable agreement with $\phi_c = 64\%$ indirectly determined by equation (6) (Fig. 4b; Table 1a).

Resulting V–z model

The expression resulting from combining the V–ϕ trend of equation (6) with the suggested exponential ϕ–z relationship (Hansen 1996a; Table 1a) is a constrained, transit-time–depth model (equation (C5); curve 1 in Fig. 4c):

$$tt = 676e^{-z/1961} + 194. \tag{7}$$

Hansen (1996b), however, chose to fit a simple, transit-time—depth model (equation (C3)) to data from normally compacted Jurassic-Miocene shale intervals in 32 wells on the Norwegian Shelf ($0.4 < z < 2.8$ km):

$$tt = 627e^{-z/3704}. \tag{8}$$

This equation predicts that the velocity approaches infinity at depth, and the two above trends are 0.8 km apart for $V = 4$ km/s (curve Ha in Fig. 4c). By contrast, the shale trend of Japsen (2000) given by equation (5) (curve V_N^{sh} in Fig. 4d, Table 1c) is almost identical to that given by equation (7). Furthermore, it is less than 100 m apart from the trend of Hansen (1996b) for $z < 2.4$ km, which is the interval that covers most of the Cenozoic shale data.

Scherbaum (1982) presented a baseline for Lower Jurassic shale in the north-west German Basin, and this trend is within 100 m of that given by equation (5) for the adjacent Danish Basin for $z < 4$ km. Corcoran and Mecklenburgh (2005) estimated a shale trend of the same form as equation (5), based on regression of sonic log data for normally compacted, Jurassic-Cenozoic shale in the Rockall and Porcupine Basins. Inclusion of data from non-shale sediments in the analysis of Corcoran and Mecklenburgh (2005) may have caused their trend to be, on average, 497 m shallower than the trend given by equation (5) for a given velocity and $z < 4$ km. Thus there is uncertainty related to the identification of a uniform lithology for which the baseline is defined and to the selection of data for similar formations for which exhumation is to be determined. Shale trends based on data from the Gulf Coast area match that given by equation (5) at intermediate depths, from where most of the Cenozoic shale data originate ($0.5 < z < 1.5$ km). Few details are, however, given about the derivation of the Gulf Coast shale trends (e.g. Hottmann and Johnson 1965; Chapman 1983).

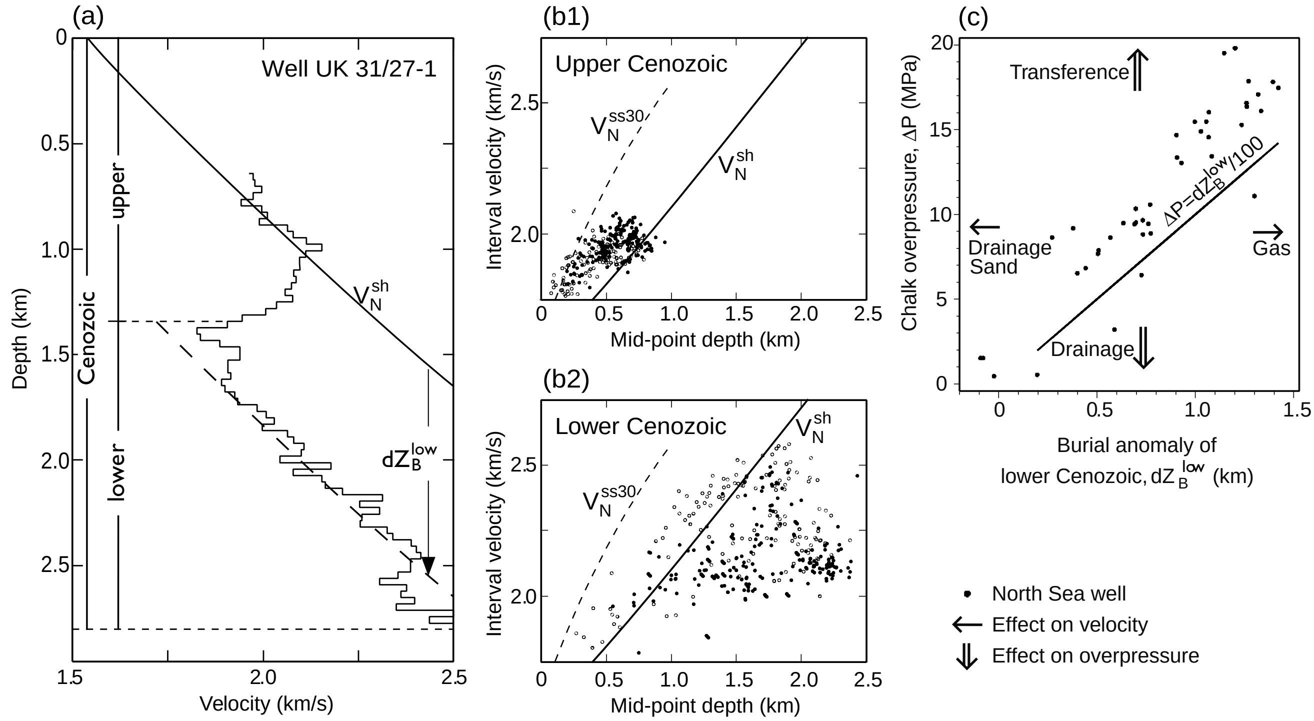

Figure 11 Prediction of overpressure in the North Sea from interval velocities of the Cenozoic deposits (excluding the Danian) (cf. Figure 1). (a) Sonic log where low velocities reveal undercompaction of the lower Cenozoic sediments corresponding to measured overpressure in the underlying chalk. (b1) and (b2) Interval velocity versus depth to the midpoint of the upper and lower Cenozoic deposits, respectively, for 322 North Sea wells. (c) Burial anomalies for the lower Cenozoic sediments (dZ_B^{low}) versus chalk formation overpressure (ΔP) in North Sea wells. The upper Cenozoic deposits are close to normal compaction whereas velocity–depth anomalies for the lower Cenozoic sediments outline a zone of undercompaction in the central North Sea. The deviations from the trend line in (c) are due to the non-compactional sources that add to the chalk overpressure from below (transference; cf. Osborne and Swarbrick 1997), the easier drainage from the more shallow Cenozoic section and sandy lithology ($\Delta P = \mathrm{d}Z_\mathrm{B}/100$; equation 9). The burial anomalies are calculated relative to the shale trend given by equation (5). Depths below top of sediments. V_N^{ss30}: modified Voigt model for sandstone, 30% clay content (equation (A2)). V_N^{sh}: marine shale trend (equation 5). Modified after Japsen (1998, 1999, 2000).

Overpressure prediction from shale velocities

Overpressure in the central North Sea was successfully predicted from velocity–depth anomalies for the Cenozoic succession, relative to a normal velocity–depth trend for shale close to that given by equation (5) (Fig. 11; Japsen 1999). Investigation of interval velocities from almost 1000 wells revealed basin-wide differences in the physical properties of the Cenozoic deposits related to disequilibrium compaction below the mid-Miocene unconformity in the central North Sea (cf. Rubey and Hubbert 1959; Osborne and Swarbrick 1997).

The overpressure of an undercompacted rock, ΔP_{comp}, is proportional to the burial anomaly, dZ_B [m] (Fig. 1). Based on North Sea data, Japsen (1998) found that

$$\Delta P_{\mathrm{comp}} \approx dZ_\mathrm{B}/100[\mathrm{MPa}], \qquad (9)$$

which means that a burial anomaly of 1000 m may reflect overpressure due to undercompaction of 10 MPa. In Fig. 11(c), we compare the degree of undercompaction of the lower Cenozoic succession in the North Sea, expressed by its burial anomaly $dZ_\mathrm{B}^{\mathrm{low}}$, with pressure data from the underlying chalk, ΔP_{ch}, because pressure measurements from the lower Cenozoic shales are rare in the central North Sea. We observe that ΔP_{ch} is proportional to $dZ_\mathrm{B}^{\mathrm{low}}$, and is of the order of the overpressure predicted by equation (9). This indicates that the burial anomaly for the lower Cenozoic succession relative to the shale trend given by equation (5) is a measure of overpressure due to undercompaction.

Comparison of *V–z* models for sandstone and shale

The velocity at the surface varies little for the sandstone and shale models presented here (approximately 1.6 km/s;

Table 1c; Fig. 9). However, different velocity gradients during normal compaction lead to a considerable range of velocities at a burial depth of 1 km for these models: sandstone velocities range from 2.6 to 3.1 km/s (30–0% clay content), while that of shale is predicted to be 2.1 km/s. For the models in Fig. 9, we predict the velocity of marine shale to be lower than that for sandstone with a clay content below 30% for $z < 3.5$ km.

The shapes of the velocity–depth trends for sandstone and shale differ markedly at shallow depth as indicated by the much higher velocity gradient for sandstone than for shale (1–1.5 s^{-1} as opposed to 0.55 s^{-1}, respectively, for z increasing from 0 to 1 km). Whereas the gradient for the sandstone trends decreases monotonously with depth, that for shale has a maximum value of 0.62 s^{-1} for $z = 2.0$ km. However, the velocity gradients are all close to 0.5 s^{-1} for the sandstone and shale models at intermediate depths.

DISCUSSION

Identification of a normal velocity–depth trend from basin-wide well data involves three steps of generalization, and this may explain differences among trends suggested for identical units by different authors. First, the model should be established for formations that are relatively homogeneous with regard to macroscopic acoustic properties, e.g. sandstone units of equal clay content or marine shale dominated by smectite/illite. Second, the trend should reflect normal compaction, but burial anomalies of ±1 km relative to the trend may be expected as the result of over- and undercompaction (Figs 1 and 11). Third, the mathematical formulation of the normal velocity–depth trends should be constrained by knowledge from rock physics.

Unconstrained trend lines fitted to local velocity–depth data may be useful for estimating the onset of overpressure or for predicting velocity within a limited depth range. However, a normal velocity–depth trend that complies with the above criteria is a prerequisite for estimating absolute values of depth, overpressure and the amount of exhumation based on sonic data for a sedimentary formation. Estimates of previous depth of burial (and hence exhumation) should thus be based on velocity data and models for specific lithologies: for example, for $V = 3$ km/s, the depth of normal compaction varies by up to 1 km, depending on whether the lithology is assumed to be shale or pure sandstone (Fig. 9). Consequently, the constrained, exponential tt–z trend given by equation (C5) that implies a V–ϕ relationship characteristic of a marine shale, should only be considered as a reference for sand/shale series (e.g. Heasler and Kharitonova 1996), for Triassic redbeds (e.g. Ware and Turner 2002) or for undefined lithologies along a seismic line (Walford and White 2005; Mackay and White 2006) (see Appendix B).

Normal compaction may be a difficult condition to prove because we do not always know if formation pressure is hydrostatic (e.g. in shale) or if a formation has been buried deeper prior to exhumation. If, for instance, a formation is exhumed, the observed minimum velocity at the surface may be mistaken for the normal velocity of the formation at zero depth prior to burial. These effects led Faust (1951) to suggest that the velocity for sand-shale sections was proportional to $(zT)^{1/6}$, where T is geological time in years (cf. Equation (C4)). Acheson (1963), however, realized that the apparent age effect observed by Faust (1951) could be explained by exhumation.

Japsen (1999) suggested that a shale trend close to that given by equation (5) could be applied more widely to marine shale dominated by smectite/illite and, thus, possibly to the Ceno-zoic shales in, for example, the Gulf Coast area. Illite and smectite are the main components of marine shale, making up 70% of the clay minerals in the major ocean basins today, and the shale of the Ceno-zoic deposits of the North Sea Basin and that in the Gulf Coast area are also dominated by smectite/illite (Weaver 1989). The validity of the baseline for marine shale given by equation (5) is indicated firstly by the successful prediction of overpressure in the North Sea (Fig. 11), secondly by the corre-spon-dence between this baseline and other suggested shale lines over significant velocity ranges (Scherbaum 1982; Hansen 1996b) and finally, by the fact that the trend is constrained by V–ϕ–z relationships for shale (Fig. 4).

CONCLUSIONS

The formulation of a normal velocity–depth trend for a formation is not an arbitrary choice of mathematical functions and regression parameters. The trend should be considered as a physical model of how the sonic velocity of a given lithology increases as porosity is reduced during burial and normal compaction in a sedimentary basin. We have investigated the properties of normal velocity–depth trends for sandstone and shale by combining typical V–ϕ trajectories and exponential ϕ–z relationships that are constrained by the critical porosity of the sediment at the surface and have shown that:

- The concave V–ϕ path for sandstone with initial grain contact leads to a monotonous decrease in the velocity gradient with depth. Therefore, V–z trends for consolidated sandstone have often been approximated by power-law V–z trends with the velocity gradient decreasing monotonously with depth, a formulation that predicts zero velocity at the surface and infinite velocity at depth. We present a constrained V–z trend for sandstone, based on a modified Voigt model (equation (A2)), and, as an approximation to this trend – a constrained, exponential V–z trend, based on a modified velocity-average equation (equation (B2)).

- The convex V–ϕ path of lithologies such as shale or chalk that are initially compliant may lead to a maximum velocity gradient at some intermediate depth before the gradient approaches zero. V–z trends for marine shale have thus often been approximated by exponential tt–z trends for which the velocity gradient increases (towards infinity) with depth. We suggest a constrained exponential tt–z model (equation 5), based on a modified time-average equation (equation (B1)), as other workers have done before us.

Different velocity-depth gradients for shale and sandstone lead to a considerable range of velocities for these lithologies at a burial depth of 1 to 2 km (normal compaction). Estimates of maximum burial (and hence exhumation) should be based on velocities for specific lithologies: depth of normal compaction may vary up to 1 km depending on whether the lithology is assumed to be shale or sand.

The case study of baselines for sandstone and shale in the North Sea underlines the importance of applying constrained models and also the difficulty of estimating such trends when the sediments are not at maximum burial due to exhumation. The baseline for the redbeds of the Triassic Bunter Shale and Sandstone is found to be in agreement with the modified Voigt model for sandstone, assuming that the onset of quartz cementation occurs below a depth of approximately 2 km. The baseline for marine shale agrees with the shale trends of previous workers, and it can be applied to predict overpressure from sonic data.

Normal velocity–depth trends derived from basinwide data thus give us the opportunity to study the rock physical behaviour of different lithologies under natural conditions that may be difficult to imitate in the laboratory.

ACKNOWLEDGEMENTS

The financial support from the Carlsberg Foundation, GEUS and Stanford Rock and Borehole Geophysics Project is gratefully acknowledged. The constructive comments of reviewers, editors, J.A. Chalmers and J. Ineson improved the paper, which has been published with permission of the Geological Survey of Denmark and Greenland.

REFERENCES

Acheson C.H. 1963. Time-depth and velocity-depth relations in western Canada. *Geophysics* **28**, 894–909.

Al-Chalabi M. 1997a. Instantaneous slowness versus depth functions. *Geophysics* **62**, 270–273.

Al-Chalabi M. 1997b. Time-depth relationships for multilayer depth conversion. *Geophysical Prospecting* **45**, 715–720.

Athy L.F. 1930. Compaction and oil migration. *American Association of Petroleum Geologists Bulletin* **14**, 25–35.

Bertelsen F. 1980. Lithostratigraphy and depositional history of the Danish Triassic. *Geological Survey of Denmark*. Series B, 4. Geological Survey of Denmark.

Bjørlykke K. and Egebjerg P.K. 1993. Quartz cementation in sedimentary basins. *American Association of Petroleum Geologists Bulletin* **77**, 1538–1548.

Bulat J. and Stoker S.J. 1987. Uplift determination from interval velocity studies, UK, southern North Sea. In: *Petroleum Geology of Northwest Europe* (eds J. Brooks and K. W. Glennie), pp. 293–305. Graham & Trotman.

Chapman R.E. 1983. *Petroleum Geology*. Elsevier. Science Publishing Co.

Chen Q. and Nur A. 1994. Critical concentration models for porous materials. In: *Advances in Porous Media* (ed. M. Y. Corapcioglu), pp. 169–308. Elsevier. Science Publishing Co.

Corcoran D.V. and Doré A.G. 2005. A review of techniques for the estimation of magnitude and timing of exhumation in offshore basins. *Earth-Science Reviews* **72**, 129–168.

Corcoran D.V. and Mecklenburgh R. 2005. Exhumation of the Corrib gasfield, Slyne Basin, offshore Ireland. *Petroleum Geoscience* **11**, 239–256.

Dvorkin J., Gutiérrez M.A. and Nur A. 2002. On the universality of diagenetic trends. *The The Leading Edge* **21**, 40–43.

Dvorkin J. and Nur A. 1996. Elasticity of high-porosity sandstones – theory for two North Sea data sets. *Geophysics* **61**, 1363–1370.

Fabricius I.L. 2003. How burial diagenesis of chalk sediments controls sonic velocity and porosity. *American Association of Petroleum Geologists Bulletin* **87**, 1755–1778.

Faust L.Y. 1951. Seismic velocity as a function of depth and geologic time. *Geophysics* **16**, 192–206.

Feng S. and Sen P.N. 1985. Geometrical model of conductive and dielectric properties of partially saturated rocks. *Journal of Applied Physics* **58**, 3236–3243.

Greenberg M.L. and Castagna J.P. 1992. Shear-wave velocity estimation in porous rocks: Theoretical formulation, preliminary verification and applications. *Geophysical Prospecting* **40**, 195–209.

Guéguen Y., Chelidze T. and Le Ravalec M. 1997. Microstructures, percolation thresholds, and rock physical properties. *Tectonophysics* **279** (1–4), 23–35.

Guéguen Y. and Palciauskas V. 1994. *Introduction to the Physics of Rocks*. Princeton University Press.

Han D.H., Nur A. and Morgan D. 1986. Effects of porosity and clay content on wave velocities in sandstones. *Geophysics* **51**, 2093–2107.

Hansen S. 1996a. A compaction trend for Cretaceous and Tertiary shales on the Norwegian Shelf based on sonic transit times. *Petroleum Geoscience* **2**, 159–166.

Hansen S. 1996b. Quantification of net uplift and erosion on the Norwegian Shelf south of 66°N from sonic transit times of shale. *Norsk Geologisk Tidsskrift* **76**, 245–252.

Haskell N.A. 1941. The relation between depth, lithology, and seismic wave velocity in Tertiary sandstones and shales. *Geophysics* **6**, 318–326.

Heasler H.P. and Kharitonova N.A. 1996. Analysis of sonic well logs applied to erosion estimates in the Bighorn Basin. *Wyoming. American Association of Petroleum Geologists Bulletin* **80**, 630–646.

Hillis R.R. 1995. Quantification of Tertiary exhumation in the United Kingdom southern North Sea using sonic velocity data. *American Association of Petroleum Geologists Bulletin* **79**, 130–152.

Hottmann C.E. and Johnson R.K. 1965. Estimation of formation pressures from log-derived shale properties. *Journal of Petroleum Technology* **17**, 717–723.

Issler D.R. 1992. A new approach to shale compaction and stratigraphic restoration, Beaufort-Mackenzie Basin and Mackenzie Corridor, northern Canada. *American Association of Petroleum Geologists Bulletin* **76**, 1170–1189.

Japsen P. 1993. Influence of lithology and Neogene uplift on seismic velocities in Denmark; implications for depth conversion of maps. *American Association of Petroleum Geologists Bulletin* **77**, 194–211.

Japsen P. 1998. Regional velocity-depth anomalies, North Sea Chalk. A record of overpressure and Neogene uplift and erosion. *American Association of Petroleum Geologists Bulletin* **82**, 2031–2074.

Japsen P. 1999. Overpressured Cenozoic shale mapped from velocity anomalies relative to a baseline for marine shale, North Sea. *Petroleum Geoscience* **5**, 321–336.

Japsen P. 2000. Investigation of multi-phase erosion using reconstructed shale trends based on sonic data. Sole Pit axis, North Sea. *Global and Planetary Change* **24**, 189–210.

Johnson H., Warrington G. and Stoker S.J. 1994. 6. Permian and Triassic of the southern North Sea. In: *Lithostratigraphic Nomenclature of the UK North Sea* (eds R. W. O'B. Knox and W. G. Cordey). British Geological Survey.

Lander R.H. and Walderhaug O. 1999. Predicting porosity through simulating sandstone compaction and quartz cementation. *American Association of Petroleum Geologists Bulletin* **83**, 433–449.

Liu G. and Roaldset R. 1994. A new decompaction model and its application to the northern North Sea. *First Break* **12**, 81–89.

Magara K. 1976. Thickness of removed sedimentary rocks, paleopore pressure, and paleotemperature, southwestern part of Western Canada Basin. *American Association of Petroleum Geologists Bulletin* **60**, 554–565.

Magara K. 1978. Compaction and Fluid Migration. *Practical Petroleum Geology*. Elsevier. Science Publishing Co.

Mackay L.M. and White N.J. 2006. Accurate estimates of the spatial pattern of denudation by inversion of stacking velocity data: An example from the British Isles. *Geochemistry, Geophysics and Geosystems 7,* Q10007, 1–34.

Marion D., Nur A., Yin H. and Han D. 1992. Compressional velocity and porosity in sand-clay mixtures. *Geophysics* **57**, 554–563.

Mavko G., Mukerji T. and Dvorkin J. 1998. *The Rock Physics Handbook*. Cambridge University Press.

Michelsen O. 1989. Revision of the Jurassic lithostratigraphy of the Danish subbasin. Geological Survey of Denmark, Copenhagen.

Nolen-Hoeksema R.C. 1993. Porosity and consolidation limits of sediments and Gassmann's elastic-wave equation. *Geophysical Research Letters* **20**, 847–850.

Nur A., Marion D. and Yin H. 1991. Wave velocities in sediments. In: *Shear Waves in Marine Sediments* (ed. J. M. Hovem), pp. 131–140. Kluwer. Academic Publishers.

Nur A., Mavko G., Dvorkin J. and Galmundi D. 1998. Critical porosity; a key to relating physical properties to porosity in rocks. *The The Leading Edge* **17**, 357–362.

Olsen R.C. 1979. Lithology. Well 17/10—1. NPD Paper 21.

Osborne M.J. and Swarbrick R.E. 1997. Mechanisms for generating overpressure in sedimentary basins. *A Re–Evaluation. American Association of Petroleum Geologists Bulletin* **81**, 1023–1041.

Pryor W.A. 1973. Permeability-porosity patterns and variations in some Holocene sand bodies. *American Association of Petroleum Geologists Bulletin* **57**, 162–189.

Raymer L.L., Hunt E.R. and Gardner J.S. 1980. An improved sonic transit time-to-porosity transform. Proceedings of SPWLA 21 Annual Logging Symposium, pp. 1–12.

Rolle F. 1985. Late Cretaceous-Tertiary sediments offshore central West Greenland: lithostratigraphy, sedimentary evolution, and petroleum potential. *Canadian Journal of Earth Science* **22**, 1001–1019.

Rubey W.W. and Hubbert M.K. 1959. Role of fluid pressure in mechanics of overthrust faulting, II. *Geological Society America Bulletin* **70**, 167–206.

Scherbaum F. 1982. Seismic velocities in sedimentary rocks; indicators of subsidence and uplift. *Geologische Rundschau* **71**, 519–536.

Scholle P.A. 1977. Chalk diagenesis and its relation to petroleum exploration; oil from chalks, a modern miracle? *American Association of Petroleum Geologists Bulletin* **61**, 982–1009.

Sclater J.G. and Christie P.A.F. 1980. Continental stretching; an explanation of the post-Mid-Cretaceous subsidence of the central North Sea basin. *Journal of Geophysical Research* **85**, 3711–3739.

Serra O. 1986. *Fundamentals of Well-Log Interpretation*. Elsevier. Science Publishing Co.

Slotnick M.M. 1936. On seismic computations, with applications, II. *Geophysics* **1**, 299–305.

Smith T. and Sondergeld C.H. 2001. Examination of AVO response in the eastern deepwater Gulf of Mexico. *Geophysics* **66**, 1864–1876.

Snieder R., Xie M.Y., Pica A. and Tarantola A. 1989. Retrieving both the impedance contrast and background velocity. A global strategy for the seismic reflection problem. *Geophysics* **54**, 991–1000.

Terzaghi K. and Peck R.P. 1968. *Soil Mechanics in Engineering Practice*. John Wiley & Sons, Inc.

Walford H.L. and White N.J. 2005. Constraining uplift and denudation of west African continental margin by inversion of stacking velocity data. *Journal of Geophysical Research-Solid Earth* **110**, B04403, 1–16.

Ware P.D. and Turner J.P. 2002. Sonic velocity analysis of the Tertiary denudation of the Irish Sea basin. In: *Exhumation of the North Atlantic Margin: Timing, Mechanisms and Implications for Petroleum Exploration*, 196 (eds A. G. Doré, J. A. Cartwright, M. S. Stoker, J. P. Turner, N. White), pp. 355–370. Geological Society.

Weaver C.E. 1989. *Clays, Muds and Shales*. Elsevier. Science Publishing Co.

Winthaegen P.L.A. and Verweij J.M. 2003. Estimating regional pore pressure distribution using 3D seismic velocities in the Dutch Central North Sea Graben. *Journal of Geochemical Exploration* **78–79**, 203–207.

Wyllie M.R.J., Gregory A.R. and Gardner L.W. 1956. Elastic wave velocities in heterogeneous and porous media. *Geophysics* **21**, 41–70.

APPENDIX A

Bounds on velocity

The simplest bounds on velocity are the Voigt and Reuss bounds (cf. Mavko *et al.* 1998). The Voigt upper bound of the effective elastic modulus, M_V, of N phases is

$$M_v = \sum_{i=1}^{N} f_i M_i,$$

where f_i is the volume fraction and M_i is the elastic modulus of the ith phase (either bulk modulus $K = \rho(V_p^2 - 4/3V_s^2)$ [GPa], P-wave modulus $M = \rho V_p^2$, or shear modulus $\mu = \rho V_s^2$, where the density of the rock is $\rho = (1-\phi)\rho_m + \phi\rho_{fl}$ [g/cm^3], ρ_m is density of the mineral material, ρ_{fl} is the fluid density, V_P and V_S are the P- and S-wave velocities [km/s]). The Reuss lower bound of the effective elastic modulus, M_R is given by

$$\frac{1}{M_R} = \sum_{i=1}^{N} f_i \frac{1}{M_i}$$

The Reuss average describes exactly the effective moduli of a suspension of solid grains in a fluid. In the suspension domain, $\phi > \phi_c$, the effective bulk and shear moduli can be estimated quite accurately using the Reuss (iso-stress) average:

$$K_R^{-1} = (1-\phi)K_m^{-1} + \phi K_{fl}^{-1}, \quad \mu_R = 0, \tag{A1}$$

where K_m and K_{fl} are the bulk moduli of the mineral material and the fluid. The effective shear modulus of the suspension is zero, because the shear modulus of the fluid is zero. We can thus calculate the P-wave velocity V_c at ϕ_c where the mineral grains are barely touching ($\mu_c = 0$):

$$V_c = \sqrt{(K_c + 4/3\mu_c)/\rho_c} = \sqrt{K_c/\rho_c},$$

where the subscript c indicates the value at critical porosity: $K_c^{-1} = (1-\phi_c)K_m^{-1} + \phi_c K_{fl}^{-1}$ and $\rho_c = (1+\phi_c)\rho_m + \phi_c \rho_{fl}$.

A linear trend of ρV^2 versus ϕ may be used to describe the compaction trend for clean sandstones at high effective pressure, leading to convenient mathematical properties (Nur *et al.* 1991; Marion *et al.* 1992). This linear dependence can be thought of as a modified Voigt average:

$$M_{MV} = (1-\phi')M_m + \phi' M_c, \tag{A2}$$

where M_m and M_c are the moduli (bulk or shear) of the mineral material at zero porosity and of the suspension at the critical porosity (M_c is given by equation (A1) with $\phi = \phi_c$). The expression is modified in the sense that the porosity is scaled by the critical porosity $\phi' = \phi/\phi_c$, so that ϕ' ranges from 0 to 1 as ϕ ranges from 0 to ϕ_c. If the low-porosity end-member is taken as the porosity at finite depth, ϕ_{fin}, rather than 0, to fit data from sedimentary basins, we have $\phi' = (\phi - \phi_{fm})(\phi_c - \phi_{fm})$. Note that using the suspension modulus M_c in this form automatically incorporates the effect of pore fluids on the modified Voigt average. The modified Voigt average (equation (A2)) can be transformed into a velocity–depth model by calculating porosity as a function of depth by assuming exponential porosity decay (equation 2). The appropriate rock physical properties for sandstone with 0, 10, 20 and 30% clay content, based on data from Han *et al.* (1986), are given in Table 1(b) and for the ϕ–z model for sandstone in Table 1(a).

APPENDIX B

V–z relationships for specific V–ϕ trends

Transit time proportional to ϕ^{α_t} (modified time-average equation)

Let transit time be dependent on porosity raised to the power of a positive constant α_t:

$$tt = (tt_c - tt_m)\left(\frac{\phi}{\phi_c}\right)^{\alpha_t} + tt_m \Rightarrow \ln\left(\frac{tt - tt_m}{tt_c - tt_m}\right) = \alpha_t \ln\left(\frac{\phi}{\phi_c}\right),$$

where tt_m is the transit time of the matrix and tt_c is that of the rock at critical porosity (the simple time-average for a rock is given by $(1-\phi)tt_m + \phi tt_{fl}$). We see that transit time varies between tt_c and tt_m for ϕ varying between ϕ_c and 0%, and that $(tt - tt_m)$ and ϕ are plotted as a straight line on a log-log plot. The V–ϕ path for this relationship is convex for all positive values of α_t. We get a linear $\ln(tt - tt_m)$–z function similar to equation (C5) by substituting the exponential ϕ–z function with decay rate β (equation 2):

$$tt = (tt_c - tt_m)e^{-z/b_2} + tt_m \Rightarrow \ln(tt - tt_m) = \ln(tt_c - tt_m) - \frac{z}{b_2},$$

where $b_2 = \beta/\alpha_t$. Conversely, we see that the above V–z trend implies that transit time is proportional to $(\phi/\phi_c)^{\beta/b_2}$ if porosity decays exponentially with depth.

If the decay rates of ϕ and tt are identical, $\beta = b_2$, we have linearity between tt and ϕ ($\alpha_t = 1$), and we get a modified time-average equation:

$$tt = (tt_c - tt_m)\phi/\phi_c + tt_m. \quad \text{(B1)}$$

This equation should be compared with the Wyllie *et al.* (1956) time-average equation that states proportionality between transit time and porosity (tt_{fl} is the transit time of the pore fluid):

$$tt = (tt_{fl} - tt_m)\phi + tt_m,$$

where $\phi = 1$ is taken as maximum porosity (and not ϕ_c), and the velocity at maximum porosity equals V_{fl} (and not V_c) (equation (A1)). The constrained transit-time–depth trend of equation (C5) can thus be derived by combining the modified time-average equation with the assumption of exponential decay of porosity (equations (B1) and (2)).

Velocity proportional to ϕ^{α_v} (modified velocity-average equation)

Let velocity be dependent on porosity raised to the power of a positive constant α_v:

$$V = V_m - (V_m - V_c)\left(\frac{\phi}{\phi_c}\right)^{\alpha_v}$$
$$\Rightarrow \ln(V_m - V) = \ln(V_m - V_c) + \alpha_v \ln\left(\frac{\phi}{\phi_c}\right),$$

where V_m is the velocity of the matrix and V_c is that of the rock at critical porosity (the simple velocity-average for a rock is defined as $(1–\phi)V_m + \phi V_{fl}$). We see that velocity varies between V_c and V_m for ϕ varying between ϕ_c and 0%, and that $(V_m - V)$ and ϕ are plotted as a straight line in a log-log plot. The V–ϕ path is concave for $\alpha_v > 1$ ($d^2V/d\phi^2 < 0$), and convex for $0 < \alpha_v < 1$, while it is a straight line for $\alpha_v = 1$ (a modified velocity-average). We get the following linear $\ln(V_m-V)$–z trend by substituting the exponential ϕ–z function with decay rate β (equation 2):

$$V = V_m - (V_m - V_c)e^{-z/b_3}$$
$$\Rightarrow \ln(V_m - V) = \ln(V_m - V_c) - \frac{z}{b_3}, \quad \text{(B2)}$$

where $\beta_3 = \beta/\alpha_v$. In the special case where $\alpha_v = 1$, velocity becomes linearly proportional to porosity and $b_3 = \beta$. The trend is a constrained velocity–depth model for which the velocity gradient decreases monotonously with depth for all values of b_3 and thus, even for convex V–ϕ paths ($0 < \alpha_v < 1$), there is no maximum velocity–depth gradient at intermediate depths.

We can estimate the parameters in equation (B2) as an approximation to the modified Voigt trend (equation (A2)) for $z < 4$ km taking $V_c = 1600$ m/s; for sandstone with varying clay content, we get

$$0\%\ \text{clay}: \quad V_m = 5065\ \text{m/s}, \quad b_3 = 1923\text{m},$$
$$5\%\ \text{clay}: \quad V_m = 4796\ \text{m/s}, \quad b_3 = 1963\text{m},$$
$$10\%\ \text{clay}: \quad V_m = 4526\ \text{m/s}, \quad b_3 = 2003\text{m},$$
$$20\%\ \text{clay}: \quad V_m = 4288\ \text{m/s}, \quad b_3 = 2042\text{m},$$
$$30\%\ \text{clay}: \quad V_m = 4056\ \text{m/s}, \quad b_3 = 2076\text{m}.$$

The depth predicted by these approximations deviates less than 90 m from the respective Voigt model for a given velocity and this is considered insignificant. The model for 5% clay corresponds to the normal velocity–depth trend for the redbeds of the Triassic Bunter Shale and Sandstone formations ($V > 3.6$ km/s; see Figs 6 and 7)

APPENDIX C

Review of analytical formulations of V–z trends

Several functions have been applied to represent the increase in velocity with depth (Table 2). A linear velocity–depth function has been used by several workers for different lithologies (e.g. Slotnick 1936; Bulat and Stoker 1987; Japsen 1993):

$$V = V_0 + kz, \quad \text{(C1)}$$

where the velocity–depth gradient k is positive (curve B&S in Fig. 10).

Hillis (1995) applied a linear function between transit time and depth for chalk, sandstone and shale:

$$tt = tt_0 + qz, \quad \text{(C2)}$$

where tt_0 is the transit time at the surface and q [μs/m^2] is the negative transit-time–depth gradient (cf. Al-Chalabi 1997a; curve H in Fig. 10).

Velocity–depth relationships for shale have often been approximated by a simple exponential model for the reduction of transit time with depth (e.g. Hottmann and Johnson 1965; Magara 1978; Hansen 1996b):

$$tt = tt_0 e^{-z/b_1} \Rightarrow \ln(tt) = \ln(tt_0) - z/b_1, \quad \text{(C3)}$$

where b_1 [m] is an exponential decay constant (curve Ha in Fig. 4).

Acheson (1963) found that velocity in sedimentary basins was proportional to depth raised to the power of (1–n):

$$V = dz^{1-n} \Rightarrow \ln(V) = \ln(d) + (1 - n)\ln(z), \quad \text{(C4)}$$

where n is a number between 0.83 and 1, and d [m^n/s] is a coefficient. The velocity at the surface is predicted to be zero, so the expression is only valid below a certain depth. Similar formulations were applied by Faust (1951).

The above four formulations are linear relationships in the V–z, tt–z, $\ln(tt)$–z and $\ln(V)$–$\ln(z)$ planes, respectively. While they may be valid approximations within a given interval, they all predict that velocity approaches infinity at depth. Only the power-law V–z trend (equation (C4)) predicts that the velocity gradient decreases with depth; the linear V–z trend (equation (C1)) has a constant gradient, and the linear tt–z and the exponential tt–z trends (equations (C2) and (C3)) have increasing gradients with depth. However, we have shown that an increasing velocity gradient at shallow depths characterizes initially compliant sediments, whereas the velocity gradient for initially stiff rocks decreases with depth. This point explains why the linear tt–z and exponential tt–z trends have been applied so successfully to initially compliant rocks, like chalk and shale (e.g. Hottmann and Johnson 1965; Hillis 1995), and why the power-law V–z model has been applied primarily to sand-shale sequences (e.g. Faust 1951; Acheson 1963).

A constrained exponential transit-time–depth model was suggested for shale by Chapman (1983), and applied for sand/shale series by Heasler and Kharitonova (1996) and for Triassic redbeds by Ware and Turner (2002):

$$tt = (tt_0 - tt_\infty)e^{-z/b_2} + tt_\infty$$
$$\Rightarrow \ln(tt - tt_\infty) = -z/b_2 \ln(tt_0 - tt_\infty), \tag{C5}$$

where tt_∞ is the transit time at infinite depth and b_2 [m] is an exponential decay constant (cf. Al-Chalabi 1997a). This model predicts finite values of transit time at the surface and at infinite depth, i.e. tt_0 and tt_∞, respectively. This formulation is linear in the $\ln(tt - tt_\infty) - z$ plane, and implies that $k \to 0$ for $z \to \infty$. The velocity gradient for this V–z trend has a maximum for $z = b_2 \ \ln[(tt_0 - tt_\infty)/tt_\infty]$. This model may thus be applied to initially compliant rocks, such as shale (e.g. Chapman 1983), or more specifically to marine shale dominated by smectite/illite (equation 5; curve V_N^{sh} in Fig. 4) (Japsen 1999, 2000).

Segmented linear velocity–depth functions have been suggested for the North Sea chalk (Upper Cretaceous-Danian) and for the Triassic Bunter Shale because no single mathematical function matched the observed trends (Japsen 1998, 2000). Such continuous and non-linear functions are defined over a velocity interval divided into n segments:

$$V = V_{0i} + k_i z, \quad z_{ai} < z < z_{bi,} \tag{C6}$$

where V_{0i} and k_i are the velocity at the surface and the velocity–depth gradient of the ith segment defined for velocities between V_{ai} and V_{bi}. The shift of the velocity gradient between the segments reflects variations in the compaction process (Japsen 1998).

Appendix C – Chalk background velocity: Influence of effective stress and texture (Japsen et al. 2005)

H027 Chalk background velocity: Influence of effective stress and texture

PETER JAPSEN[1], GARY MAVKO[2], LARS GOMMESEN[3], IDA L. FABRICIUS[4], FINN JACOBSEN[1], OLE VEJBÆK[1], RASMUS RASMUSSEN[1], CHRISTIAN RAU SCHIØTT[5]

[1] Geological Survey of Denmark and Greenland (GEUS) (pj@geus.dk), Øster Voldgade 10, DK-1350 Copenhagen; [2] Stanford University, California, USA; [3] Ødegaard A/S, Copenhagen, Denmark; [4] Danish Technical University (DTU), [5]Amerada Hess Aps.

Abstract

The relative variations in acoustic impedance and hence porosity may be determined by inversion of seismic data. The estimation of the absolute level of these parametres, however, requires a priori knowledge about the low-frequent, background velocity. We find that the background velocity of the North Sea chalk is primarily controlled by effective stress: velocity and porosity log data for chalk in two wells plotted versus effective depth match published reference lines for normally compacted chalk above c. 1.8 km. Effective depth is depth corrected for the effect of overpressure. Below that depth we observe a significant drop in porosity and an increase in velocity that possibly may be explained by a decrease in the Biot factor leading to an increase in effective stress and hence in pore-filling cementation originating from pressure dissolution along stylolites. Moreover, we observe different velocity-porosity relation for the chalk in the two wells leading to differences in porosity of some 5% for identical values of velocity for apparently pure chalk. These variations may be related to differences in contact cementation between the poorly cemented and stiffer pore shapes (possibly affected by quartz-overcoating). The non-unique velocity-porosity relation for chalk will lead to variability in the estimation of porosity from seismic data because one impedance value may represent a range of porosities.

Introduction

The background velocity of a depth interval – or the low-frequency velocity variations – define the absolute level of the sonic velocity. This background velocity cannot be resolved from reflection seismic data that depend on relatively high-frequency variations of the acoustic impedance. Consequently, the background velocity has to be estimated from e.g. near-by wells before seismic data can be inverted to porosity of the right magnitude. Here we investigate the controls on the regional variations of the background velocity of the Upper Cretaceous-Danian Chalk Group in the central North Sea.

Terzaghi's principle states that the weight of the overburden per unit area, S, is borne partly by the rock matrix and partly by the pore fluid: $S = S_{eff} + \beta \cdot P$, where S_{eff} is the effective stress transmitted through the matrix, P is the formation pressure and β the Biot factor that ranges between 0 and 1 (β=1 for high-porosity rocks). If a rock is more deeply buried without change in effective stress, the added load is carried by an increase in pore pressure, ΔP. We can rewrite Terzaghi's equation in terms of the gravitational acceleration, g=9.807 m/s^2, average bulk density, $\rho_b \approx 2$ g/cm^3, and pore fluid density, $\rho_{fl} \approx 1$ g/cm^3, of the added overburden:

$$Z_{eff} = Z - \frac{\beta}{g(\rho_b - \beta \cdot \rho_{fl})} \Delta P \qquad (1)$$

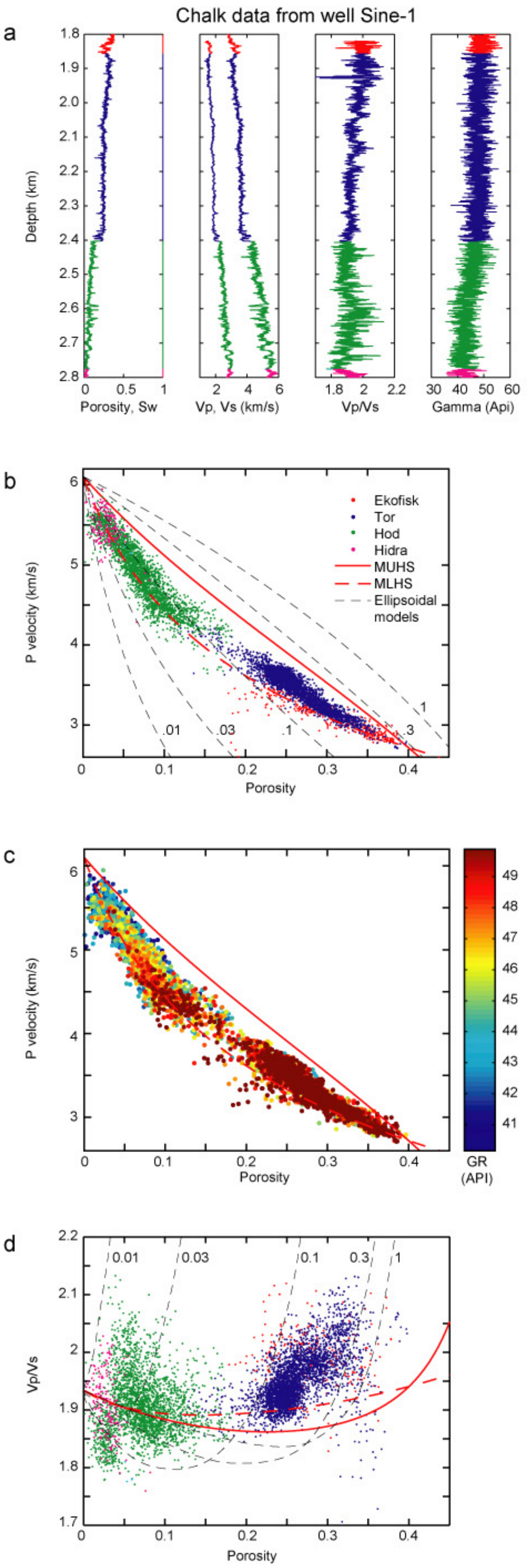

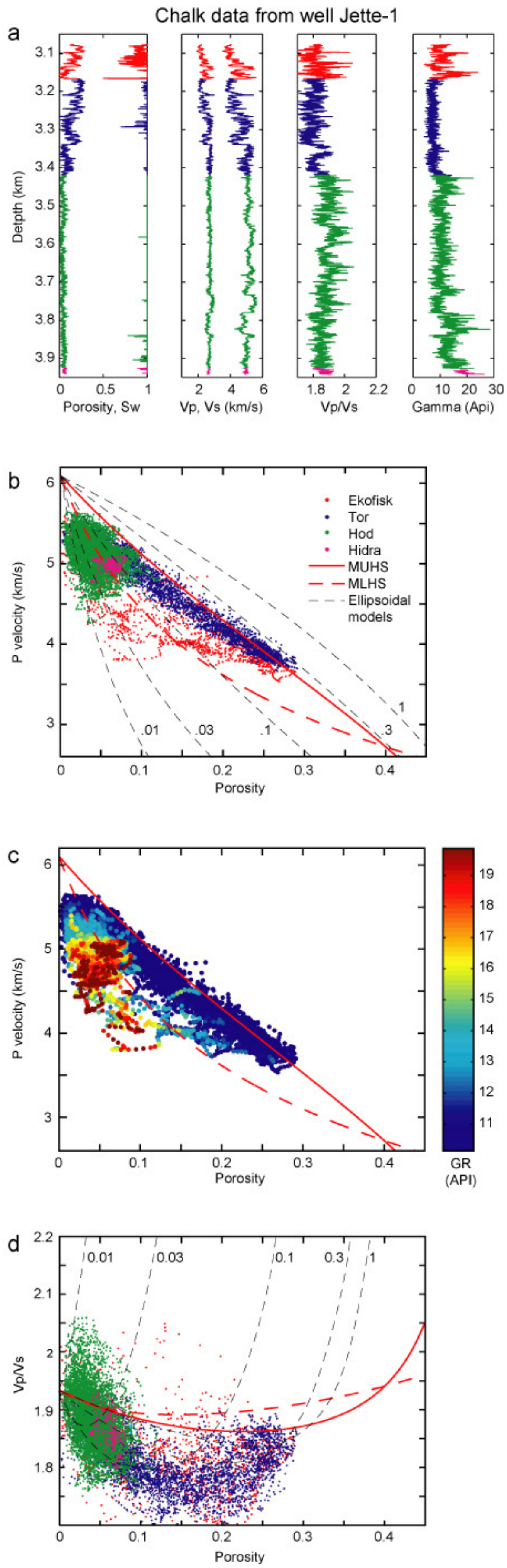

Figure 1 (left). Log data from the chalk in the Sine-1 well: a. Log data vs depth; b. and c. V_P vs porosity; d. V_P/V_S vs porosity. Figure 2 (right). Log data from the chalk in the Jette-1 well. Same panels as in Fig. 1. Figs a, b, d colorcoded by formation and Fig. c by gamma. Superimposed: Ellipsoidal pore models for different aspect ratios (Berryman 1995) and empirical modified upper and lower Hashin-Shtrikman chalk models (Walls et al. 1998).

where Z is the actual depth of the rock and Z_{eff} is the effective depth corresponding to the depth where the effective stress would occur during normal compaction. For β=1 we get $Z_{eff} \approx Z - \Delta P \cdot 100$, and for β=0.5 we get $Z_{eff} \approx Z - \Delta P \cdot 33$ (Z in metres, ΔP in MPa) (cf. Japsen 1998).

Data

We have analyzed the variation of the acoustic properties of chalk based on log data from 29 Danish wells in the central North Sea. All wells had P-wave sonic logs and 8 also S-wave logs. Of these wells we present data from the Sine-1 and Jette-1 wells both penetrating c. 1 km thick, dry chalk sections (Figs 1, 2). The absolute level of the gamma-readings in the wells is not comparable because of insufficient calibration of the gamma tools. Chalk formation overpressure was 6.5 MPa in the Sine-1 well, whereas the overpressure in the 1.2 km more deeply buried chalk in the Jette-1 well is estimated to be 14.5 MPa as in a near-by well.

Results

Figure 3 shows a plot of the sonic and porosity logs for the chalk in the Sine-1 and Jette-1 wells versus actual depth and effective depth assuming $\beta = 1$ (eq. 1). We observe that for effective depths less than c. 1.8 km, the data plot along the V–Z and V–ϕ reference curves for normally compacted chalk of Japsen (1998) and Sclater & Christie (1980). Below that depth a pronounced porosity drop and a corresponding velocity increase is observed over a short depth interval for both data sets. These observations imply that porosity reduction and velocity increase for chalk is governed by the effective stress for porosities less than c. 40% and that below some 20% a rapid increase in pore-filling cementation takes place.

Figs. 1 and 2 show different V–ϕ relations for the chalk in the two wells. Chalk with low gamma-response has higher porosity for a given velocity in the Jette-1 well than in the Sine-1 well; e.g. for V=4.5 km/s, porosity is c. 15% and only c. 10% in the two wells, respectively. The difference between the two data sets is clear from the much lower V_P–V_S ratios measured in the Jette-1 well compared to the Sine-1 well (Figs 1d, 2d). There is a general symmetry between gamma log and the V_P/V_S log: low gamma readings for the Tor Formation in the Jette-1 well correspond to low values of V_P/V_S, and high values of these parameters for the Ekofisk and Hod formations (Figs 1a, 2a). This indicates that both gamma readings and V_P–V_S ratios are indicators of the mineralogical composition.

Discussion

Pore-filling cementation

Mechanical compaction is limited in chalk with porosity less than 40%, whereas porosity reduction due to cementation originating from pressure dissolution at stylolites starts around that porosity (Fabricius 2003). The match seen in Fig. 3 between velocity and porosity data versus effective depth and the reference curves (that were defined by identifying normally compacted chalk) above c. 1.8 km implies that the Biot factor must be close to 1 for chalk with porosities between c. 40 and 20%. The drop in porosity below that depth could imply the initiation of a new process related to pressure dissolution, but the drop could also be explained by a sharp reduction in the Biot factor for chalk with porosities less than some 20%: equation (1) shows that such a reduction would lead to an increase in effective depth as well as effective stress, and thus to accelerated pressure dissolution. A reduction of the Biot factor below 20% porosity has been observed for chalk based on acoustic (Gommesen et al. *in review*) and geotechnical data (Engstrøm 1992). A similar behavior may be expected for the Biot factor estimated from loading of chalk across a geological basin over million of years.

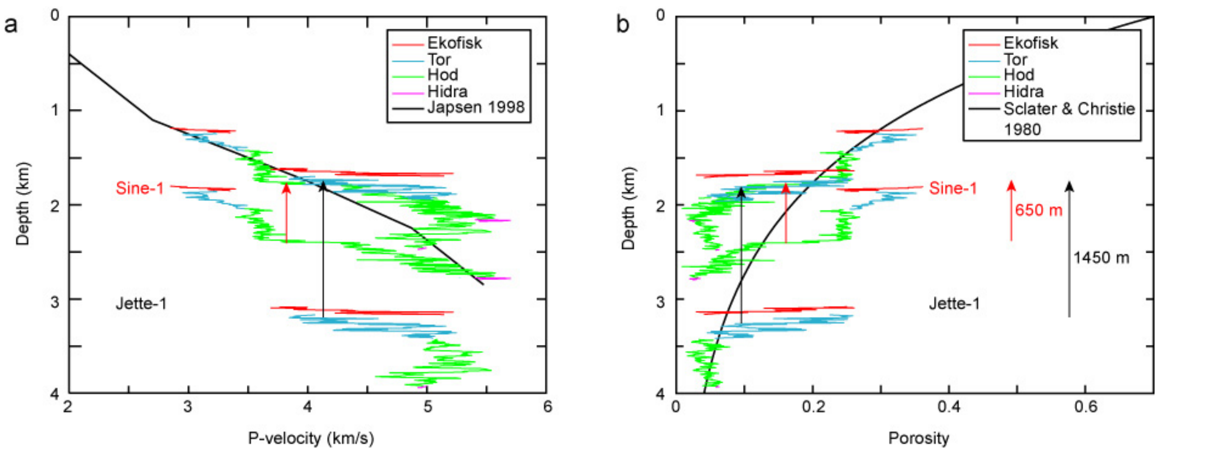

Figure 3. Sonic and porosity log data vs actual depth and effective depth for β=1 (colorcoded by formation). The data are averaged over 20 m intervals. After correction for the effect of overpressure (arrows; see eq. 1) the log data overlap and reveal a pronounced change for effective depths around c. 1.8 km. These observations indicate that porosity-reduction in chalk is controlled by effective stress.

Contact cementation

We can compare the V-ϕ data with models that represent the pore space as a collection of ellipsoidal inclusions, ranging from flat penny-shaped cracks to spherical pores (Figs 1, 2; Berryman 1995). The comparison suggests that the Jette-1 chalk has rounder, stiffer pores whereas the Sine-1 chalk has more compliant pores. The fact that the Sine-1 data are consistent with a penny-shaped crack model does not mean that there must be cracks in the rock; poorly cemented, compliant grain contacts will yield the same elastic behavior.

The causes behind these differences in pore stiffness are neither related to effective stress nor temperature. The chalk in the Sine-1 and Jette-1 wells are subjected to effective stress in the same range (Fig. 3) and the Jette-1 chalk differs from chalk in wells in the same temperature interval as it does relative to the more shallow and hence cooler Sine-1 chalk.

One hypothesis for explaining the differences is that earlier in their burial history, chalk from both wells had similar microstructures with compliant grain-to-grain contacts, but that the Jette-1 chalk later gained more cement preferentially deposited at grain contacts. An alternative hypothesis is that the greater stiffness of the chalk in the Jette-1 well is due to quartz-coating of the calcite grains and consequently that the observed low V_P–V_S ratio reflects the mineral properties of quartz. Both hypotheses thus suggest that the post-depositional development of the chalk in the Jette-1 well differs from that in the Sine-1 well.

Acknowledgement

This study was funded by the South Arne Group (Amerada Hess Aps, Dong E&P, Denerco Oil). Data from the Jette-1 well are courtesy of Amerada Hess.

Berryman,J.G. 1995. Mixture theories for rock properties. In: Ahrens, T. J. (ed.) *A Handbook of Physical Constants*. American Geophysical Union, Washington. 236 pp.

Engstrøm,F. 1992. Rock mechanical properties of Danish North Sea chalk. In: *Fourth North Sea Chalk symposium*. Joint Chalk Research, Deauville. 23 pp.

Fabricius, I. L. 2003. How burial diagenesis of chalk sediments controls sonic velocity and porosity. *AAPG Bulletin*, **87**, 1755–1778.

Gommesen, L., Fabricius, I. L., Mukerji, T., Mavko, G., and Pedersen, J. M. in review Elastic behaviour of North Sea chalk: A well log study. *Geophysical Prospecting*.

Japsen, P. 1998. Regional velocity-depth anomalies, North Sea Chalk: a record of overpressure and Neogene uplift and erosion. *AAPG Bulletin*, 82, 2031–2074.

Sclater, J. G. & Christie, P. A. F. 1980. Continental stretching; an explanation of the post-Mid-Cretaceous subsidence of the central North Sea basin. *Journal of Geophysical Research*, **85**, 3711–3739.

Walls, J. D., Dvorkin, J. & Smith, B. A. 1998. Modeling seismic velocity in Ekofisk Chalk. *Society of Exploration Geophysicists 68th annual conference*. 1016–1019.